XUV OPTICS

Luca Poletto

National Research Council - Institute of Photonics and Nanotechnologies (CNR-IFN)

Padova, Italy

luca.poletto@cnr.it

Course topics

Introduction to science and technology of extreme-ultraviolet (XUV) radiation

Wave propagation and refractive index in the XUV

XUV optical systems: mirrors, gratings, multilayer, diffractive optics

Research topic: **photon handling of XUV and soft X-rays ultrashort pulses**

INTRODUCTION

The XUV region

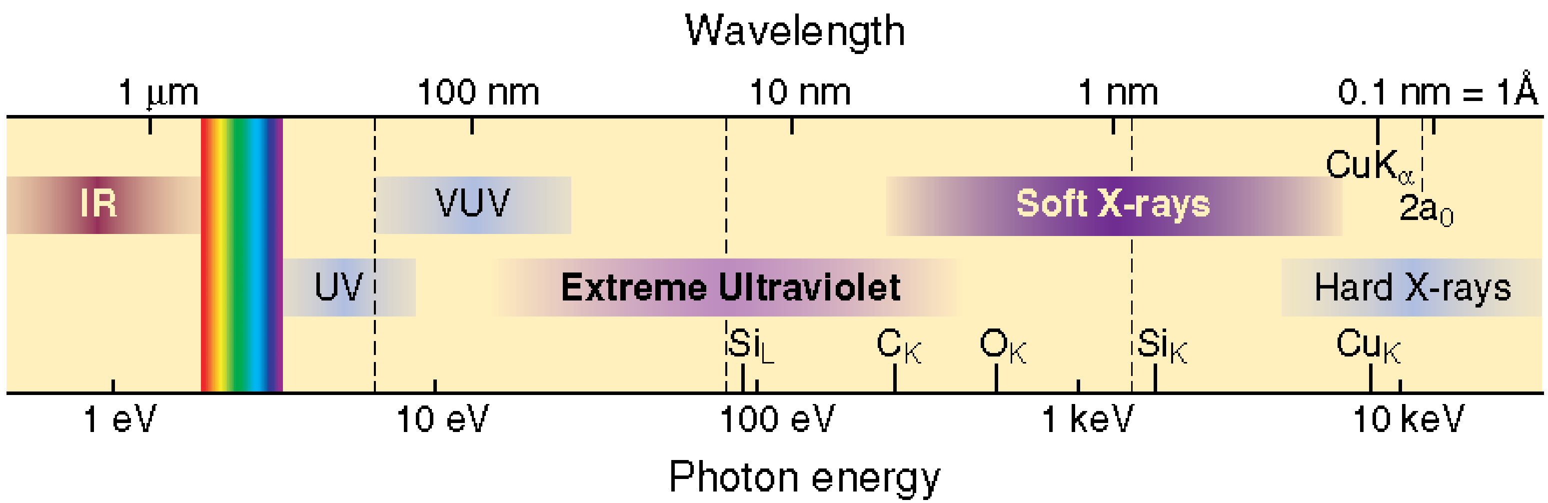

- See smaller features
- Write smaller patterns
- Elemental and chemical sensitivity

XUV to increase the resolution

Optical phenomena have a natural length scale defined by the wavelength of radiation.

Resolution is limited by λ. This limits:

– the minimum size of any patterning/machining

– the smallest particular that can be observed

Optical microscope

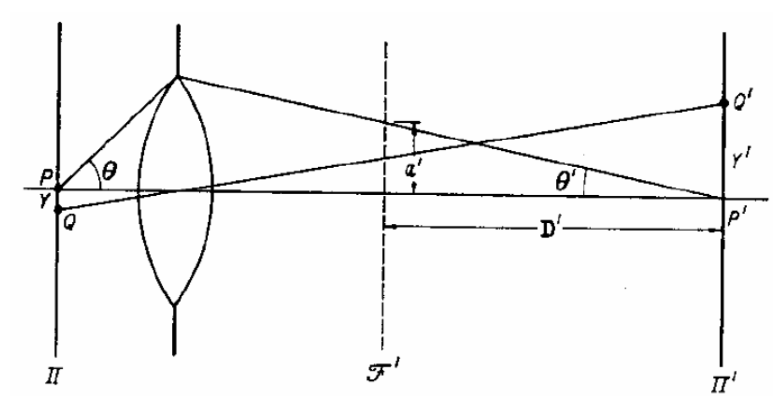

Fig. 8.31. Illustrating the theory of resolving power of the microscope.

$$|Y| \sim 0{\cdot}61 \frac{\lambda_0}{n \sin \theta}.$$

This formula gives the distance between two object points which a microscope can just resolve when the illumination is *incoherent* and the aperture is circular.

High-resolution imaging

nature Vol 435|30 June 2005|doi:10.1038/nature03719

LETTERS

Soft X-ray microscopy at a spatial resolution better than 15 nm

Weilun Chao[1,2], Bruce D. Harteneck[1], J. Alexander Liddle[1], Erik H. Anderson[1] & David T. Attwood[1,2]

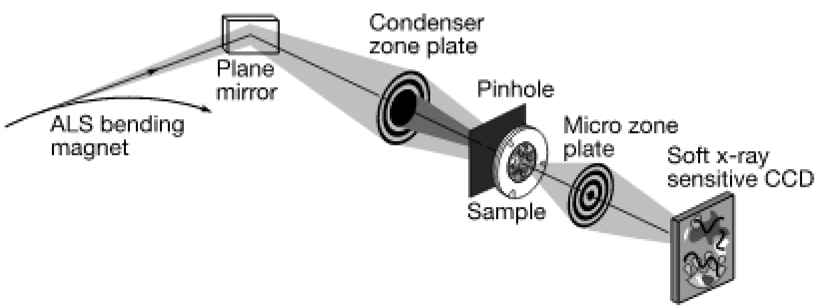

Figure 1 | A diagram of the soft X-ray microscope XM-1. The microscope uses a micro zone plate to project a full field image onto a CCD camera that is sensitive to soft X-rays. Partially coherent, hollow-cone illumination of the sample is provided by a condenser zone plate. A central stop and a pinhole provide monochromatization.

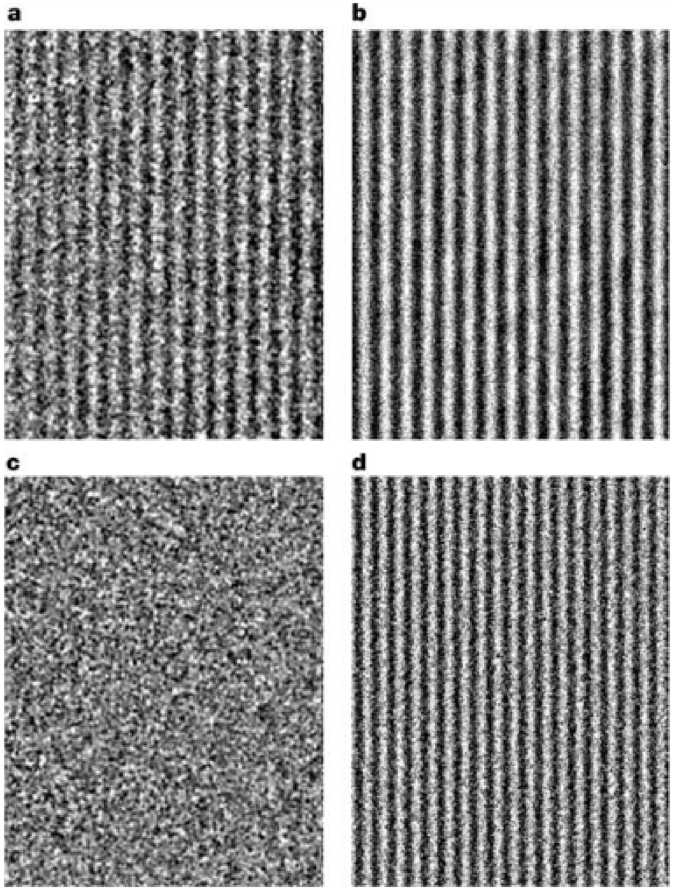

Figure 4 | Soft X-ray images of 15.1 nm and 19.5 nm half-period test objects, as formed with zone plates having outer zone widths of 25 nm and 15 nm. The test objects consist of Cr/Si multilayers, with 15.1 nm and 19.5 nm half-periods, respectively. Significant improvements are noted between the images obtained with the new 15 nm zone plate, as compared to earlier results obtained with the 25 nm zone plate. This is particularly evident for the 15 nm half-period images, for which the earlier result shows no modulation, whereas the image obtained with the 15 nm zone plate shows excellent modulation. **a,** Image of 19.5 nm half-period test object obtained previously with a 25 nm zone plate. **b,** Image of 19.5 nm half-period object with the 15 nm zone plate. **c,** Image of 15.1 nm half-period with the previous 25 nm zone plate. **d,** Image of 15.1 nm half-period with the 15 nm zone plate. Images **a** and **c** were obtained at a wavelength of 2.07 nm (600 eV photon energy); **b** and **d** were obtained at a wavelength of 1.52 nm (815 eV). The equivalent object plane pixel size for images **a** and **c** is 4.3 nm; the size for **b** and **d** is 1.6 nm.

XUV lithoghraphy

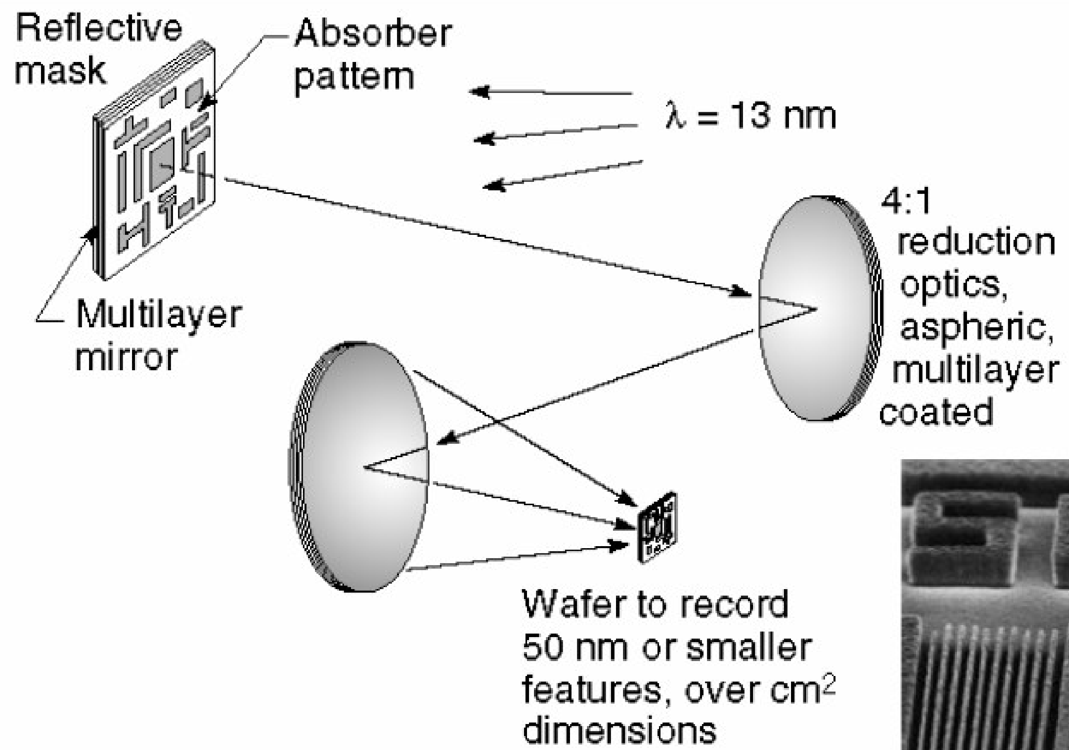

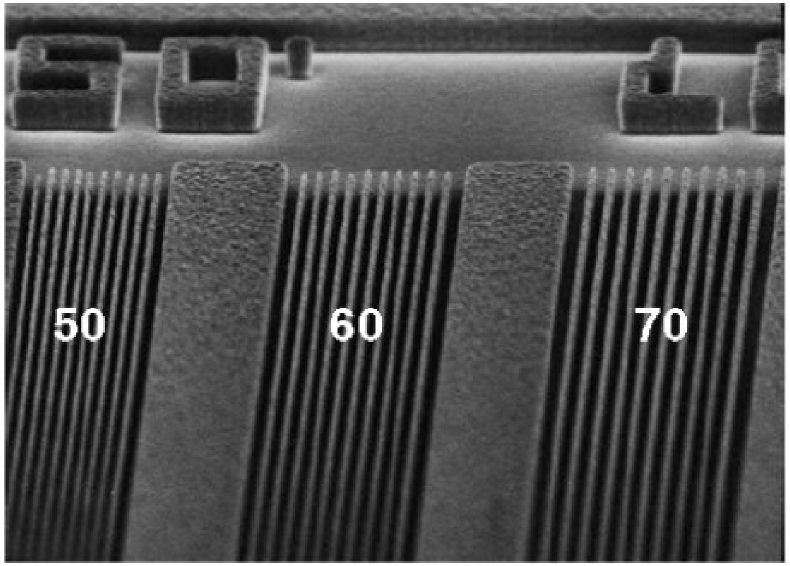

XUV astronomy

Multilayer-based telescopes for the observation of the Solar disk and solar corona in the XUV at 19 nm wavelength, Fe XVIII emission.

SOHO-EIT, SOHO-CGS, ROSAT XUV, FUSE, HINODE

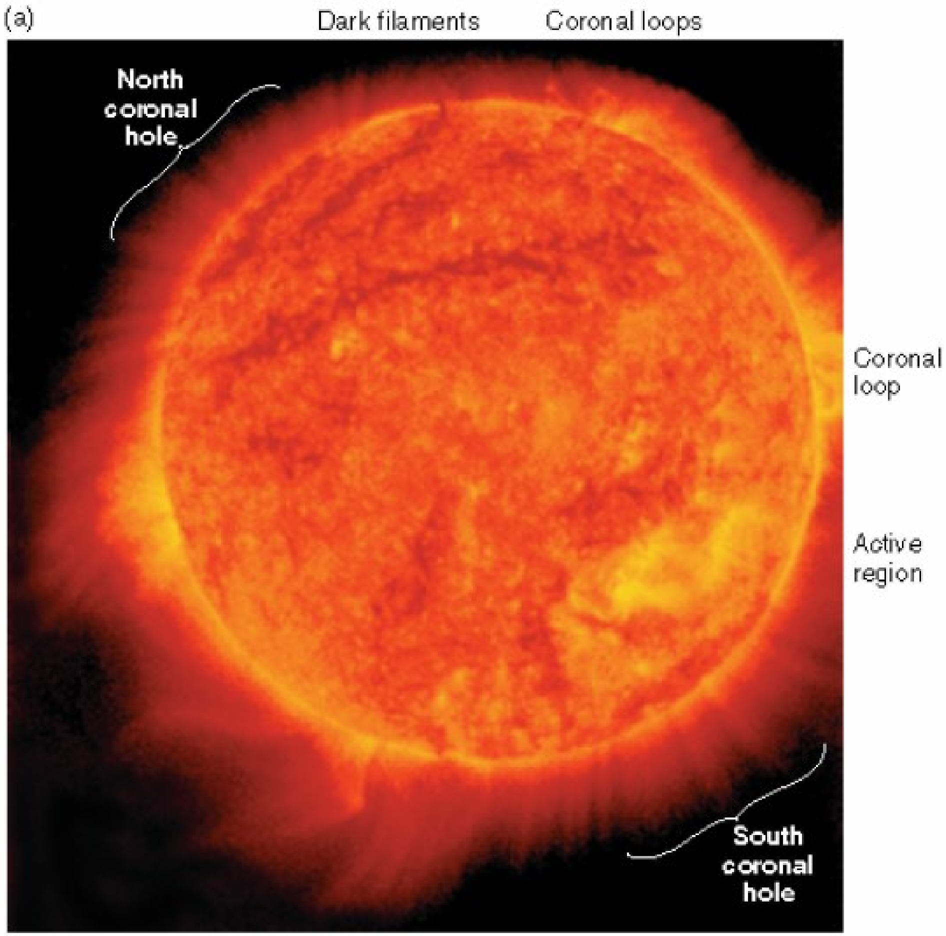

(A. Walker, Stanford)

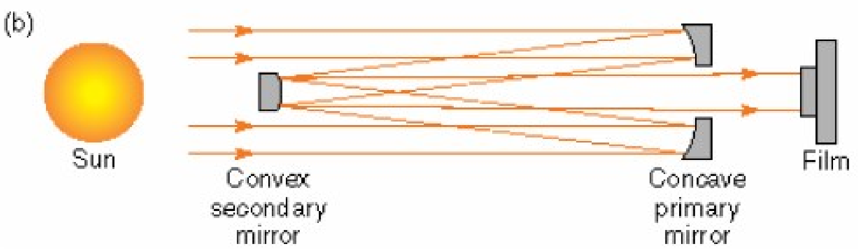

XUV for ultrafast phenomena

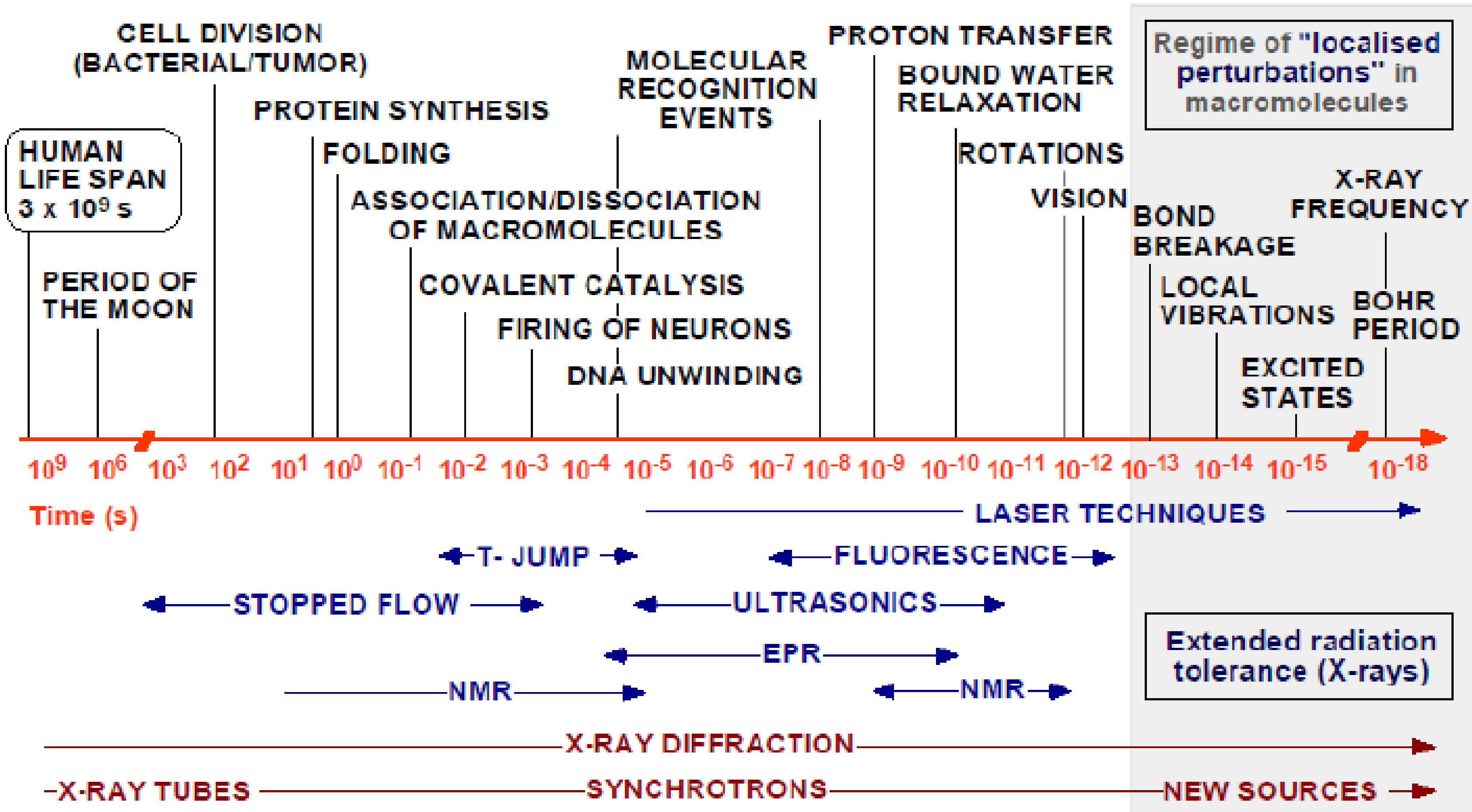

XUV and soft X-ray radiation

XUV and soft X-ray radiation spans over a range of photon energies from above 10 eV to few keV.

Such energetic radiation is emitted from the stars, mainly from electrons from both external and core levels (10% of the Sun emission is in the UV, XUV and soft X-rays). Sun UV emissions have sufficient energy to ionize atoms and molecules on the outer Earth atmosphere, giving raise to the ionosphere. Fortunately, the ozone layer (O_3) shields radiation below 280 nm. Therefore, XUV telescopes have to be operated on satellite from space.

UV and soft X-ray radiation is absorbed by air at atmospheric pressure (few centimeters of air are sufficient to block any photon between 10 and 1000 eV). Therefore, XUV beamlines are operated in vacuum

SCATTERING IN THE XUV

Wave propagation (1)

Maxwell's equations

$$\nabla \times \mathbf{H} = \frac{\partial \mathbf{D}}{\partial t} + \mathbf{J} \qquad \text{(Ampere's law)}$$

$$\nabla \times \mathbf{E} = -\frac{\partial \mathbf{B}}{\partial t} \qquad \text{(Faraday's law)}$$

$$\nabla \cdot \mathbf{B} = 0$$

$$\nabla \cdot \mathbf{D} = \rho$$

E is the electric field, **H** and **B** the magnetic field, **D** the electric dispacement field, **J** the current density, ρ the charge density, ε_0 the dielectric constant, μ_0 the magnetic permeability

In vacuum

$$\mathbf{D} = \varepsilon_0 \mathbf{E}$$

$$\mathbf{B} = \mu_0 \mathbf{H}$$

Wave propagation (2)

Wave equation

$$\left(\frac{\partial^2}{\partial t^2} - c^2\nabla^2\right)\mathbf{E}(\mathbf{r},t) = -\frac{1}{\varepsilon_0}\left[\frac{\partial \mathbf{J}(\mathbf{r},t)}{\partial t} + c^2\nabla\rho(\mathbf{r},t)\right]$$

$$c \equiv \frac{1}{\sqrt{\varepsilon_0\mu_0}}$$

c = phase velocity in vacuum

The current density is the product of charge density and velocity

$$\mathbf{J}(\mathbf{r},t) = q\, n(\mathbf{r},t)\, v(\mathbf{r},t)$$

Scattered fields (1)

Fourier-Laplace transform

$$\mathbf{E}(\mathbf{r},t) = \int_{\mathbf{k}}\int_{\omega} \mathbf{E}_{k\omega} e^{-i(\omega t - \mathbf{k}\cdot\mathbf{r})} \frac{d\omega\, d\mathbf{k}}{(2\pi)^4}$$

and its inverse

$$\mathbf{E}_{k\omega} = \int_{\mathbf{r}}\int_{t} \mathbf{E}(\mathbf{r},t) e^{i(\omega t - \mathbf{k}\cdot\mathbf{r})} d\mathbf{r}\, dt$$

Wave equation

$$(\omega^2 - k^2 c^2)\,\mathbf{E}_{k\omega} = \frac{1}{\varepsilon_0}[(-i\omega)\,\mathbf{J}_{k\omega} + ic^2\mathbf{k}\,\rho_{k\omega}]$$

where k = 2π/λ is the wave vector

Scattered fields (2)

We apply the charge conservation

$$\nabla \cdot \mathbf{J} + \frac{\partial \rho}{\partial t} = 0 \qquad\qquad \rho_{k\omega} = \frac{\mathbf{k} \cdot \mathbf{J}_{k\omega}}{\omega}$$

to obtain

$$\mathbf{E}_{k\omega} = -\frac{i\omega}{\varepsilon_0} \frac{\mathbf{J}_{k\omega} - \mathbf{k}_0(\mathbf{k}_0 \cdot \mathbf{J}_{k\omega})}{\omega^2 - k^2 c^2}$$

$\Rightarrow$ **E**(**r**,t) is finally calculated

The electron as a point radiator (1)

Oscillating electron: the current density is the Dirac delta function

$$\int_{-\infty}^{\infty} \delta(x)\, dx = 1 \qquad \int_{-\infty}^{\infty} f(x)\, \delta(x-a)\, dx = f(a)$$

$$\mathbf{J}(\mathbf{r},t) = -e\, \delta(\mathbf{r})\, \mathbf{v}(t)$$

$$\mathbf{J}_{k\omega} = \int_{\mathbf{r}} \int_{t} \text{-}e\, \delta(\mathbf{r})\, \mathbf{v}(t) e^{i(\omega t\text{-}\mathbf{k}\cdot\mathbf{r})} d\mathbf{r}\, dt \qquad \mathbf{J}_{k\omega} = -e\, \mathbf{v}(\omega)$$

The transverse component is $\mathbf{J}_{\mathrm{T}\,k\omega} = -e\, \mathbf{v}_{\mathrm{T}}(\omega)$

The electron as a point radiator (2)

Electric field

$$\mathbf{E}(\mathbf{r},t) = \frac{ie}{\varepsilon_0} \int_{\mathbf{k}} \int_{\omega} \frac{\omega\, \mathbf{v}_{\mathrm{T}}(\omega)\, e^{-i(\omega t - \mathbf{k}\cdot\mathbf{r})}}{\omega^2 - k^2 c^2} \frac{d\omega\, d\mathbf{k}}{(2\pi)^4}$$

$$\mathbf{E}(\mathbf{r},t) = \frac{e}{4\pi\varepsilon_0 c^2 r} \int_{-\infty}^{\infty} (-i\omega)\, \mathbf{v}_{\mathrm{T}}(\omega)\, e^{-i\omega(t - r/c)} \frac{d\omega}{2\pi}$$

in spherical coordinates

$$\mathbf{E}(\mathbf{r},t) = \frac{e}{4\pi\varepsilon_0 c^2 r} \frac{d\mathbf{v}_{\mathrm{T}}(t - r/c)}{dt}$$

$$\mathbf{E}(\mathbf{r},t) = \frac{e\, \mathbf{a}_{\mathrm{T}}(t - r/c)}{4\pi\varepsilon_0 c^2 r}$$

The radiated electric field is due to the component of electron acceleration transverse to the propagation direction, observed at a retarded time due to the wave propagation at speed *c* on a distance *r*

Radiated power (1)

Radiated power (W/m^2) is described by the **Poynting vector**

$$\mathbf{S} = \mathbf{E}(\mathbf{r},t) \times \mathbf{H}(\mathbf{r},t)$$

$$\nabla \cdot \underbrace{(\mathbf{E} \times \mathbf{H})}_{\mathbf{S}} = -\frac{\partial}{\partial t}\left(\frac{\mu_0 H^2}{2}\right) - \frac{\partial}{\partial t}\left(\frac{\varepsilon_0 E^2}{2}\right) - \mathbf{E} \cdot \mathbf{J}$$

The time derivatives indicate the rate of change of energy density stored in the magnetic and electric fields. The rightmost term is the rate of energy dissipation per unit volume associated to the current density

$$\iint_{\text{surface}} \underbrace{(\mathbf{E} \times \mathbf{H})}_{\mathbf{S}} \cdot \mathrm{d}\mathbf{A} = -\frac{\partial}{\partial t} \iiint_{\text{vol}} \underbrace{\left(\frac{\mu_0 H^2}{2} + \frac{\varepsilon_0 E^2}{2}\right)}_{\text{energy density}} dV - \iiint_{\text{vol}} \underbrace{(\mathbf{E} \cdot \mathbf{J})}_{\text{energy dissipation}} \, dV$$

Radiated power (2)

For plane waves in free space

$$\mathbf{H}(\mathbf{r},t) = \sqrt{\frac{\varepsilon_0}{\mu_0}}\mathbf{k}_0 \times \mathbf{E}(\mathbf{r},t)$$

$$\mathbf{S}(\mathbf{r},t) = \sqrt{\frac{\varepsilon_0}{\mu_0}} \, |\mathbf{E}|^2 \, \mathbf{k}_0$$

The power per unit area radiated by an oscilalting electron is

$$\mathbf{S}(\mathbf{r},t) = \frac{e^2 \, |\mathbf{a}|^2 \, \sin^2 \Theta}{16\pi^2 \varepsilon_0 c^3 r^2} \mathbf{k}_0$$

The $\sin^2\theta$ is the **dipole radiation factor**. Power scales as $1/r^2$.

Oscillating dipole

Radiated power per unit solid angle

$$\frac{dP}{d\Omega} = \frac{e^2 |\mathbf{a}|^2 \sin^2 \Theta}{16\pi^2 \varepsilon_0 c^3}$$

Total radiated power

$$P = \frac{8\pi}{3} \frac{e^2 |\mathbf{a}|^2}{16\pi^2 \varepsilon_0 c^3}$$

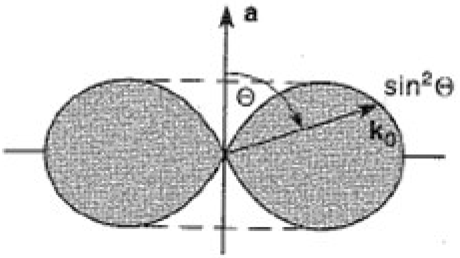

The $\sin^2 \Theta$ radiation pattern of a small accelerated charge

Scattering by a free electron (1)

The incident e.m. field causes oscillations of the free electron [acceleration **a**(**r**,t)], which radiates power $\Rightarrow$ *scattering*

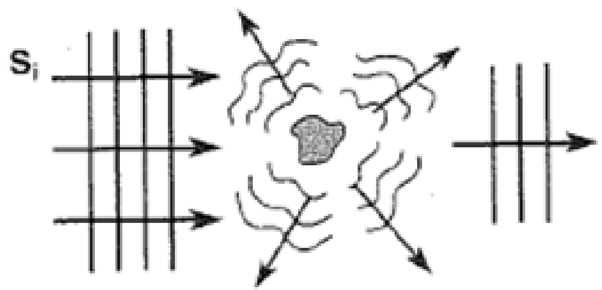

Scattering of incident radiation into many directions, leaving a less intense wave in the forward direction.

Scattering cross-section: ratio between the average power radiated and the average incident power per unit area

$$\sigma \equiv \frac{\overline{P}_{scatt}}{|\overline{\mathbf{S}}_i|}$$

Scattering by a free electron (2)

Oscillating electron ⇒ Newton's law **F** = m**a** (**F** is the Lorentz force)

$$m\mathbf{a} = -e\,[\mathbf{E}_i + \mathbf{v}\times\mathbf{B}_i]$$

The term linked to the magnetic field is neglected in non-relativistic conditions [it scales as (v/c)$\mathbf{E_i}$]. The acceleration is

$$\mathbf{a}(\mathbf{r},t) = -\frac{e}{m}\mathbf{E}_i(\mathbf{r},t)$$

The scattered electric field depends only on the transverse component

$$\mathbf{E}(\mathbf{r},t) = -\frac{r_e\,E_i\sin\Theta}{r}\,e^{-i\omega(t-r/c)}$$

$$r_e = \frac{e^2}{4\pi\varepsilon_0\,mc^2} = 2.82\cdot 10^{-13}\ \mathrm{cm}$$

Scattering by a free electron (3)

Average scattered power

$$\overline{P}_{\text{scatt}} = \frac{1}{2}\frac{8\pi}{3}\frac{e^2\left(e^2/m^2\,|\mathbf{E}_i|^2\right)}{16\pi^2\varepsilon_0 c^3}$$

Cross section σ for the single electron (**Thomson cross-section**)

$$\sigma = \frac{\overline{P}_{\text{scatt}}}{|\overline{\mathbf{S}}|} = \frac{\dfrac{4\pi}{3}\left(\dfrac{e^4\,|\mathbf{E}_i|^2}{16\pi^2\varepsilon_0 m^2 c^3}\right)}{\dfrac{1}{2}\sqrt{\dfrac{\varepsilon_0}{\mu_0}}\,|\mathbf{E}_i|^2} \quad\Rightarrow\quad \sigma_e = \frac{8\pi}{3}\mathrm{r}_\mathrm{e}^2 = 6.65\cdot 10^{-25}\,\mathrm{cm}^2$$

Cross-section independent from the wavelength

Differential cross-section $$\frac{d\sigma_e}{d\Omega} = r_e^2\sin^2\Theta$$

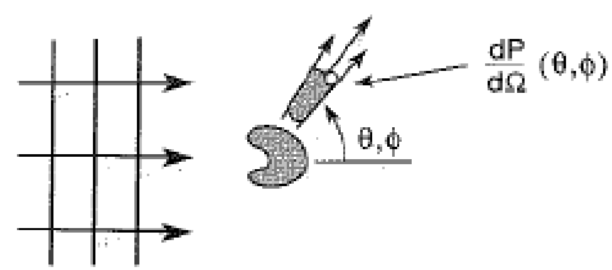

Angle-dependent scattering

Scattering by bound electrons (1)

Semi-classical model (massive positively charged nucleous + Z*e*, surrounded by Z electrons orbiting at discrete binding energies).

Answer of electrons at frequency ω depends on $\omega - \omega_s$, where ω_s is the resonance frequency. A dissipative term is introduced to take into account collisions.

$\Rightarrow$ **Dumpened harmonic oscillator**

$$m\frac{d^2\mathbf{x}}{dt^2} + m\gamma\frac{d\mathbf{x}}{dt} + m\omega_s^2\mathbf{x} = -e\mathbf{E}_i$$

For a monochromatic field $\mathbf{E} = \mathbf{E}_i\, e^{-i\omega t}$

$$m(-i\omega)^2\mathbf{x} + m\gamma(-i\omega)\mathbf{x} + m\omega_s^2\mathbf{x} = -e\mathbf{E}_i$$

$$\mathbf{x} = \frac{1}{\omega^2 - \omega_s^2 + i\gamma\omega}\frac{e\mathbf{E}_i}{m} \qquad \mathbf{a} = \frac{-\omega^2}{\omega^2 - \omega_s^2 + i\gamma\omega}\frac{e\mathbf{E}_i}{m}$$

Scattering by bound electrons (2)

Scattering cross-section for a bound electron

$$\sigma = \frac{8\pi}{3} r_e^2 \frac{\omega^4}{(\omega^2 - \omega_s^2)^2 + (\gamma\omega)^2}$$

Near resonance, the shape is a Lorentzian with width $\gamma/2$.

Far from resonance, $\omega >> \omega_s$, the cross-section approaches Thomson's result, since the oscilaltions forced by the incident radiation are too rapid to be affected by the natural response of the resonant system.

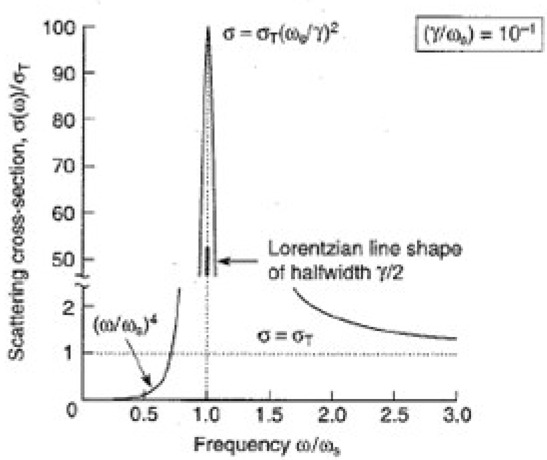

The semi-classical scattering cross-section for a bound electron of resonant energy $\hbar\omega_s$ and an assumed damping factor $\gamma/\omega_s = 0.1$.

Application: the color of the sky

For $\omega << \omega_s$, the cross-section has a form described by Reileigh, with a strong dependence on the wavelength λ^{-4}.

$$\sigma_R = \frac{8\pi}{3} r_e^2 \left(\frac{\omega}{\omega_s}\right)^4 = \frac{8\pi}{3} r_e^2 \left(\frac{\lambda_s}{\lambda}\right)^4$$

We can explain the color of the sky. In air, the resonances of O_2 e N_2 are respectively at 145 nm and 152 nm. Reileigh formula gives a cross-section for the blue (400 nm) 16 times higher than the red (800 nm). This explains the blue appearance of the sky when looking overhead, and the red appearance of the setting sun when observed in direct view.

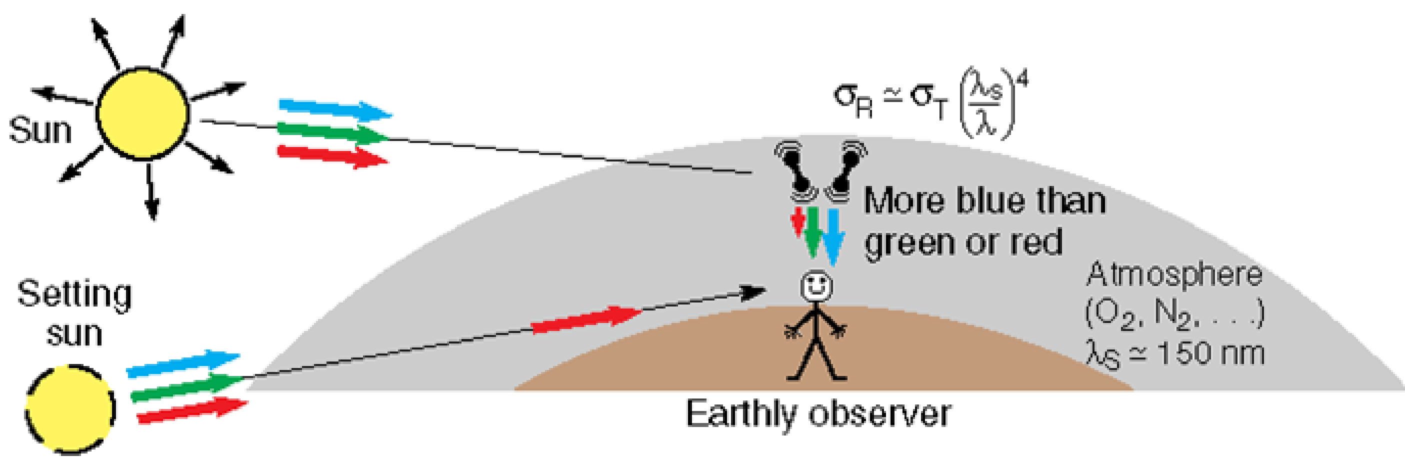

Scattering by multi-electrons atoms (1)

The size of the atom is not negligible with respect to the wavelength (this is true for XUV and X-rays). Each electrons has separate coordinates

$$n(\mathbf{r},t)=\sum_{s=1}^{Z}\delta[\mathbf{r}-\Delta\mathbf{r}_S(t)] \qquad \mathbf{J}(\mathbf{r},t)=-e\sum_{s=1}^{Z}\delta[\mathbf{r}-\Delta\mathbf{r}_S(t)]\,\mathbf{v}_S(t)$$

The displacement is dominated by the incident e.m. field, ignoring the effect of waves scattered by neighboring electrons.

$$\mathbf{J}_{k\omega}=\int_{\mathbf{r}}\int_{t}\mathbf{J}(\mathbf{r},t)\,e^{i(\omega t-\mathbf{k}\cdot\mathbf{r})}d\mathbf{r}\,dt \qquad \mathbf{J}_{k\omega}=-\sum_{s=1}^{Z}e^{-i\mathbf{k}\cdot\Delta\mathbf{r}_s}\mathbf{v}_s(\omega)$$

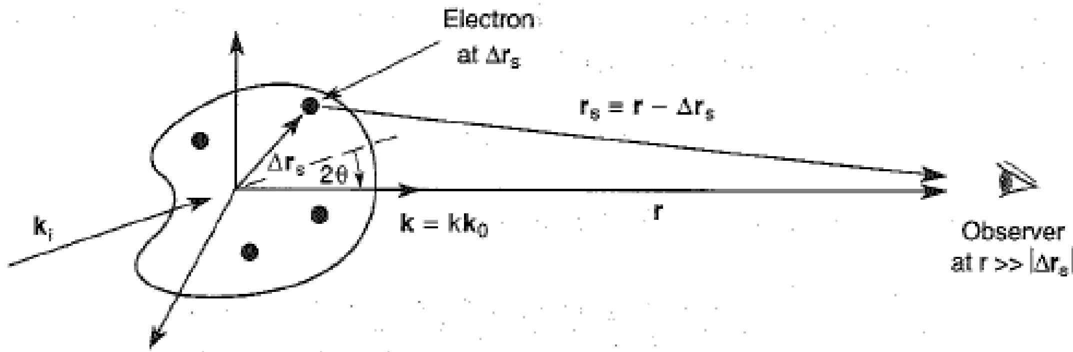

Scattering by multi-electrons atoms (2)

As from the single radiating electron $\mathbf{E}(\mathbf{r},t) = \frac{e}{4\pi\varepsilon_0 c^2} \sum_{s=1}^{Z} \frac{\mathbf{a}_{T,s}(t - r_s / c)}{r_s}$

Equation of motion $m\frac{d^2\mathbf{x}_S}{dt^2} + m\gamma\frac{d\mathbf{x}_S}{dt} + m\omega_s^2\mathbf{x}_S = -e\mathbf{E}_i$

Differing phase seen by each electron $\mathbf{E}_i(\mathbf{r},t) \rightarrow \mathbf{E}_i\, e^{-i(\omega t - \mathbf{k}_i \cdot \Delta\mathbf{r}_S)}$

$$\mathbf{x}_S(t) = \frac{1}{\omega^2 - \omega_s^2 + i\gamma\omega}\frac{e}{m}\mathbf{E}_i\, e^{-i(\omega t - \mathbf{k}_i \cdot \Delta\mathbf{r}_S)} \qquad \mathbf{a}_S(t) = \frac{-\omega^2}{\omega^2 - \omega_s^2 + i\gamma\omega}\frac{e}{m}\mathbf{E}_i\, e^{-i(\omega t - \mathbf{k}_i \cdot \Delta\mathbf{r}_S)}$$

$$\mathbf{E}(\mathbf{r},t) = -\frac{r_e}{r}\underbrace{\left[\sum_{s=1}^{Z}\frac{\omega^2\, e^{-i\Delta\mathbf{k}\cdot\Delta\mathbf{r}_S}}{\omega^2 - \omega_s^2 + i\gamma\omega}\right]}_{f(\Delta\mathbf{k},\omega)} E_i \sin\Theta\, e^{-i\omega(t - r/c)}$$

$\mathbf{r}_S \equiv \mathbf{r} - \Delta\mathbf{r}_S$

$r_S \cong r - \mathbf{k}_0 \cdot \Delta\mathbf{r}_S \quad \text{for } r >> \Delta r_S$

$f(\Delta\mathbf{k},\omega)$ ***complex atomic scattering factor***

The complex atomic scattering factor (1)

It depends on the incident wave frequency ω, the resonance frequencies ω_s of the bound electrons and the phase terms due to the position of the bound electrons within the atom

$$f(\Delta\mathbf{k},\omega)=\sum_{s=1}^{Z}\frac{\omega^2\, e^{-i\Delta\mathbf{k}\cdot\Delta\mathbf{r}_S}}{\omega^2-\omega_s^2+i\gamma\omega}$$

It describes the relation between the scattering from a single electron and from a multi-electron system. For the single electron $\Rightarrow$ $f(\Delta\mathbf{k},\omega)=1$

Differential and total cross-section $\quad \dfrac{d\sigma(\omega)}{d\,\Omega}=r_e^2\,|\,f(\omega)\,|^2\,\sin^2\Theta \qquad \sigma(\omega)=\dfrac{8\pi}{3}r_e^2\,|\,f(\omega)\,|^2$

The complex atomic scattering factor (2)

The charge distribution within the atom is largely constrained within dimensions the Bohr radius (a_0 = 0.5 Å for the ground state of the hydrogen atom)

$$\Delta k = \frac{4\pi}{\lambda}\sin\theta \qquad\qquad |\Delta\mathbf{k}\cdot\Delta\mathbf{r}_S| \leq \frac{4\pi\, a_0}{\lambda}\sin\theta$$

Two special cases

$$|\Delta\mathbf{k}\cdot\Delta\mathbf{r}_S| \to 0 \ \text{ for } a_0/\lambda << 1 \qquad \text{(long wavelength limit)}$$

$$|\Delta\mathbf{k}\cdot\Delta\mathbf{r}_S| \to 0 \ \text{ for } \theta \approx 0 \qquad \text{(forward scattering)}$$

$$f^0(\omega) = \sum_{s=1}^{Z} \frac{\omega^2}{\omega^2 - \omega_s^2 + i\gamma\omega}$$

Oscillator strengths g_s: indicate the number of electrons associated with a given resonance frequency ω_s (e.g. 2 for K shell, 6 for L, 10 for M). Also fractional values are given to take into account transition probabilities.

$$\sum g_S = Z$$

The complex atomic scattering factor (3)

For long wavelengths ($\lambda >> a_0$) and/or small angles ($\theta << \lambda/a_0$)

$$f^0(\omega) = \sum_{s=1}^{Z} \frac{g_s \omega^2}{\omega^2 - \omega_s^2 + i\gamma\omega}$$

$$\frac{d\sigma(\omega)}{d\,\Omega} = r_e^2 \,|\, f^o(\omega)\,|^2 \sin^2\Theta \qquad\qquad \sigma(\omega) = \frac{8\pi}{3} r_e^2 \,|\, f^0(\omega)\,|^2$$

For low-Z atoms and relatively long wavelengths $\omega^2 >> \omega_s^2$ and $\lambda/a_0 >> 1$

$$f(\Delta\mathbf{k},\omega) \rightarrow f^0(\omega) \rightarrow \sum g_S = Z$$

$$\frac{d\sigma(\omega)}{d\,\Omega} \cong Z^2\, r_e^2 \sin^2\Theta \qquad\qquad \sigma(\omega) \cong \frac{8\pi}{3} r_e^2\, Z^2 = Z^2\, \sigma_e$$

The complex atomic scattering factor (4)

Exmple: C atom (Z = 6), 0.4 nm wavelength. The scattering is 36 times higher than a single electron. The 6 electrons are scattering coherently in all directions.

1) λ= 0.4 nm >> a_0 = 0.05 nm
2) E_{ph}=3 keV >> binding energy of the most tightly held electrons 284 eV

The scattering factor is tabulated $f^0(\omega) = f_1^0(\omega) - i\, f_2^0(\omega)$

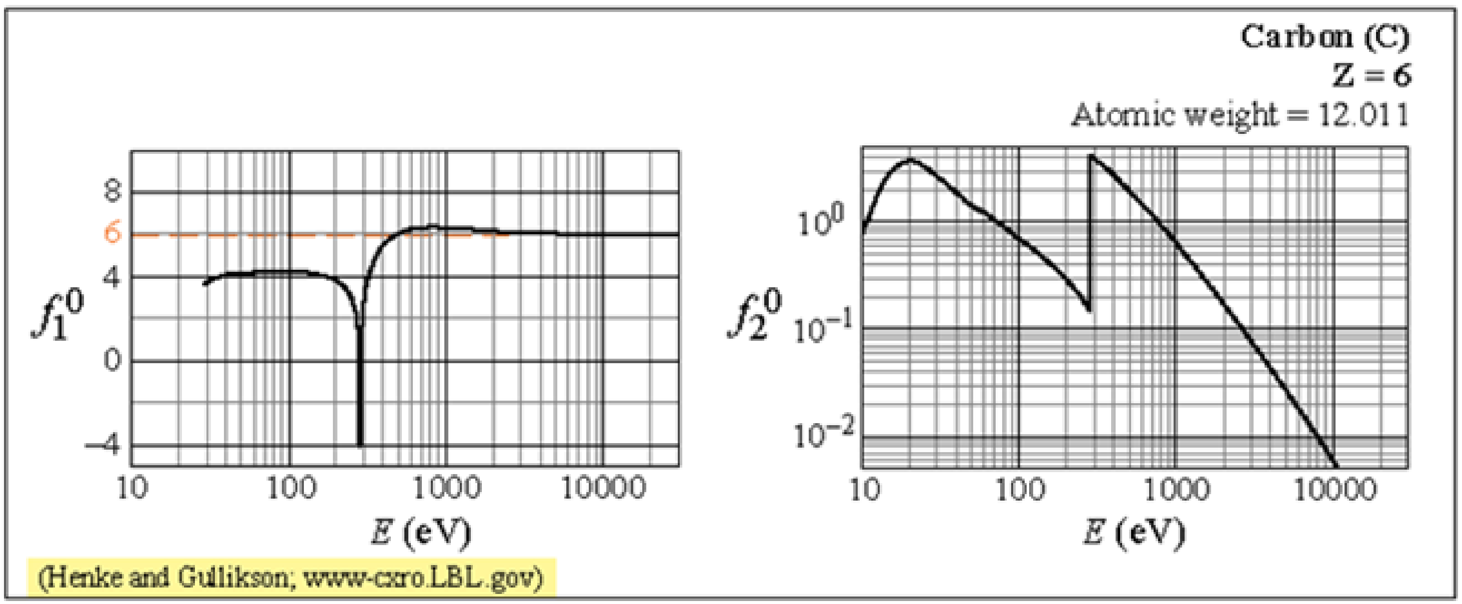

WAVE PROPAGATION AND REFRACTION INDEX IN THE XUV

Wave propagation in the XUV

The photon energy is comparable with the binding energy of electrons

Vector wave equation for transverse waves (**E** perpendicular to **k**)

$$\left(\frac{\partial^2}{\partial t^2} - c^2\nabla^2\right)\mathbf{E}_T(\mathbf{r},t) = -\frac{1}{\varepsilon_0}\frac{\partial \mathbf{J}_T(\mathbf{r},t)}{\partial t} \qquad \mathrm{c} \equiv \frac{1}{\sqrt{\varepsilon_0 \mu_0}}$$

Propagation in the **forward direction**

It is the sum of forward-scattered radiation from all atoms that interferes with the incident wave to produce a modified propagation wave, compared to that in vacuum.

As the scattering process involves both inelastic (lossless) and elastic (dissipative) processes, the refractive index is a complex quantity: it describes a modified phase velocity and a wave amplitude that decays as it propagates

Wave propagation

The interaction between the incident wave and the scattered waves modifies the propagation characteristics $\Rightarrow$ refraction index

The current density is

$$\mathbf{J}_0(\mathbf{r},t) = -e\, n_a \sum_S g_s \mathbf{v}_s(\mathbf{r},t) \qquad \mathbf{J}_0(\mathbf{r},t) = -\frac{e^2\, n_a}{m} \sum_S \frac{g_s}{\omega^2 - \omega_s^2 + i\gamma\omega} \frac{\partial \mathbf{E}(\mathbf{r},t)}{\partial t}$$

where in the semi-classical model of the atom ω_s is the electron's natural frequency of oscillation, γ is a dissipative factor, g_s is the oscillator strength and n_a is the average density of atoms

The wave equation becomes $\left(\frac{\partial^2}{\partial t^2} - \frac{c^2}{n^2(\omega)} \nabla^2 \right) \mathbf{E}_T(\mathbf{r},t) = 0$

With the **complex refraction index** defined as

$$n(\omega) \equiv 1 - \frac{1}{2} \frac{e^2\, n_a}{\varepsilon_0 m} \sum_S \frac{g_s}{\omega^2 - \omega_s^2 + i\gamma\omega}$$

Refraction index

$n(\omega)$ is dispersive since it varies with ω, i.e., waves at different wavelengths propagate with different phase speed

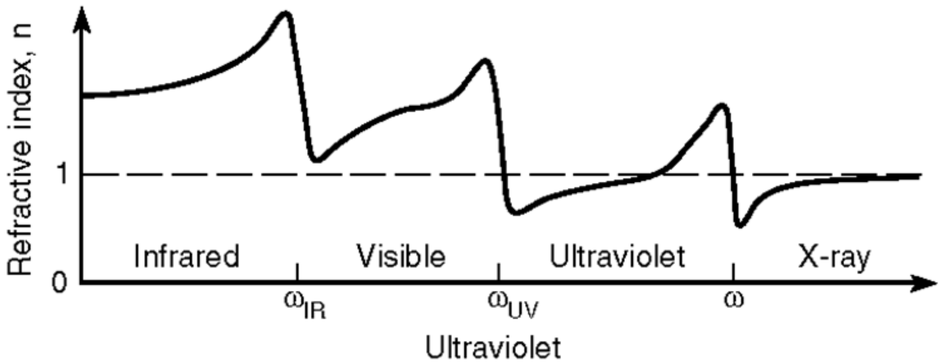

$n(\omega)$ depends on the complex atomic scattering factor

$$n(\omega) \equiv 1 - \frac{n_a\, r_e\, \lambda^2}{2\pi}[f_1^0(\omega) - i\, f_2^0(\omega)] = 1 - \delta + i\beta$$

In the XUV the refraction index is close to the unity

$$\delta = \frac{n_a\, r_e\, \lambda^2}{2\pi} f_1^0(\omega) \qquad \delta << 1$$

$$\beta = \frac{n_a\, r_e\, \lambda^2}{2\pi} f_2^0(\omega) \qquad \beta << 1$$

Phase variation and absorption

Plane wave $\mathbf{E}(\mathbf{r},t) = \mathbf{E}_0 e^{-i(\omega t - \mathbf{k}\cdot\mathbf{r})}$

$$\frac{\omega}{k} = \frac{c}{n} = \frac{c}{1-\delta+i\beta}$$

$$\mathbf{E}(\mathbf{r},t) = \underbrace{\mathbf{E}_0\, e^{-i(t-r/c)}}_{\text{propagation in vacuum}}\ \underbrace{e^{-i(2\pi\delta/\lambda)r}}_{\text{phase variation}}\ \underbrace{e^{-(2\pi\beta/\lambda)r}}_{\text{attenuation}}$$

The wave intensity is calculated from the Poynting vector

$$\bar{I} = \frac{1}{2}\mathrm{Re}(n)\sqrt{\frac{\varepsilon_0}{\mu_0}}\,|\mathbf{E}_0|^2\, e^{-2(2\pi\beta/\lambda)r} = \bar{I}_0 e^{-(4\pi\beta/\lambda)r}$$

The wave decays with an exponential decay length

$$\ell_{abs} = \frac{\lambda}{4\pi\beta} = \frac{1}{2n_a r_e \lambda f_2^0(\omega)} = \frac{1}{\rho\mu}$$

The scattering coefficient is related to the macroscopic absorption coefficient μ

XUV absorption

The absorption of any material in the XUV is very high.

Only thin foils (thickness of fraction of micrometers) can be used as filters, but no substrates

$\Rightarrow$ **lenses cannot be used in the XUV**

$\Rightarrow$ **mirrors have to be adopted as the main optical components**

Thin foils as filters for the XUV

Thin metallic foils as filters for the XUV

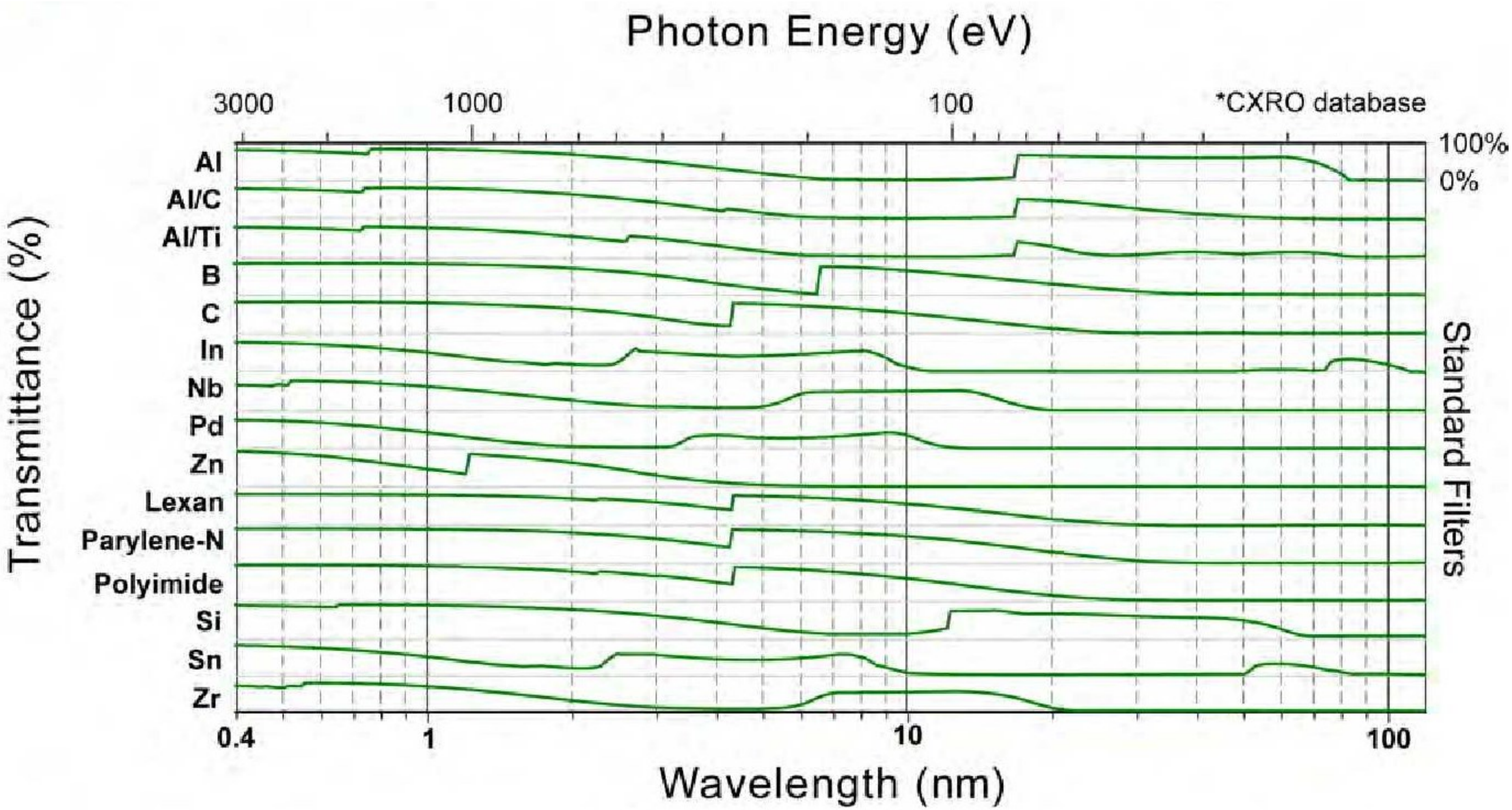

Reflection and refraction at the interfaces

At an interface, reflected and refracted waves obey the Snell's law

$$\phi = \phi'' \quad , \quad \sin\phi' = \frac{\sin\phi}{n}$$

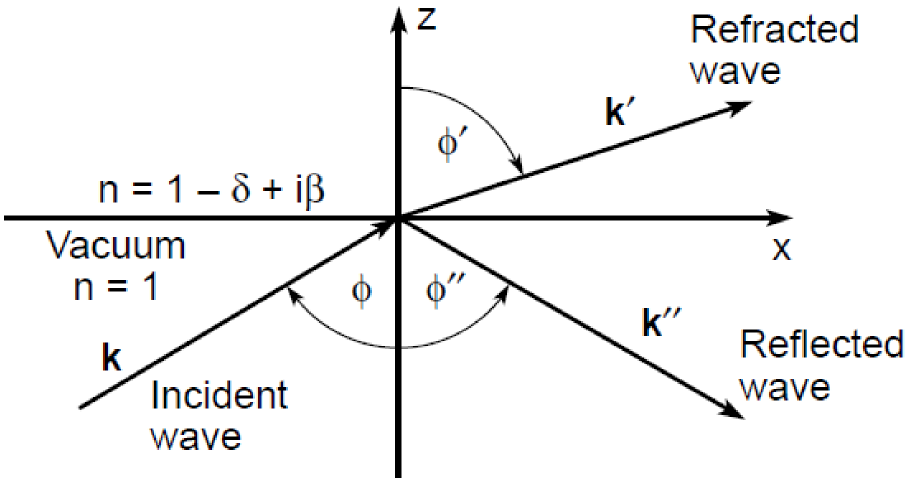

Total external reflection (1)

For n close to the unity $n \cong 1-\delta$ (neglecting absorption)

$$\sin\phi' = \frac{\sin\phi}{1-\delta}$$

Therefore $\phi' \geq \phi$ and if ϕ approaches 90° (**extreme grazing incidence**), ϕ' approaches 90° faster.

The **critical angle of incidence** ϕ_c is defined as the incidence angle that gives $\phi' = 90°$

$$\sin\phi_c = 1-\delta$$

For incidence angles beyond the critical angle, the radiation is completely reflected $\Rightarrow$ **total external reflection**

Glancing incidence ($\theta < \theta_c$) and total external reflection

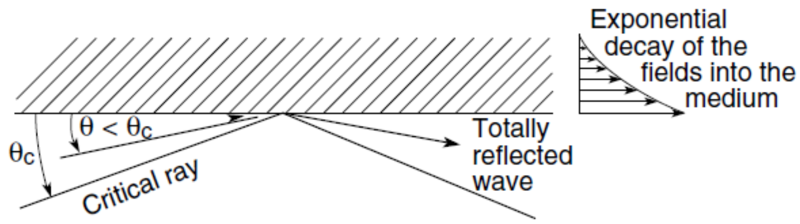

Total external reflection (2)

We define the critical angle as measured from the tangent to the surface (**grazing angle)**: $\theta+\phi = 90°$

The critical angle is $\cos\theta_c = 1-\delta$ $\quad \theta_c = \sqrt{2\delta} == \sqrt{\dfrac{n_a\, r_e\, \lambda^2 f_1^0(\lambda)}{\pi}}$

Since the scattering factor is approximated by Z (atomic number) $\theta_c \propto \lambda\sqrt{Z}$

The obtain a conveniently large critical angle at given wavelength, it is convenient to use higher Z materials

Material	*Critical wavelength (nm)*	*10°*	*5 °*
Glass		6.6	3.3
Aluminum oxide		5.4	2.7
Silver		3.5	1.8
Gold		2.7	1.3
Platinum		2.6	1.3
Iridium		2.5	1.2

Reflection coefficient at the interfaces

S polarization (**E** polarized perpendicularly to the incident plane)

$$\frac{E_0'}{E_0} = \frac{2\cos\phi}{\cos\phi + \sqrt{n^2 - \sin^2\phi}} \qquad \frac{E_0''}{E_0} = \frac{\cos\phi - \sqrt{n^2 - \sin^2\phi}}{\cos\phi + \sqrt{n^2 - \sin^2\phi}} \qquad R_s = \frac{\left|\cos\phi - \sqrt{n^2 - \sin^2\phi}\right|^2}{\left|\cos\phi + \sqrt{n^2 - \sin^2\phi}\right|^2}$$

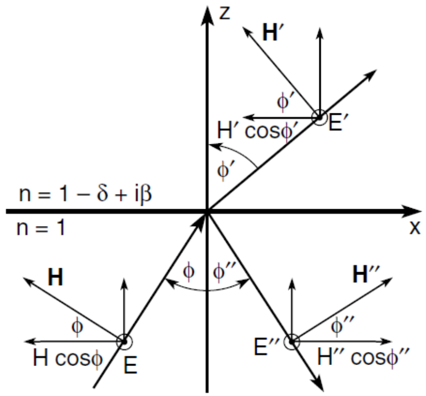

P polarization (**E** polarized parallel to the incident plane)

$$\frac{E_0''}{E_0} = \frac{n^2\cos\phi - \sqrt{n^2 - \sin^2\phi}}{n^2\cos\phi + \sqrt{n^2 - \sin^2\phi}} \qquad \frac{E_0'}{E_0} = \frac{2n\cos\phi}{n^2\cos\phi + \sqrt{n^2 - \sin^2\phi}} \qquad R_p = \frac{\left|n^2\cos\phi - \sqrt{n^2 - \sin^2\phi}\right|^2}{\left|n^2\cos\phi + \sqrt{n^2 - \sin^2\phi}\right|^2}$$

Normal incidence

For ***normal incidence*** (ϕ = 0°)

$$R_{0^\circ} = R_s = R_p = \frac{|1-n|^2}{|1+n|^2}$$

For n = 1 - δ – iβ

$$R_{0^\circ} = \frac{\delta^2 + \beta^2}{(2-\delta)^2 + \beta^2}$$

In the XUV $\delta \ll 1$ and $\beta \ll 1$

Therefore ***the XUV reflectivity in normal incidence of a single interface is very small***

$$R_{s,\perp} \cong \frac{\delta^2 + \beta^2}{4}$$

MIRRORS ARE USED AT GRAZING INCIDENCE

Comparison between normal and grazing incidence in the XUV

Example: reflectivity of a platinum-coated mirror at normal (left) and grazing (right) incidence

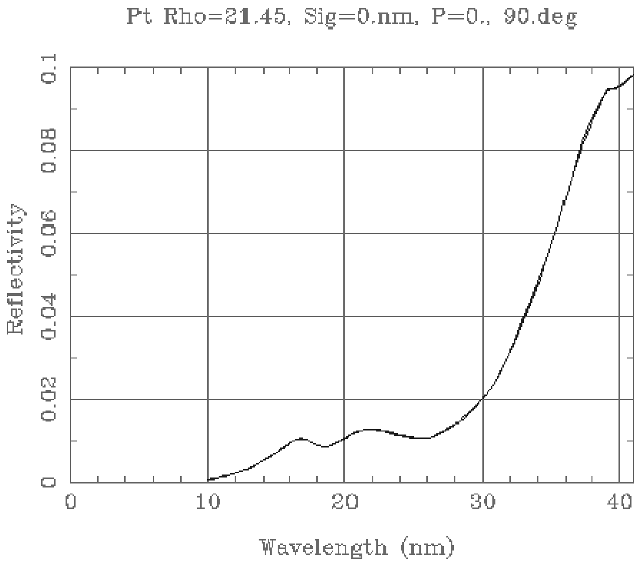

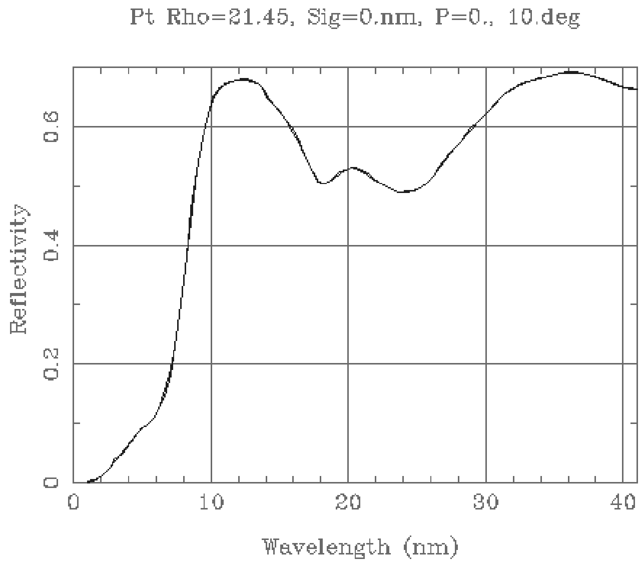

- **Normal incidence reflection is weak for wavelengths below 35 nm**
- **Grazing-incidence operation required for broad-band applications below 35 nm**

Coatings for mirrors at grazing incidence

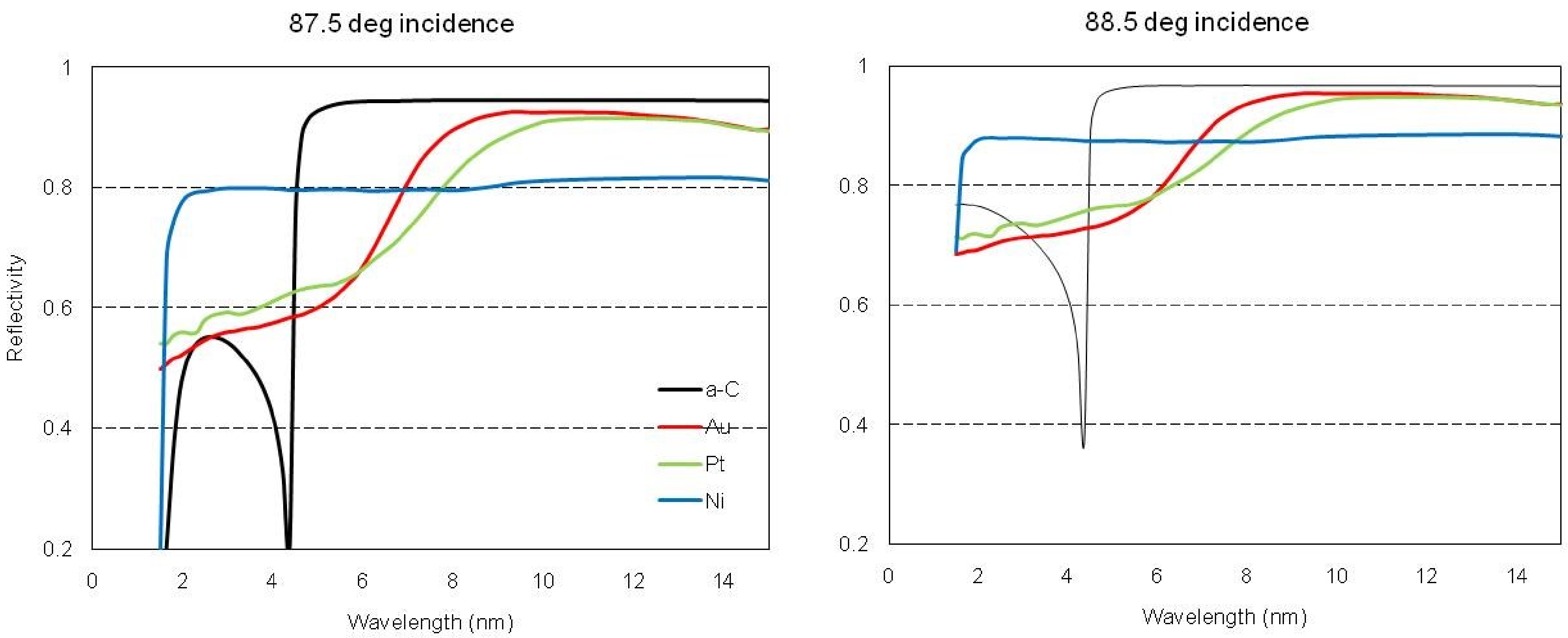

Normal incidence vs. grazing incidence

NORMAL INCIDENCE
Small mirrors
Good correction of aberrations
High angular acceptance

GRAZING INCIDENCE
Long mirrors
Difficult correction of aberrations
Lower angular acceptance

Effect of coatings on ultrafast pulses at grazing incidence

Due to total reflection, grazing incidence mirrors always exhibit a high and almost flat reflectivity and a linear spectral phase (within the bandwidth of the attosecond pulses/high-order harmonics).

Moreover, the variation of the incidence angle of the rays on the mirror surface is by far too small to induce any changes of the coating response in space related to the angle of incidence.

Therefore, the influence of the coating on the reflected pulses can be neglected. Only the losses due to non-unity reflectivity have to be considered.

OPTICAL SYSTEMS FOR THE XUV

Optical systems

- **Optical configurations to form images**
- Optical systems to select one particular wavelength: **monochromators**
- Optical systems to disperse the radiation and measure the spectrum: **spectrometers**

Optical instruments:

- Mirrors
- Multilayer-coated optics
- Gratings
- Diffractive optics

Aim of the optical design

- ***The most important element of any photon beamline is the sample***

- The beamline has to:

  transport the radiation from the source to the sample

  handle the photon beam such as to obtain the proper energy, energy band, focusing, polarization, position, intensity

Broad-band mirrors

Imaging systems and aberrations

Optical aberrations are deformation of the shape of an image given by an optical system. They are due to the departure of the performance of an optical system from the predictions of paraxial optics (i.e., from the formulas for small angles of propagation).

$$\frac{1}{p}+\frac{1}{q}=\frac{1}{f}$$

p = source distance

q = image distance

f = focal length

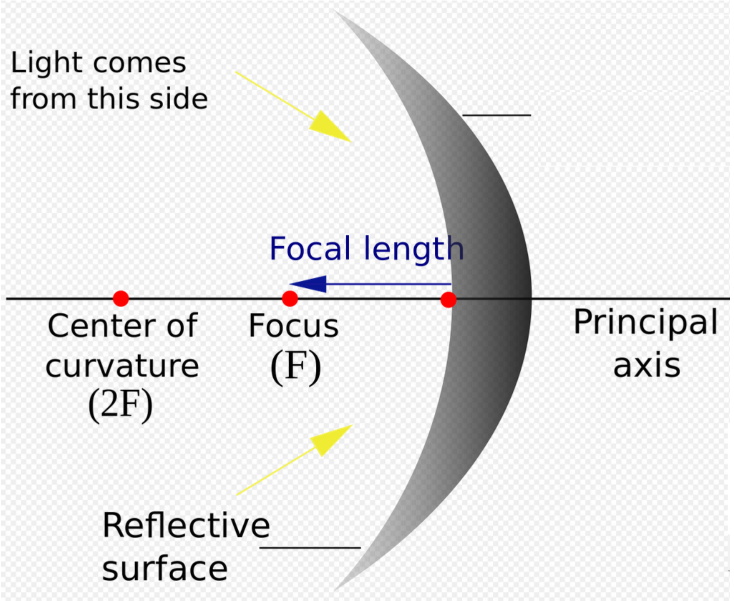

On-axis aberration-free mirrors

OPTICAL SURFACES FOR ON-AXIS ABERRATION-FREE IMAGING

The optical performances are independent from the angular aperture of the rays

1. **Ellipse**
2. **Parabola**
3. **Hyperbola**

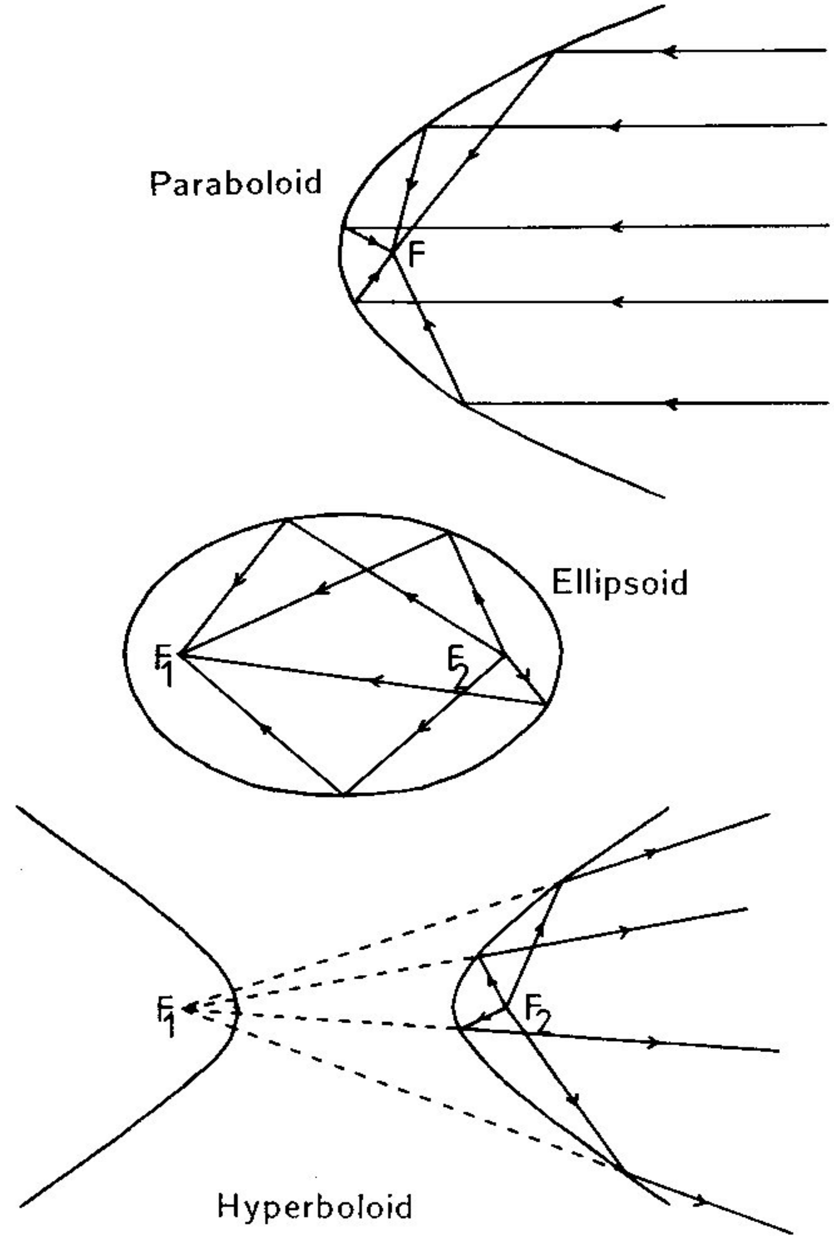

Aberrations: defocus

Out of the nominal focus

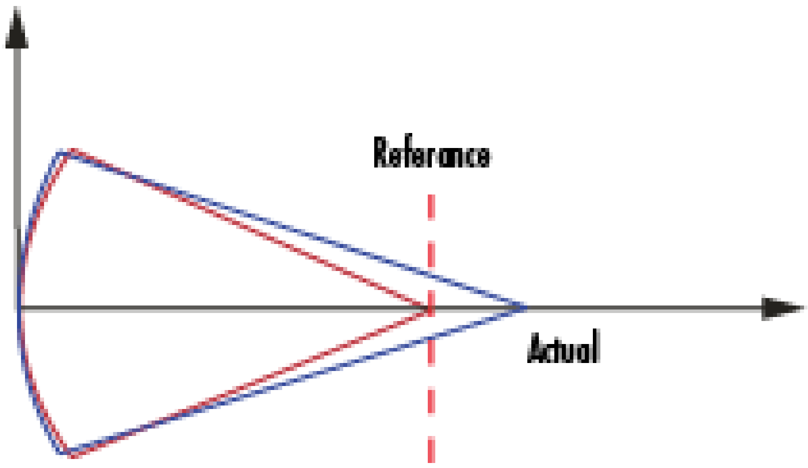

Aberrations: astigmatism

The rays propagating in perpendicualr planes have different foci

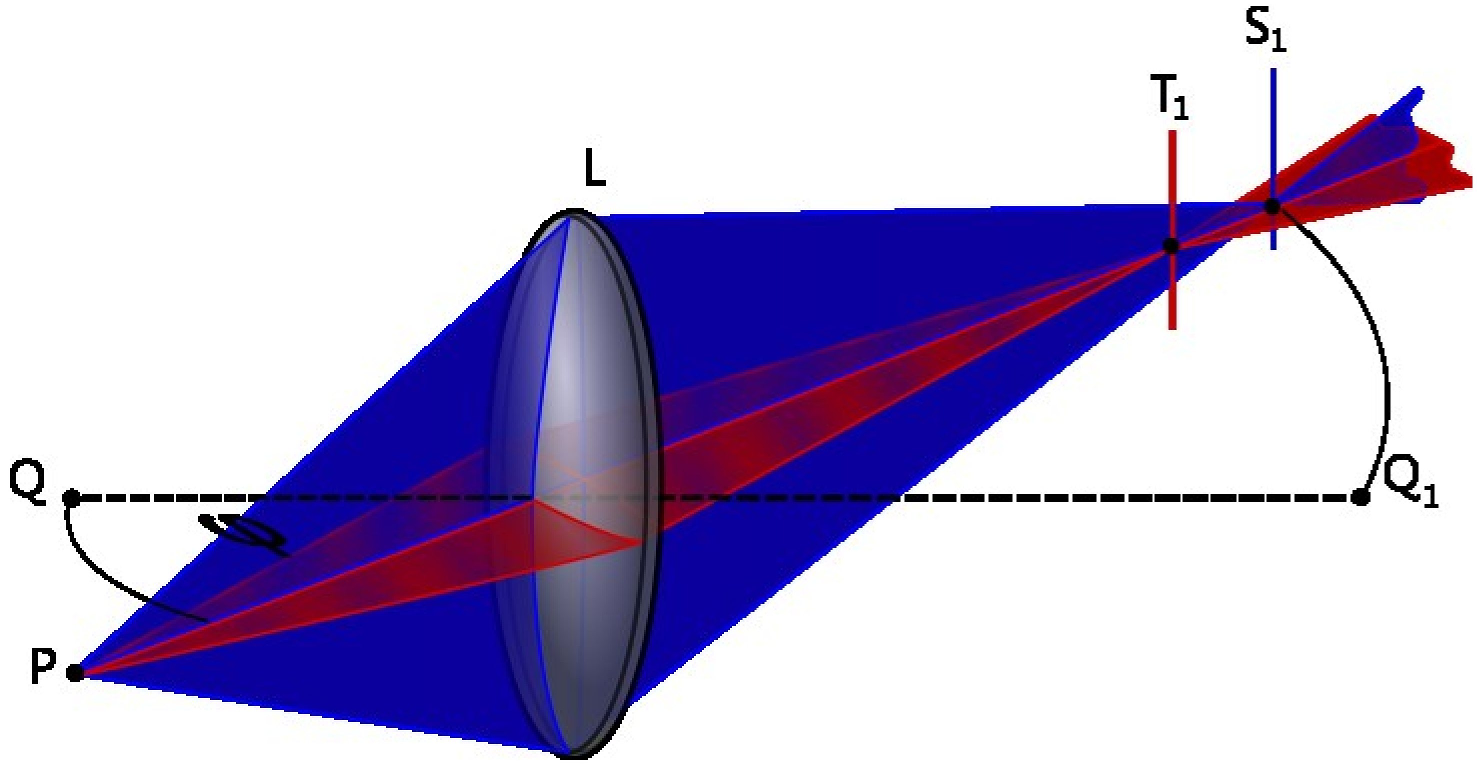

Aberrations: spherical aberration

The position of the focal plan depends on the distance from the optical axis. On a spherical surface, incoming rays from different height from the axis do not bend at the same position and focus at slightly different distance along the axis.

Perfect lens

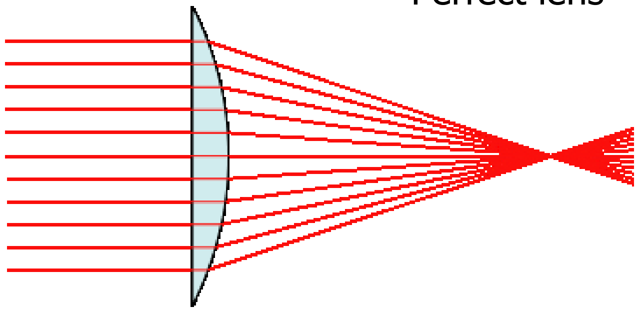

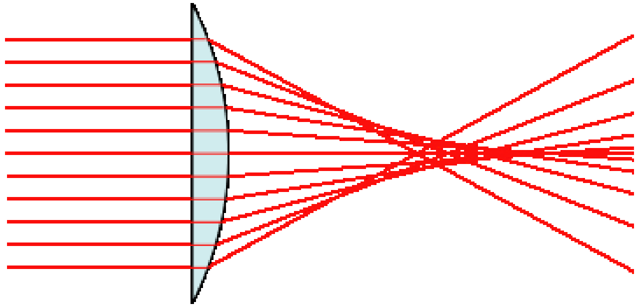

Aberrations: coma

Rays incoming from the periphery of the lens focus closer to the axis and produce a larger blurry spot than the paraxial rays. As coma is proportional to the distance to the central axis, more the rays are away from the center, more the focal point changes of position and get blurry images.

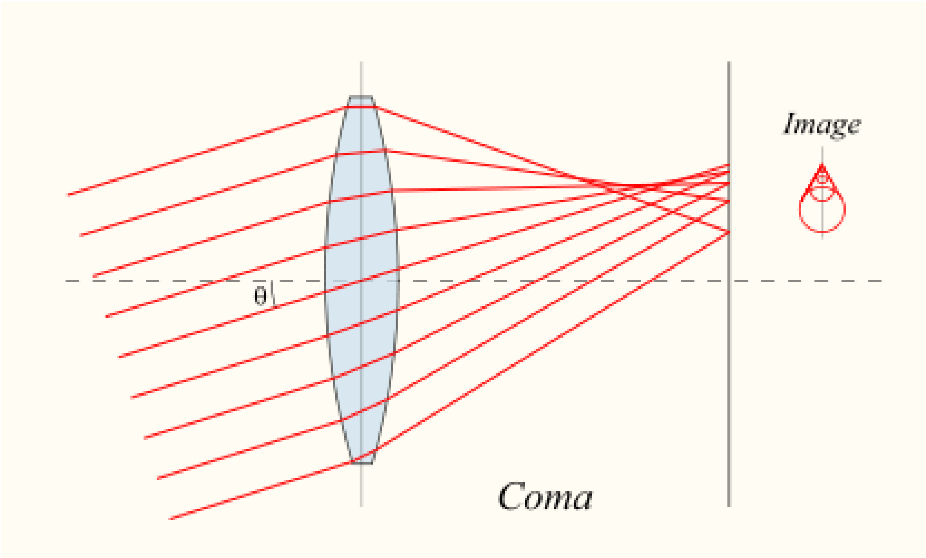

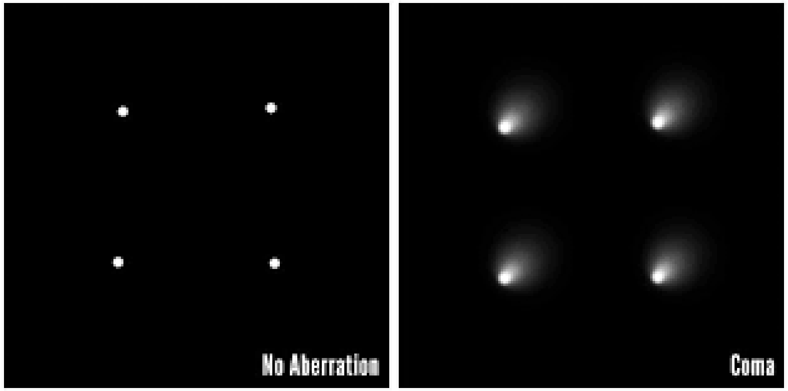

The spherical mirror

Mirror equation

$1/p + 1/q = 2/(R \cos\alpha)$ tangential plane

$1/p + 1/q` = (2 \cos\alpha)/R$ sagittal plane

α : incidence angle

p : source-mirror distance

q : mirror-image distance in the tangential plane

q': mirror-image distance in the sagittal plane

R : radius

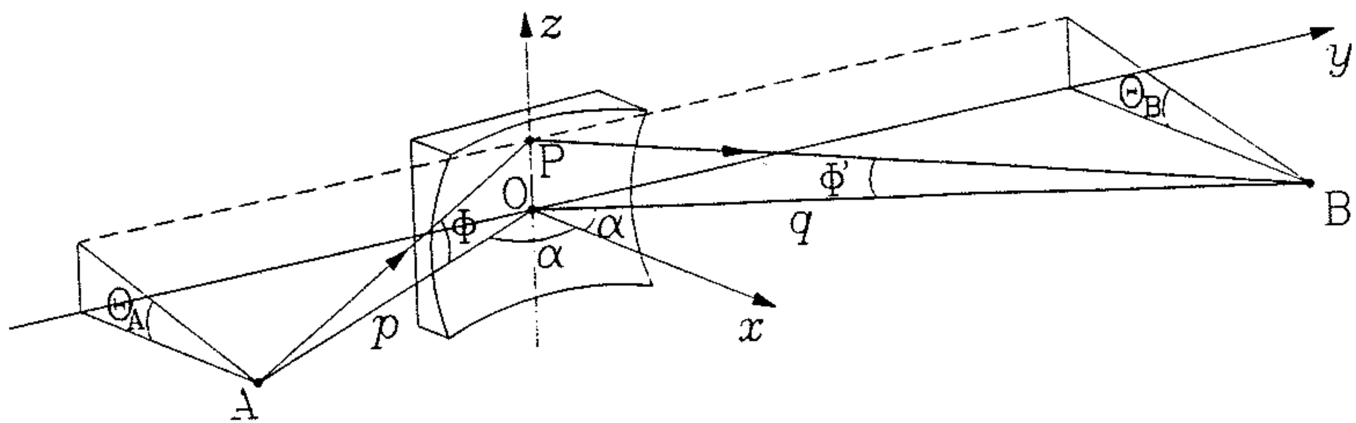

Spherical mirror at normal incidence

q and q' are equal $\Rightarrow$ no astigmatism

At near-normal incidence the astigmatism introduced by a spherical mirror is negligible.

When the angle deviates from the normal, the astigmatism is more evident

$$\Delta q \cong q^2 \frac{2}{R} \frac{\sin^2 \alpha}{\cos \alpha}$$

Spherical mirror at grazing incidence

A spherical mirror at grazing incidence has only tangential focusing capabilities, since q′ becomes negative (virtual image) and almost equal to *p*

Example:

$p = q = 1$ m , $\alpha = 87°$

R $\cong$ 19100 mm

$q' \doteq -1005$ mm, therefore $|q'| \cong p$.

In the sagittal plane, rays propagates as from a plane mirror.

A point is focused on a line.

Kirkpatrick-Baez configuration: 2 spherical mirrors

- Two crossed spherical mirrors both for tangential focusing
- KB system is stigmatic: a source point is focused on a point

$1/p_1 + 1/q_1 = 2/(R_1 \cos\alpha)$

$1/p_2 + 1/q_2 = 2/(R_2 \cos\alpha)$

$p_1 + q_1 = p_2 + q_2$

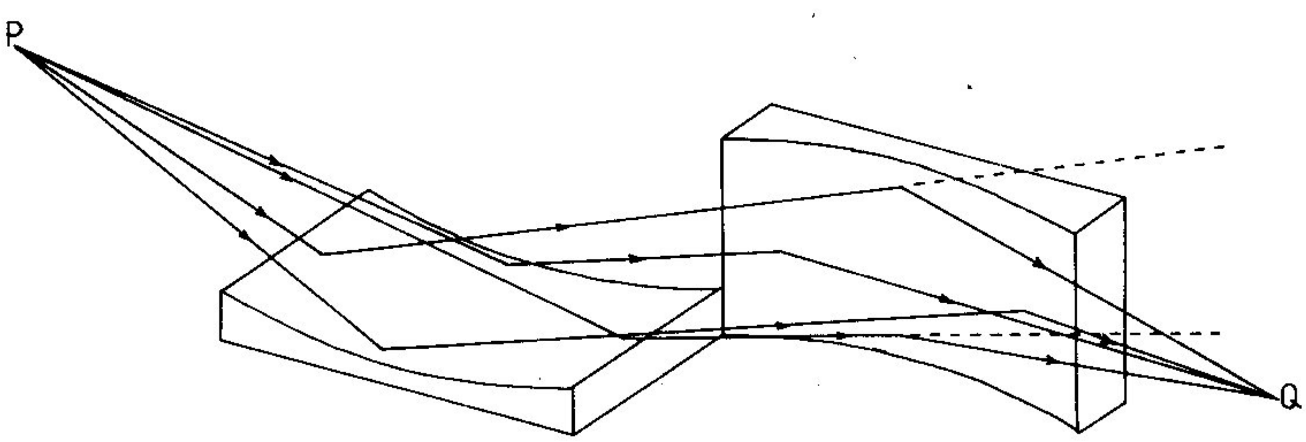

KB for sub-micrometric focusing

KB systems at extreme grazing incidence are used for nanometric focusing on synchrotron and free-electron laser beamlines

- 10 keV FEL pulses have been focused on 1 um X 1 um spot (Yumoto et al, Nat. Photonics, 7, 43, 2013)
- KB systems with variable numerical aperture for variable focusing from ≈100 nm to ≈ 600 nm have been realized (Matsuyama et al, Sci. Rep. 6, 24801, 2016)

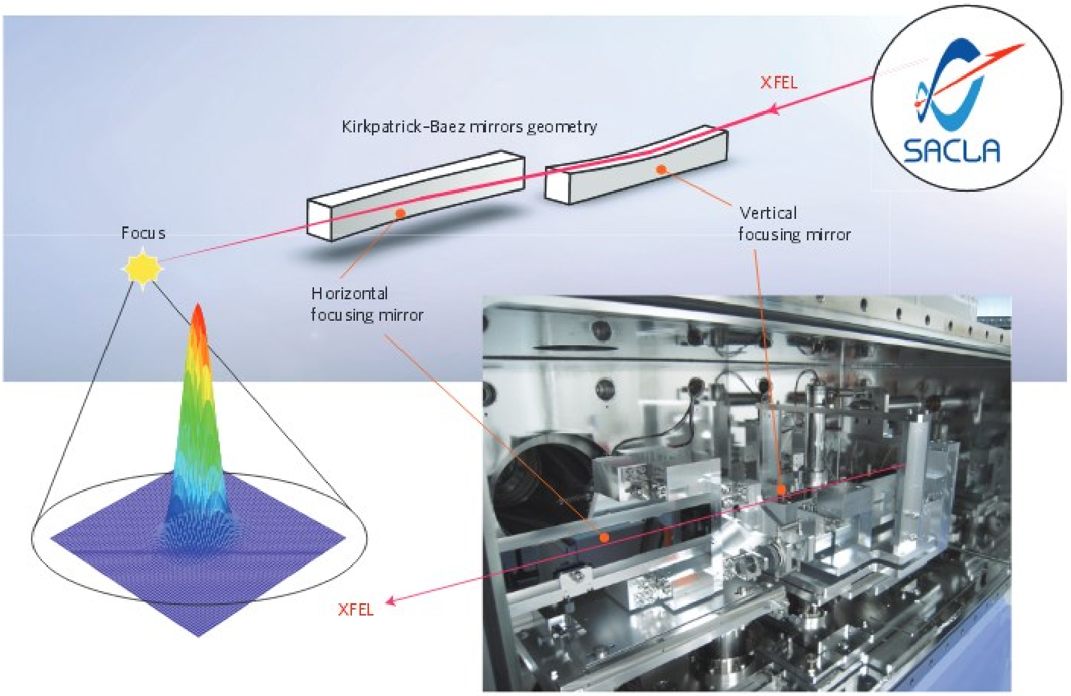

The toroidal mirror

Toroidal: two different radii in the tangential and sagittal directions

Mirror equation

$1/p + 1/q = 2/(R\cos\alpha)$ tangential plane

$1/p + 1/q' = (2\cos\alpha)/\rho$ sagittal plane

α : incidence angle

p : source-mirror distance

q : mirror-image distance in the tangential plane

q' : mirror-image distance in the sagittal plane

R : tangential radius

ρ : sagittal radius

Toroidal mirror for stigmatic focusing

The condition to have stigmaticity ($q = q'$) is

$\rho / R = \cos^2 \alpha \quad (\rho << R)$

A point is imaged on a point

Example:

$p = q = q' = 1$ m , $\alpha = 87°$

R $\cong$ 19100 mm, ρ = 52 mm

Rowland mounting for a toroidal mirror

A toroidal mirror at grazing incidence has minima aberrations (no coma) if used in the ***Rowland mounting***, that is, unity magnification

$\rho / R = \cos^2 \alpha$	astigmatism correction
$p = q = q' = R \cos\alpha$	coma correction

If the mirror is used with magnification different from unity, coma is the dominant aberration.

Focal plane image of a toroidal mirror with demagnification of 10, three angular apertures. Coma aberration is evident.

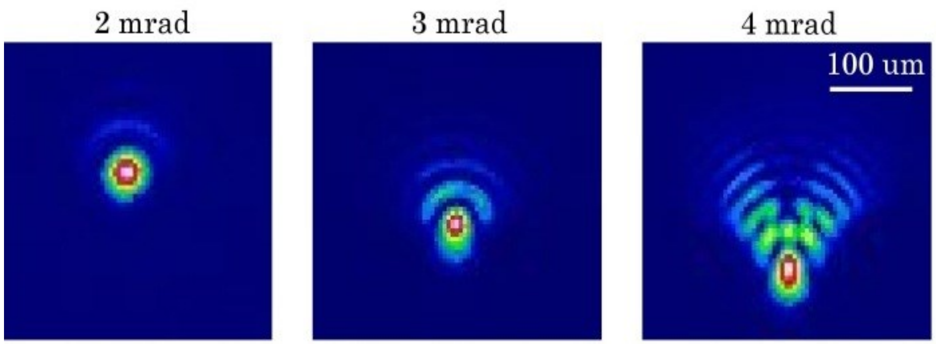

Wolter configurations

- Optical systems used in reflection – they use the properties of the conical surfaces by combining two of them
- They are designed for grazing incidence
- The are normally used to realize telescopes for space applications, since they give reduced aberrations on an extended field-of-view, as required to image multiple stars in the same image

Coma compensation with magnification different from unity

- The **Abbe sine condition** is a condition that must be fulfilled by an optical system to produce sharp images of off-axis as well as on-axis objects
- The sine of the output angle has to be proportional to the sine of the input angle $\sin\alpha'/\sin\alpha$ = cost
- Two reflections are required

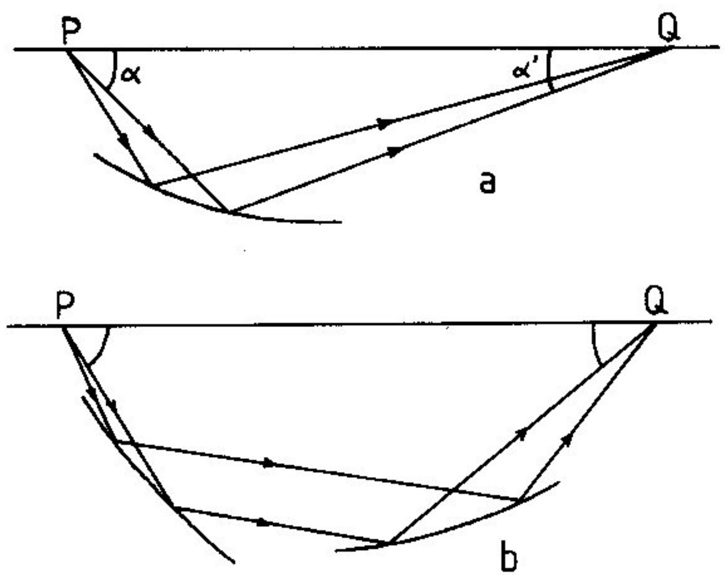

Figure 2.15. Reduction of coma in Kirkpatrick–Baez systems. In (a), the Abbe sine condition is not satisfied and coma is significant. In (b), coma is reduced by ensuring that the Abbe sine condition is satisfied.

Wolter type 1

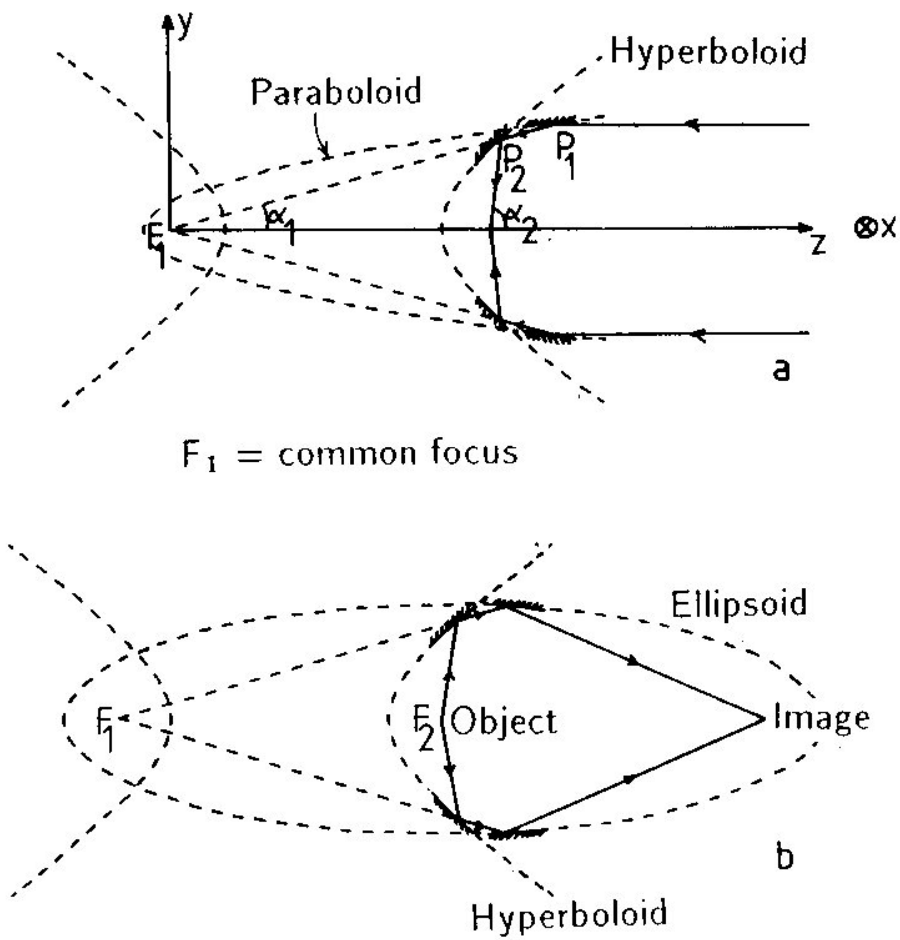

Figure 2.17. Wolter type I optics: (a) telescope; (b) microscope.

Wolter type 2

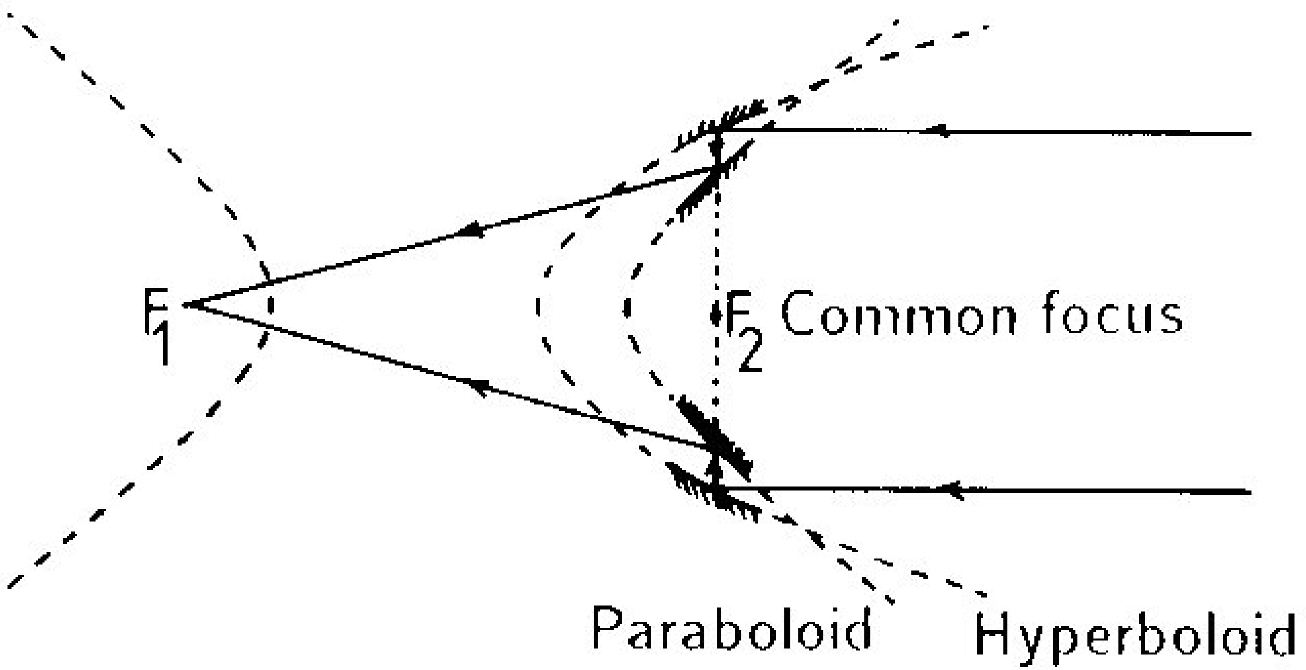

Figure 2.18. Wolter type II telescope.

Wolter type 3

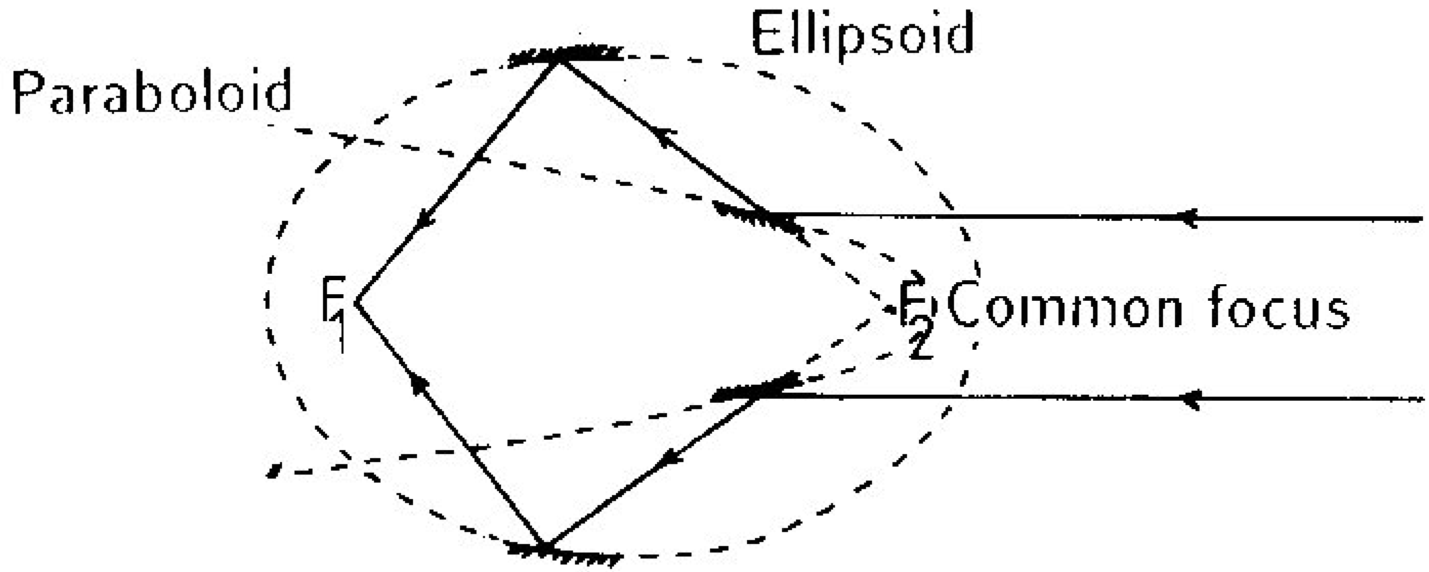

Figure 2.19. Wolter type III telescope.

Aberrations and ultrafast response

Optical path and Fermat's principle: mirror

The optical path function describes, for any point B within the optical surface, the contribution of all rays to the image in B

$$F = AP + PB$$

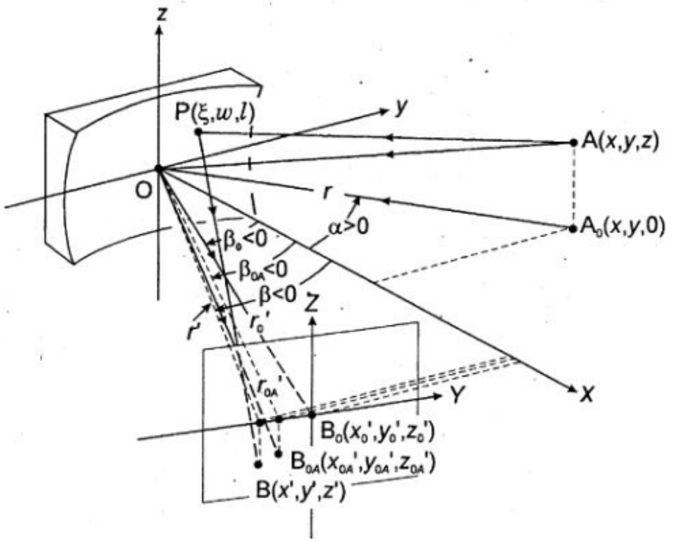

Theory of aberrations from Fermat's principle

Fermat's principle is the principle that the path taken between two points by a ray of light is the path that can be traveled in the least time. A more modern statement of the principle is that rays of light traverse the path of stationary optical length with respect to variations of the path.

Following the Fermat's principle with no aberrations, the position of B (image point) is that giving P(*u,w,l*) a stationary point for F(*w,l*)

$$\frac{\partial F}{\partial w} = 0 \qquad \frac{\partial F}{\partial l} = 0$$

Any violation of the Fermat's principle gives raise to an aberration on the image point B $\Rightarrow$ deformation of the image

Theory of aberrations from Fermat's principle

Series development $$F = \sum F_{i\,j} w^i l^j$$

- The violation of Fermat's principle for the point B occurs with aberrations. The non-zero terms F_{ij} describe the type and the order of the aberration: low orders of i and j describe more important aberrations, while the variation with *w* and/or *l* gives the direction (tangential or sagittal) affecting the aberration

- Aberrations are corrected by varying the geometry of the configuration, the shape of the surface and the law of variation of the groove density (for gratings) in order to cancel or mimimize the terms F_{ij}

The condition F_{10}=0 gives the Snell's law for reflection $\alpha = -\beta$

Theory of aberrations for a mirror (1)

TOROIDAL SURFACE

Taking into account the equation of the toroidal surface, the distances <AP> and <PB> can be expressed as functions of the variables α, p, q, y and z, where α is the angle of incidence, p and q are the entrance and exit arms (the distances between A and the mirror center, O, and between O and B), y and z span on the mirror surface

$$F = p + q + F_{20} y^2 + F_{02} z^2 + F_{30} y^3 + F_{12} yz^2 + O(y^4, z^4)$$

Theory of aberrations for a mirror (2)

For a toroidal surface (tangential radius R, sagittal radius ρ), the first terms F_{ij} are

$$F_{20} = \frac{1}{2}\cos^2\alpha\left(\frac{1}{p}+\frac{1}{q}-\frac{2}{R\cos\alpha}\right)$$

$$F_{02} = \frac{1}{2}\left(\frac{1}{p}+\frac{1}{q}-\frac{2\cos\alpha}{\rho}\right)$$

$$F_{30} = \frac{1}{2}\sin\alpha\cos\alpha\left[\frac{1}{p}\left(\frac{\cos\alpha}{p}-\frac{1}{R}\right)-\frac{1}{q}\left(\frac{\cos\alpha}{q}-\frac{1}{R}\right)\right]$$

$$F_{12} = \frac{1}{2}\sin\alpha\left[\frac{1}{p}\left(\frac{1}{p}-\frac{\cos\alpha}{\rho}\right)-\frac{1}{q}\left(\frac{1}{q}-\frac{\cos\alpha}{\rho}\right)\right]$$

Theory of aberrations for a mirror (3)

According to Fermat's principle, point B is located such that F will be an extreme for any point P. Since points A and B are fixed while point P can be any point on the surface of the mirror, aberration-free image focusing is obtained by the conditions $\delta F/\delta y = \delta F/\delta z = 0$, which must be satisfied simultaneously by any pair of y and z values.

This is possible only if ***all F_{ij} terms are equal to zero***.

The F_{20} and F_{02} terms control the tangential and sagittal defocusing respectively, which are the main optical aberrations to be cancelled. Therefore, in order to have stigmatic imaging, two conditions must be fulfilled: $F_{20} = 0$ and $F_{02} = 0$, which give

$$\frac{1}{p} + \frac{1}{q} = \frac{2}{R\cos\alpha} = \frac{2\cos\alpha}{\rho}$$

The tangential and sagittal radii of the mirror have to be calculated from these equations

Theory of aberrations for a mirror (4)

The remaining parts of the derivatives of the optical path function F give rise to the aberration terms. Since the partial derivatives have the geometrical significance of angles, the maximum tangential (y) and sagittal (z) displacements of the reflected rays from the true focus B can be calculated as

$$\Delta_{\tan} = \frac{q}{\cos\alpha} \left.\frac{\partial F}{\partial y}\right|_{y = L_{\tan},\, z = L_{\mathrm{sag}}}, \quad \Delta_{\mathrm{sag}} = q \left.\frac{\partial F}{\partial y}\right|_{y = L_{\tan},\, z = L_{\mathrm{sag}}}$$

where $(2L_{\tan})\times(2L_{\mathrm{sag}})$ is the illuminated area on the mirror surface.

For the partial derivatives of order n that do not vanish, these displacements correspond to **aberrations of order *n* in the focal plane.**

Tangential and sagittal defocusing: II-order aberration

Tangential and sagittal coma: III-order aberration

For M=1 (i.e., $p=q$), the coma is zero $\Rightarrow$ Rowland configuration

Ultrafast pulses

An ultrafast pulse is a "sheet of light" with micrometric or sub-micrometric thickness that is traveling at 300.000 km/s

The thickness of the "sheet" is proportional to the duration of the pulse

100 fs $\Rightarrow$ **30** μ**m**
10 fs $\Rightarrow$ **3** μ**m**
1 fs $\Rightarrow$ **0.3** μ**m**
100 as $\Rightarrow$ **30 nm**

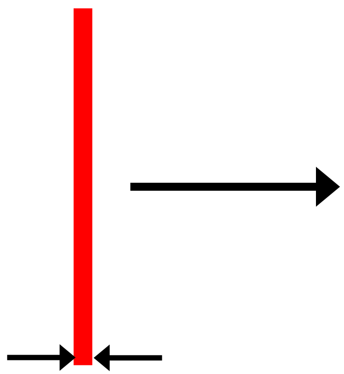

c = $3 \cdot 10^8$ m/s

$\boldsymbol{\Delta s = c \cdot \Delta T}$

Pulse-front deformation

Since aberrations are violation of the Fermat's principle (rays with different directions travel different paths), they give deformation of the pulse-front ⇒ pulse stretching of ultrafast pulses

Aberrations have to be studied not only in space but also in time

Toroidal mirror, p = 1000 mm, α = 87°, 5 mrad accepted aperture

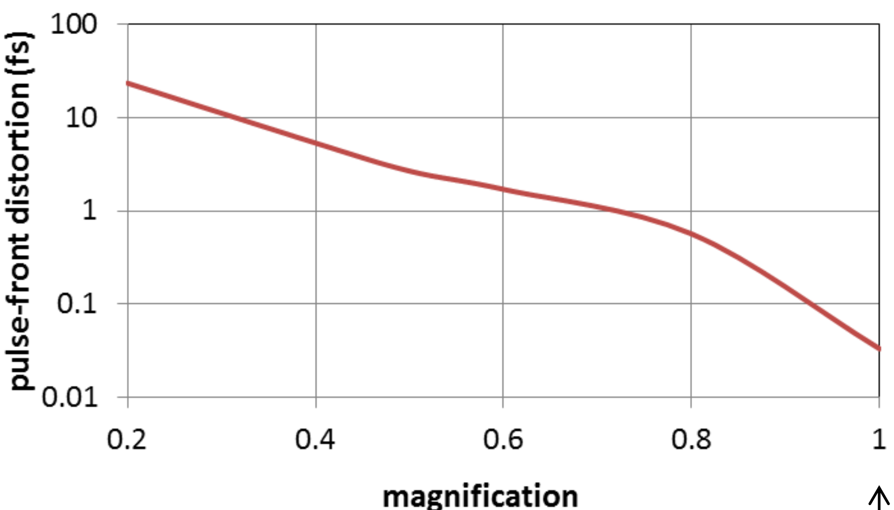

Rowland mounting

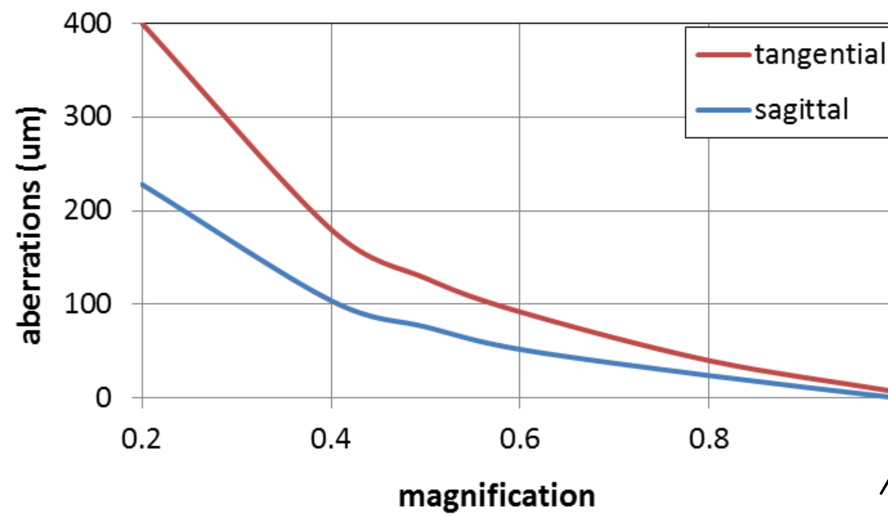

Rowland mounting

Spatio-temporal coupling (1)

Advanced simulation techniques allow to study the space-time coupling given by aberrations, that means that the pulse profile is spatially dependent.

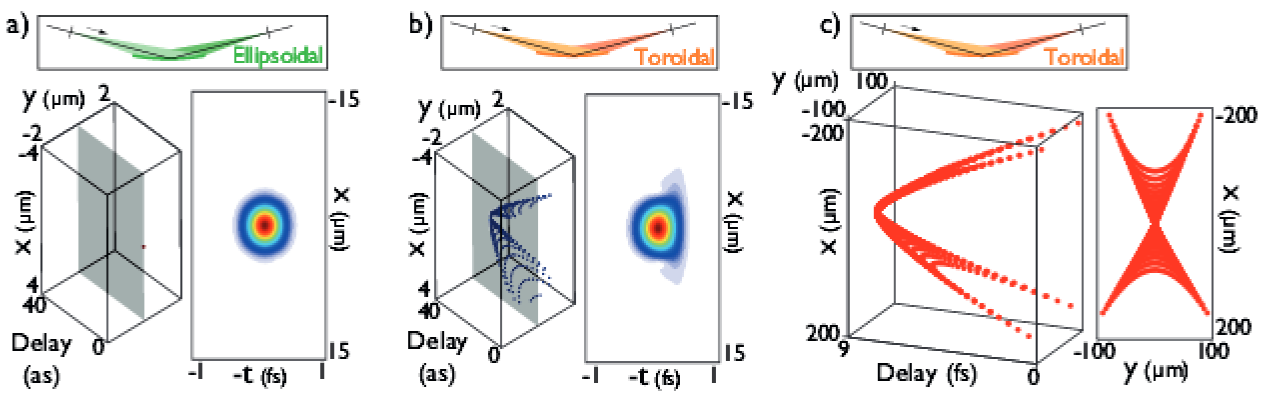

Fig. 9. Diffractive and geometric structures of pulses focused by toroidal and ellipsoidal mirrors in a $2f-2f$ geometry. Upper panels: description of the focusing geometry. (a-b) Evolution of the 3D spot diagrams (left) and of the modulus of the electric field in the $y=0$ plane (right) at the paraxial focus, in the case of (a) an ellipsoidal and (b) toroidal mirror. The shaded plane on the 3D spot diagrams at the paraxial focus indicates the $y=0$ plane. (c) 3D spot diagram at the paraxial focus of the toroidal mirror if considering the rays reflected off the full surface of the mirror.

Bourassin-Bouchet et al, Opt. Express 19, 17357 (2011)
Bourassin-Bouchet et al, Opt. Express 21, 2506 (2012)

Spatio-temporal coupling (2)

Magnification different from unity or misalignment error

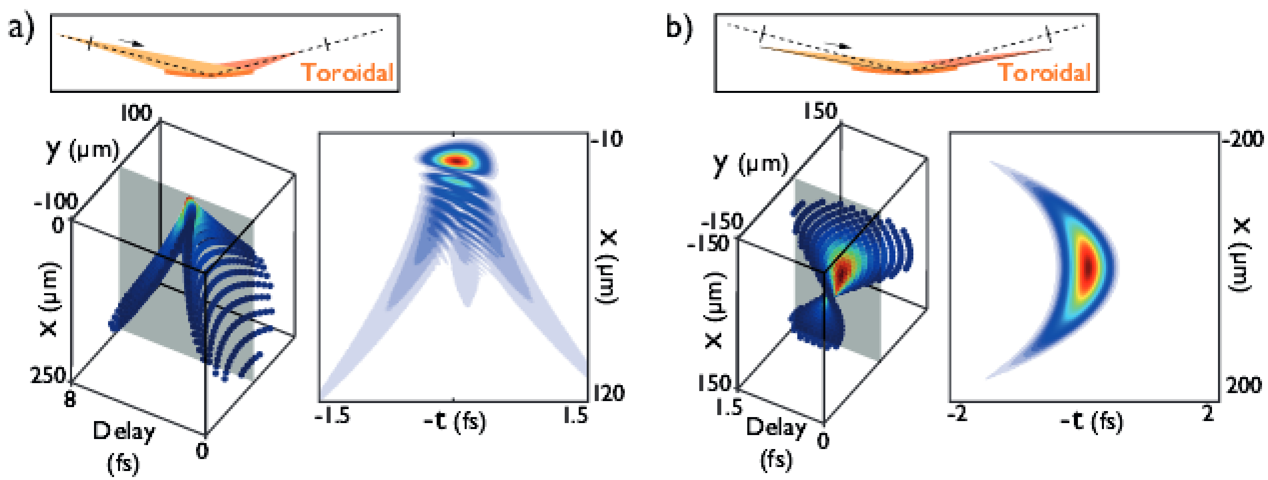

Fig. 10. Detailed evolution of a pulse focused by a toroidal mirror in the case of (a) a 0.5 magnifying power and (b) an error of 0.1° on the grazing angle with a magnification of 1. Upper panel: studied focusing geometry. Left panel: 3D spot diagram. Right panel: evolution of the modulus of the electric field in the $y = 0$ plane, shaded in grey on the 3D spot diagrams.

Rule of thumb

Toroidal mirror for ultrashort pulses have to be used with almost unity magnification.

For magnification different from unity, ellipsoidal mirrors have to be preferred.

High attention to be given in the alignment procedure to avoid misalignment errors.

Micro-focusing of ultrashort pulses

Micro-focusing is required to:

- Increase the peak intensity in the focus (as required for nonlinear effects)
- Increase the spatial resolution (as required for microscopy)

Micro-focusing of HHs with an ellipsoidal mirror

HHs have been focused by a platinum-coated ellipsoidal mirror at moderate grazing incidence (60 deg) to a spot size of 2.4 um

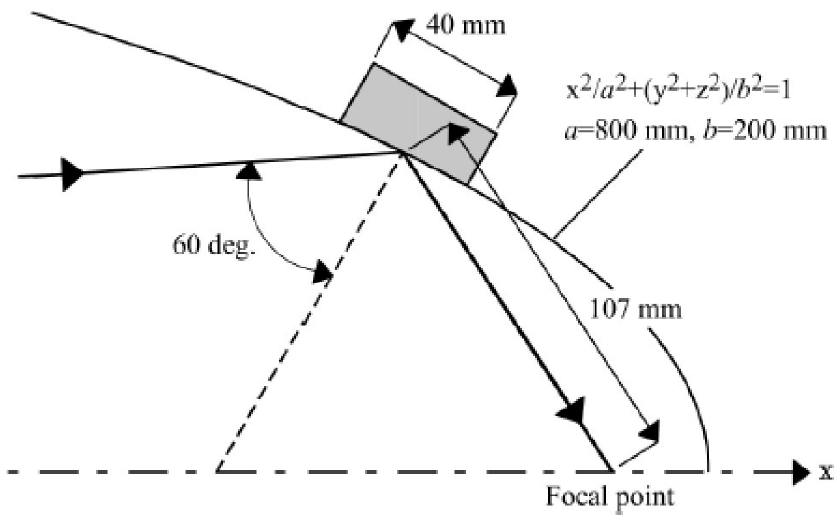

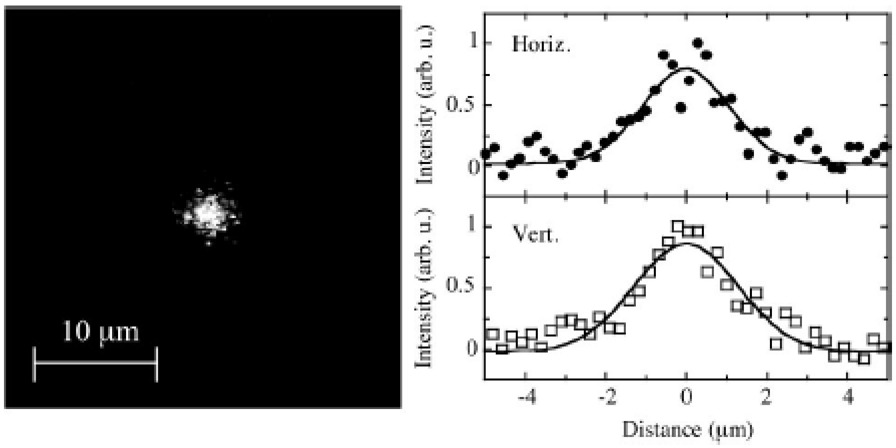

Entrance arm: 1600 mm

Exit arm: 107 mm

Demagnification factor: 15

Mashiko et al, Appl. Opt. 45, 573, 2006

Micro-focusing and output arm

Micro-focusing is normally achieved on a short output arm, since a large demagnification is required ($p/q >> 1$).

If microfocusing and a long output arm are simultaneously required, there are two solutions:

- increase also p to maintain the same demagnification
- add an additional relay mirror to make a 1:1 image of the focus

Micro-focusing of HHs with compensated toroidal mirrors

HHs have been focused by two toroidal mirrors at grazing incidence (80 deg) to a spot size of 8 um. The first mirror gives the high demagnification, the second mirror compensates for the coma

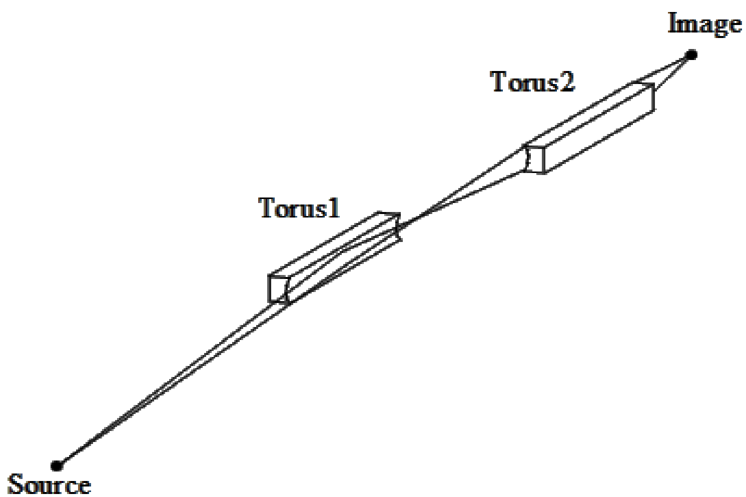

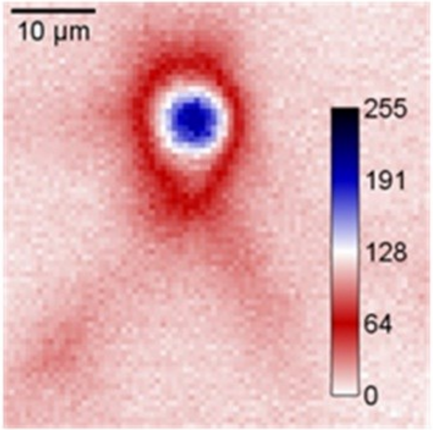

Demagnification factor: 11

Output arm: 600 mm

Total length of the beamline: <3 m

L. Poletto et al, Opt. Express 21, 13040, 2013

F. Frassetto et al, Rev. Sci. Inst. 85, 103115, 2014

Design consideration

⇒ The ideal mirror to demagnify a source with no aberrations is the ellipsoidal

Drawback of single-mirror configuration

⇒ A configuration with high demagnification using a single mirror has a short exit arm

⇒ The short exit arm may be not suitable to accommodate the experimental chamber.

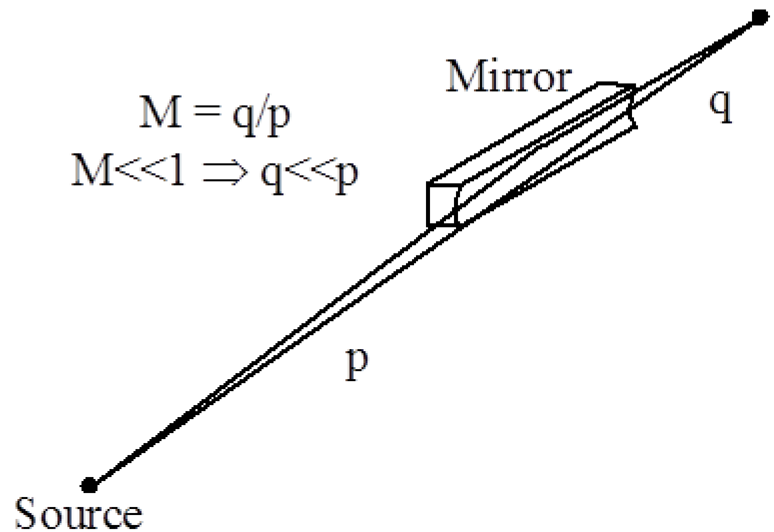

Toroidal mirrors for micro-focusing

⇒Toroidal mirrors are a cheaper alternative to the use of expensive Cartesian surfaces

⇒ A single toroidal mirror gives large aberrations (coma) when used to give high demagnification

PROPOSAL: two sections with toroidal mirrors in a compensated configuration: M1 provides the large demagnification, M2 is the relay section to increase the length of the exit arm. M2 compensates for the coma given by the couple M1.

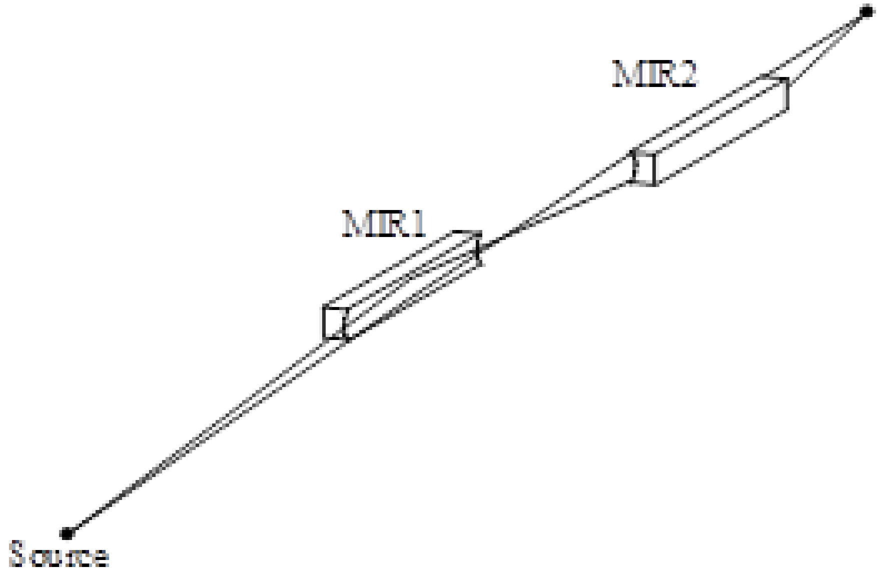

Study of the aberrations

From the light-path function, the coma aberration is calculated as

$$\Delta C_{\tan} = 3\frac{q}{\cos\alpha}F_{30}L_{\tan}^2 = \frac{3}{4}p\mathcal{D}^2\frac{M^2-1}{M}\tan\alpha$$

$$\Delta C_{\mathrm{sag}} = 2qF_{12}L_{\tan}L_{\mathrm{sag}} = \frac{1}{2}p\mathcal{D}^2\frac{M^2-1}{M}\tan\alpha = \frac{2}{3}\Delta C_{\tan}$$

$$\Delta C_{\tan,1} = \frac{3}{4}p_1\mathcal{D}^2\frac{M_1^2-1}{M_1}\tan\alpha$$

first mirror

$$\Delta C_{\tan,2} = \frac{3}{4}q_2\mathcal{D}^2\mathrm{M}_1^2\left(\mathrm{M}_2^2-1\right)\tan\alpha$$

second mirror

$$\mathrm{M}_2 \cong \sqrt{1+\frac{p_1}{q_2\mathrm{M}_1}}$$

Coma compensation

Preliminary test of the beamline with He:Ne laser

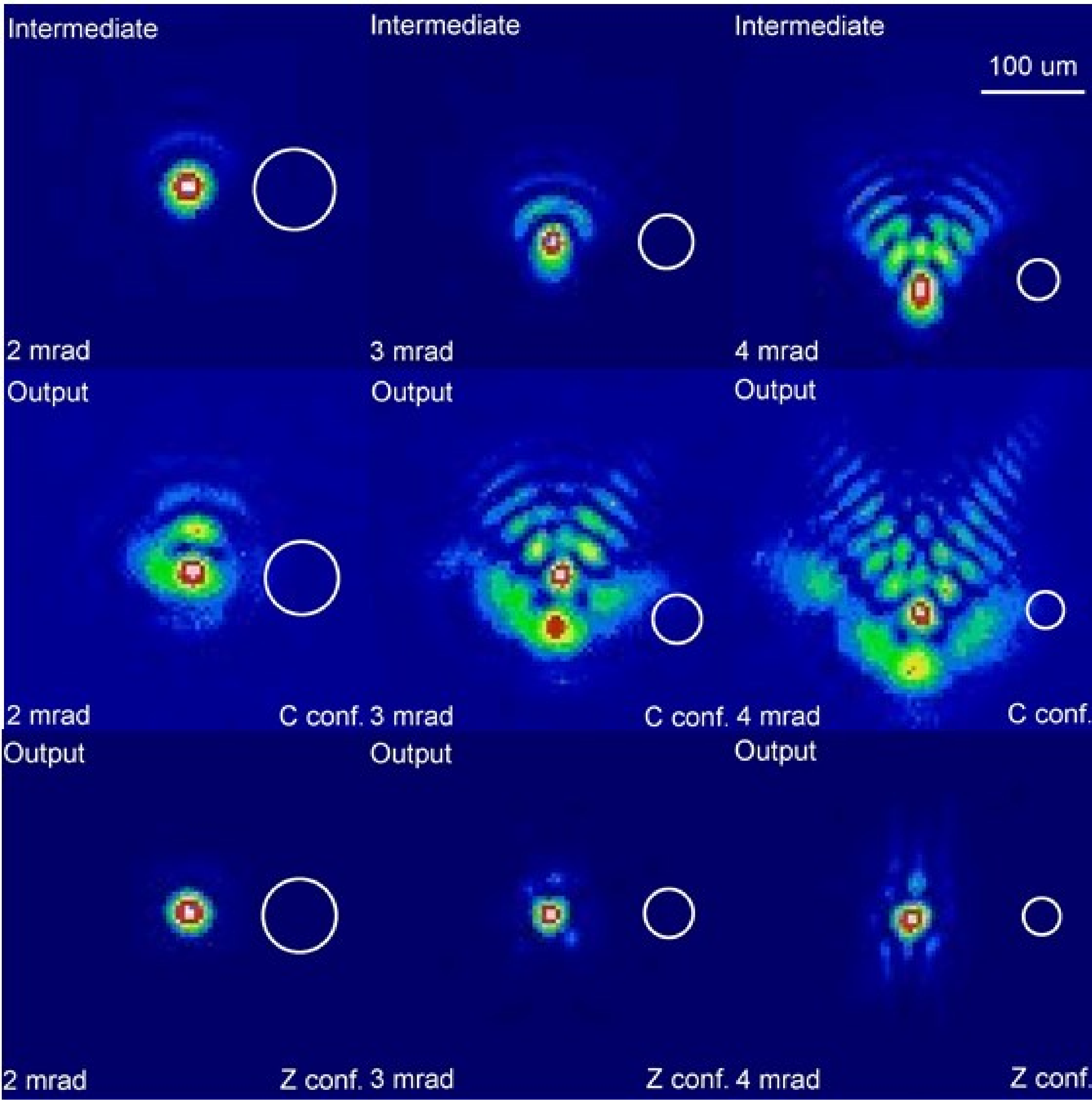

Aberrations from the first mirror

Case a) M3 in C configuration with respect to M2

Case b) M3 in Z configuration with respect to M2

Z configuration effective in coma compensation

Test of the beamline with XUV high-order laser harmonics

Spot size: 8 um FWHM

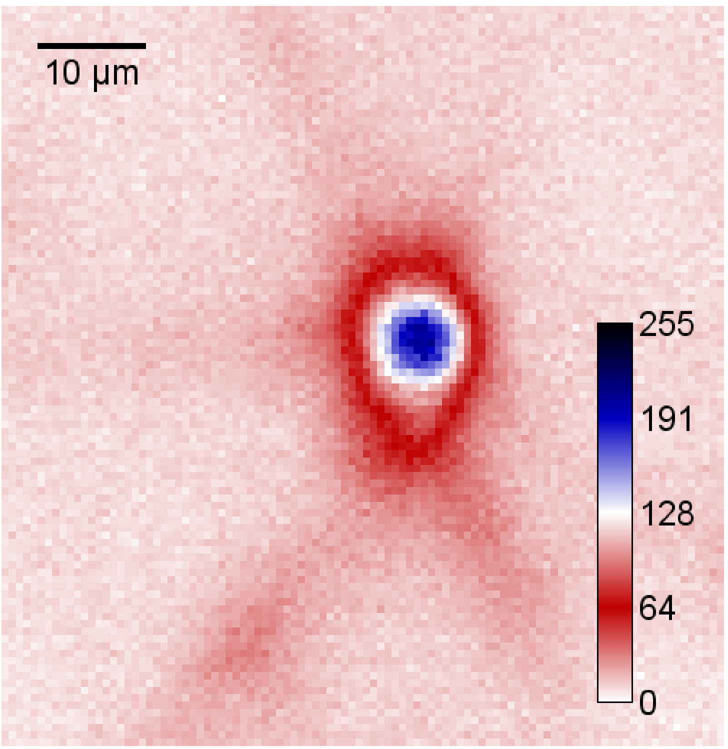

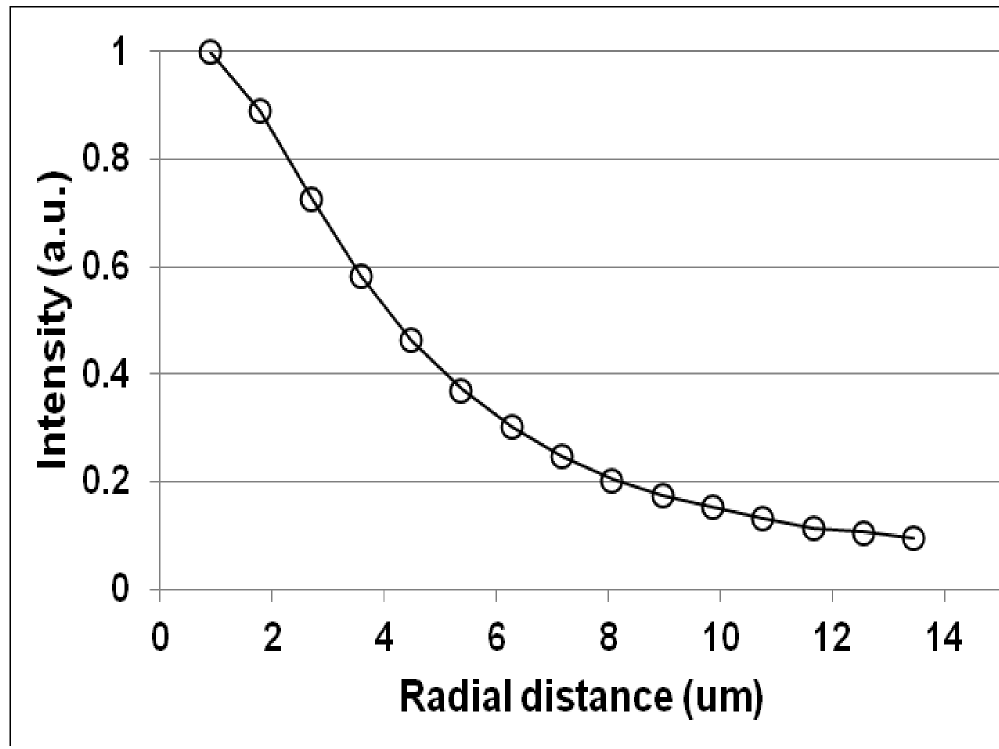

Gratings

Diffraction gratings

Diffraction grating

- Different wavelengths exit with different directions (dispersion)
- The same wavelength is deviated in different directions (diffraction orders)

$$sin\alpha + sin\beta = m\lambda\sigma$$

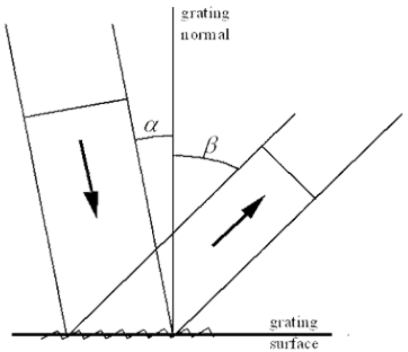

α = incidence angle ($\alpha > 0$)
β = diffraction angle ($\beta < 0$ if opposite to α with respect to the normal)
m = diffraction order (m = 0, 1, -1, 2, -2, ...)
λ = wavelength
σ = groove density

Monochromator: system which gives at the output a monochromatic beam from a polychromatic beam (it is a filter with variable wavelength and variable bandwidth)

Spectrometer: it allows to analyze spectrally the radiation, it gives the spectrum on a defined bandwidth

Spectral resolution

It is the capacity to distinguish two close wavelenths separated by $\Delta\lambda$.

From the grating theory, the maximum resolution is $\lambda/\Delta\lambda = m\mathrm{N}$ where m is the diffraction order and N is the total number of illuminated grooves.

E.g.: m=1, 1200 l/mm grating, 10 cm illuminated area $\Rightarrow$ the highest theoretical resolution is 120.000

From the practical point of view, the resolution is limited by the finite width of the slits or by the pixel size of the detector.

Dispersion

Angular dispersion

$$\frac{d\beta}{d\lambda} = \frac{m\sigma}{\cos\beta}$$

Plate factor

$$\frac{d\lambda}{dl} = \frac{\cos\beta}{mq\sigma} \cdot 10^6 \quad \mathrm{nm}/mm$$

Bandwidth on a slit of width W (or on a detector pixel of size W)

$$\Delta\lambda = W\frac{\cos\beta}{mq\sigma} \cdot 10^6 \quad \mathrm{nm}$$

Czerny-Turner configuration

The beam entering is collimated from the first mirror, the grating diffracts the radiation, the second mirror focuses the radiation.

The spectral scanning is done by rotating the grating around an axis parallel to the grooves.

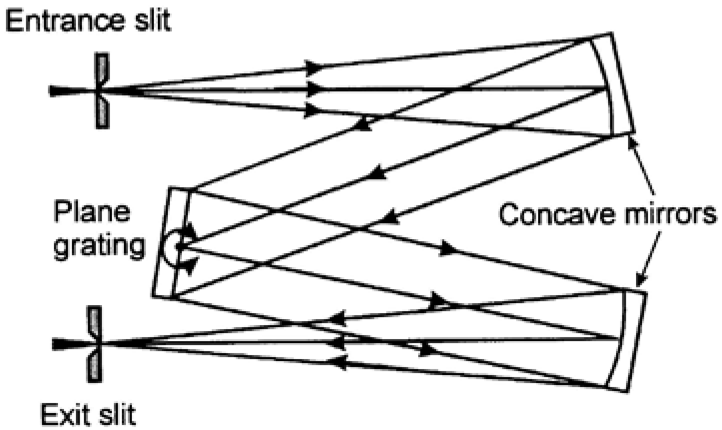

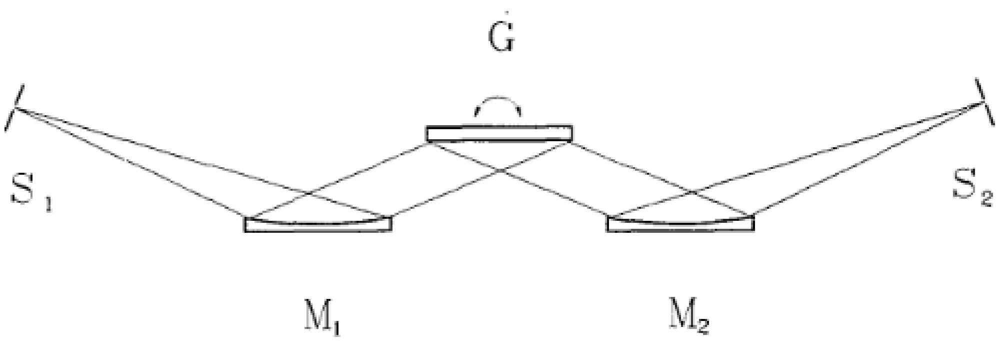

Grating types

Two categories:

- ***constant groove spacing***

$$\sigma = \sigma_0$$

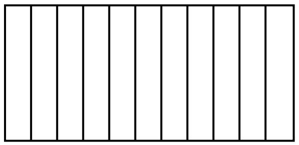

- ***variable groove spacing***

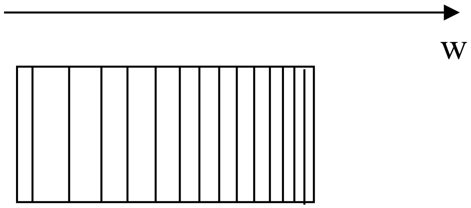

$$\sigma = \sigma_0 + \sigma_1 w + \sigma_2 w^2 + \sigma_3 w^3 + \sigma_4 w^4$$

Grating surfaces are normally ***plane, spherical or toroidal***

R indicates the tangential radius and ρ the sagittal radius

Plane grating: $\rho = R = \infty$

Spherical grating: $\rho = R$

Toroidal grating: $\rho \neq R$

Optical path and Fermat's principle: grating

The optical path function describes, for any point B within the optical surface, the contribution of all rays to the image in B

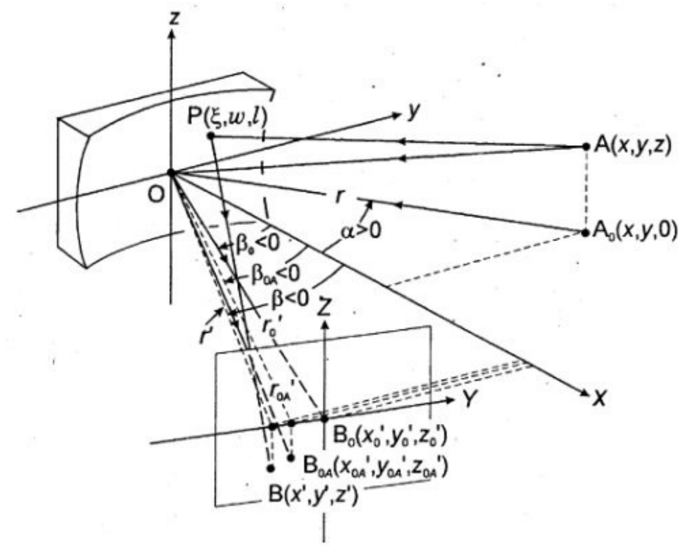

$$F = AP + PB + nm\lambda$$

where $n = w/d$ is the groove number in P, d is the groove density ($n=0$ is the groove passing through the center O), m is the diffraction order.

Following the Fermat's principle with no aberrations, the position of B (image point) is that giving P(u,w,l) a stationary point for F(w,l)

$$\frac{\partial F}{\partial w} = 0 \qquad \frac{\partial F}{\partial l} = 0$$

Any violation of the Fermat's principle gives raise to an aberration on the image point B

The concave grating

Concave grating, radii R, ρ

$$F_{20} = \frac{1}{2}\left(\frac{\cos^2\alpha}{p} - \frac{\cos\alpha}{R}\right) + \frac{1}{2}\left(\frac{\cos^2\beta}{q} - \frac{\cos\beta}{R}\right) + \frac{1}{2} m\lambda\sigma_1$$

Spectral defocusing

$$F_{02} = \frac{1}{2}\left(\frac{1}{p} - \frac{\cos\alpha}{\rho}\right) + \frac{1}{2}\left(\frac{1}{q'} - \frac{\cos\beta}{\rho}\right)$$

Astigmatism

Spectral focusing curve: $F_{20}=0 \Rightarrow$ the image of a point-like source consists of vertical lines at the different wavelengths

Spatial focusing curve: $F_{02}=0 \Rightarrow$ the image of a point-like source consists of horizontal lines at the different wavelengths

For spectroscopy, the spectral focus is preferred to the spatial focus to achieve the best spectral resolution

Rowland configuration for constant-spaced concave gratings (1)

If the source (the slit) and the grating are on a circle with diameter equal to the grating tangential radius, and the grating normal is on a diameter, the spectral focus is on the circle

$$p = R \cos \alpha$$

$$q = R \cos \beta$$

This configuration has been used for many instruments for lab and space applications

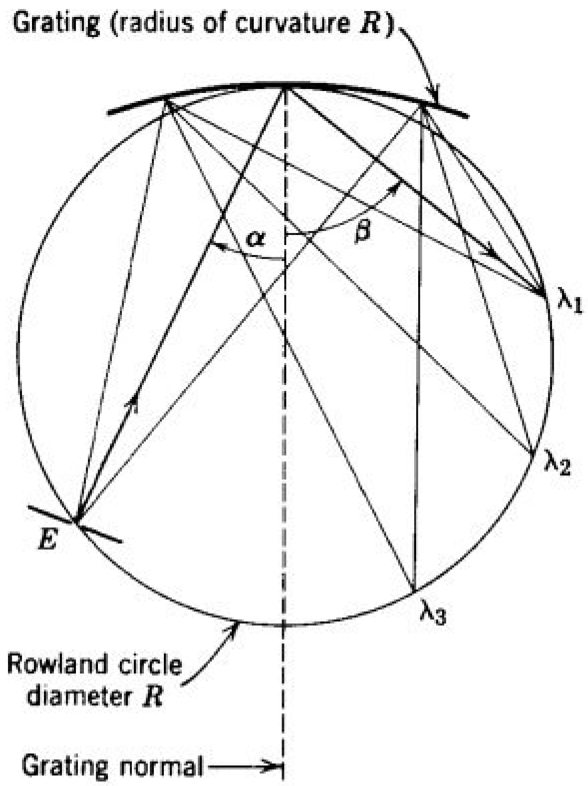

Rowland configuration for constant-spaced concave gratings (2)

For a spherical grating, the spectral and spatial foci are not coincident $\Rightarrow$ ***astigmatism*** (given by the spherical surface)

Astigmatism is corrected by a toroidal surface

$$\rho = R\cos\alpha \cos\beta$$

Stigmaticity is realized on two points on the Rowland circle (stigmatic points) for two wavelengths (stigmatic wavelengtyhs), corresponding to (α, β) and (α,- β)

Space application of toroidal gratings at n.i.: UVCS spectrometer on SOHO

UVCS is an UV solar coronagraph launched in 1995 with SOHO satellite and operated till 2012. It acquires spectroscopic images of the solar corona at the HI-Lya line at 121.6 nm and O-VI lines centered at 103.2 nm.

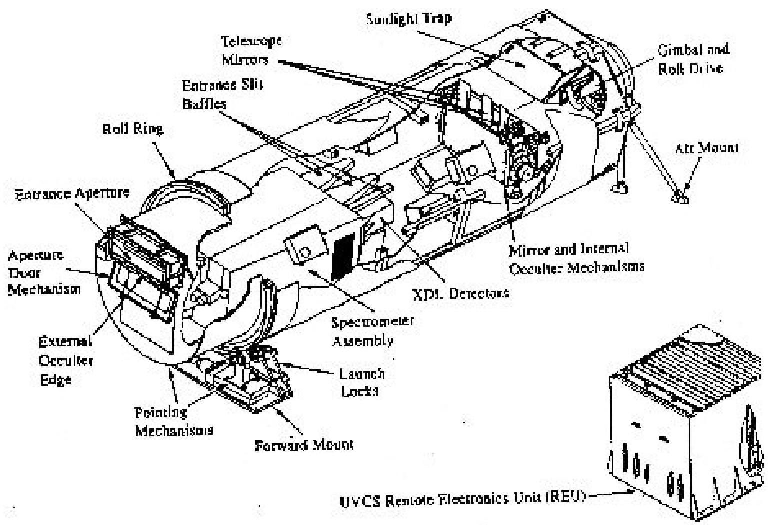

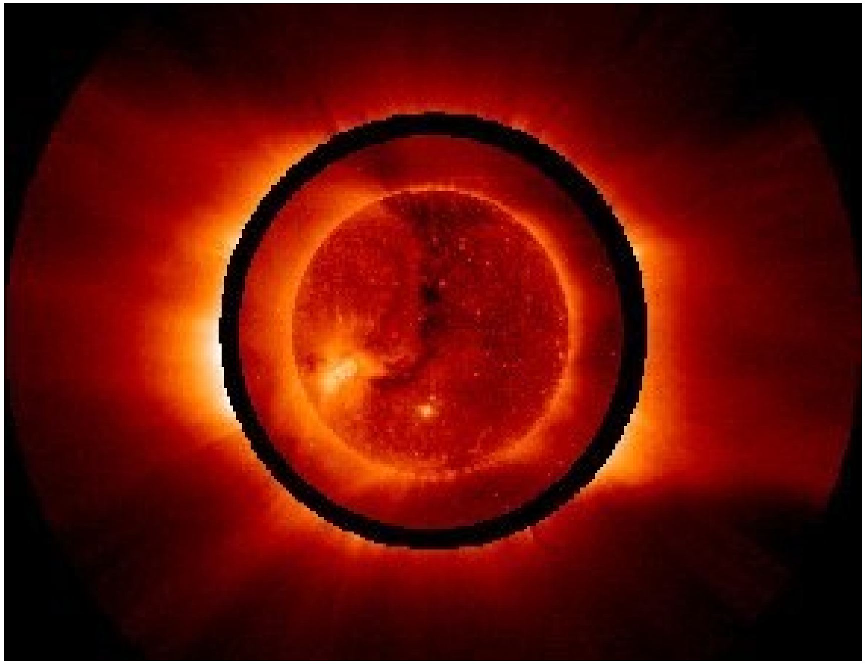

Composite image of the solar disk and solar corona with EIT and UVCS.

Constant-spaced spherical grating at grazing incidence

$$\frac{\cos^2\alpha}{p}+\frac{\cos^2\beta}{q}-\frac{\cos\alpha+\cos\beta}{\mathrm{R}}=0$$

Spectral focusing

$$\frac{1}{p}+\frac{1}{q'}-\frac{\cos\alpha+\cos\beta}{R}=0$$

Spatial focusing

At grazing incidence, when the term F_{20} is canceled (Rowland circle), the term F_{20} is highly different from zero, since a sphere at grazing incidence has no focusing capabilities in the sagittal plane.

The image of a point-like source is a series of vertical lines at the different wavelengths.

CHARACTERISTICS

The input arm is p = R cosα

The output arm is q = R cosβ

Space application of toroidal gratings at g.i.: CDS spectrometer on SOHO

CDS is a solar disk spectrometer on SOHO, to acquire monochromatic images in the 15-78 nm region.

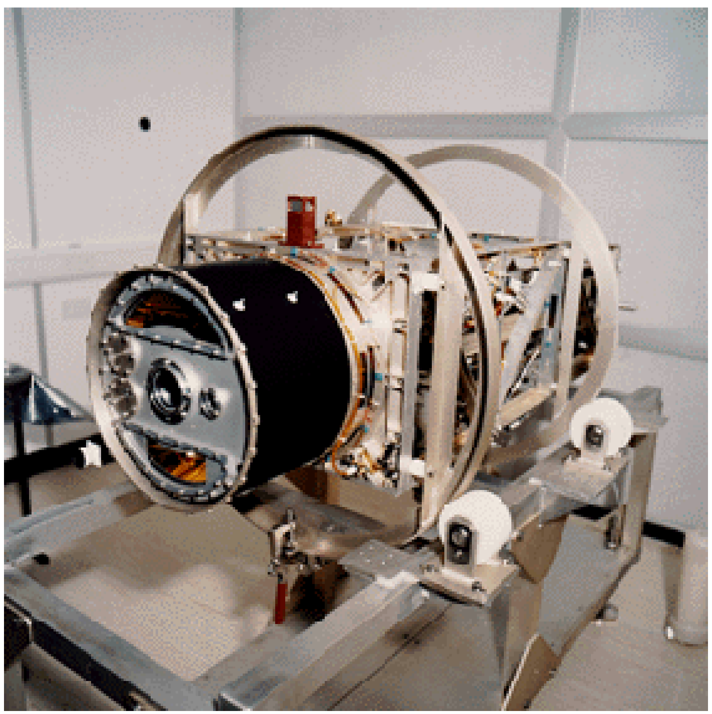

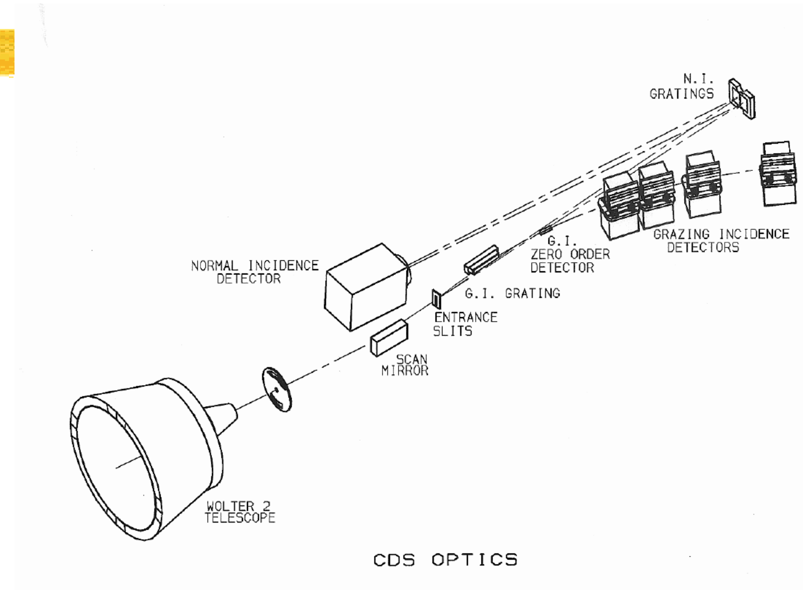

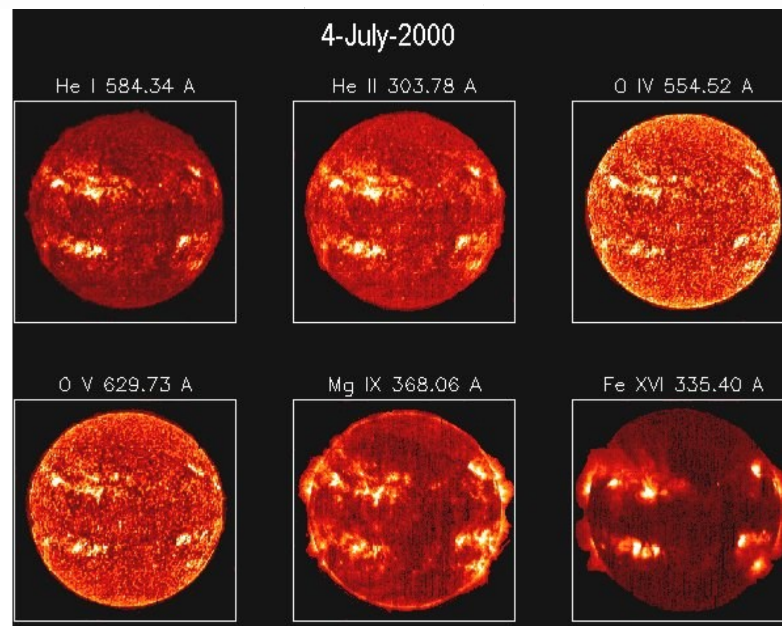

The varied-line-spaced (VLS) grating at grazing incidence

$$\frac{\cos^2\alpha}{p}+\frac{\cos^2\beta}{q}-\frac{\cos\alpha+\cos\beta}{\mathrm{R}}+m\lambda\sigma_1=0$$

Spectral defocusing

$$\frac{1}{p}+\frac{1}{q}-\frac{\cos\alpha+\cos\beta}{R}=0$$

Spatial defocusing

At grazing incidence, when the term F_{20} is canceled, the term F_{20} is highly different from zero, since a sphere at grazing incidence has no focusing capabilities in the sagittal plane $\Rightarrow$ astigmatism

Once the incidence angle has been fixed, R and $\sigma 1$ can be chosen to have the spectral focusing on a curve that is a line almost normal to the tangent to the grating surface.

Furthermore, parameters $\sigma 2$ and $\sigma 3$ are chosen to minimize coma and spherical aberration.

Hitachi Aberration-Corrected Concave Gratings for Flat-Field Spectrographs

Grazing-Incidence Type

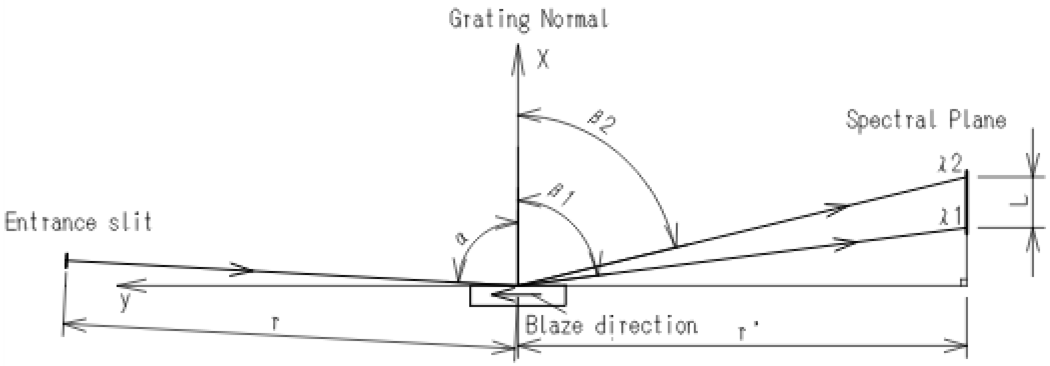

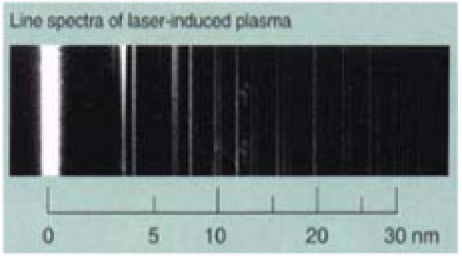

Grazing-incidence soft X-ray spectrograph with flat-field image focusing

The spectra of the soft X-ray region can be observed on a flat photographic plate when the grating is mounted at an incidence angle of 87°(001-0437, 001-0266).

Part No.	Grooves per mm	Radius of curvature (mm)	Blaze WL (nm)	Blank size H×W×T (mm)	Blaze angle (degree)	α (degree)	r (mm)	β1 (degree)	β2 (degree)	r' (mm)	WL Rang λ1 to λ2 (nm)	L (mm)	Material
001-0437 *1,2	1200	5649	10	30×50×10	3.2	87	237	-83.04	-77.07	235.3	5~20	25.3	Pyrex
001-0266 *1,2	1200	5649	10	30×50×10	3.2	87	237	-83.04	-77.07	235.3	5~20	25.3	Zero Dur
001-0450 *2	2400	15920	1.5	30×50×10	1.9	88.7	237	-85.81	-81.01	235.3	1~5	19.99	Pyrex
001-0471 *2	2400	15920	1.5	30×50×10	1.9	88.7	237	-85.81	-81.01	235.3	1~5	19.99	Zero Dur
001-0639	600	5649	31	30×50×10	3.7	85.3	350	-79.56	-67.26	469	22~124	110.16	Pyrex
001-0640	1200	5649	16	30×50×10	3.7	85.3	350	-79.56	-67.26	469	11~62	110.16	Pyrex
001-0659 *3	2400	57680	3	40×70×12	3	89	564	-85.91	-80.21	563.2	1~6	56.83	BK7
001-0660 *3	1200	13450	9	40×70×12	3	87	564	-83.04	-75.61	563.2	5~25	75.73	BK7

References

1. T. Kita, T. Harada , N. Nakano and H. Kuroda, "Mechanically ruled aberration-corrected concave gratings for a flat-field grazing-incidence spectrograph", Appl. Opt. 22, 512-513 (1983)
2. N. Nakano, H. Kuroda, T. Kita and T. Harada, "Development of a flat-field grazing-incidence XUV spectrometer and its application in picosecond XUV spectroscopy", Appl. Opt. 23, 2386-2392 (1984)
3. T. Harada, K. Takahashi, H. Sakuma and A. Osyczka, "Optimum design of a grazing-incidence flat-field spectrograph with a spherical varied-line-space grating", Appl. Opt. 38, 2743-2748(1999)

Example of flat-field spectrograph

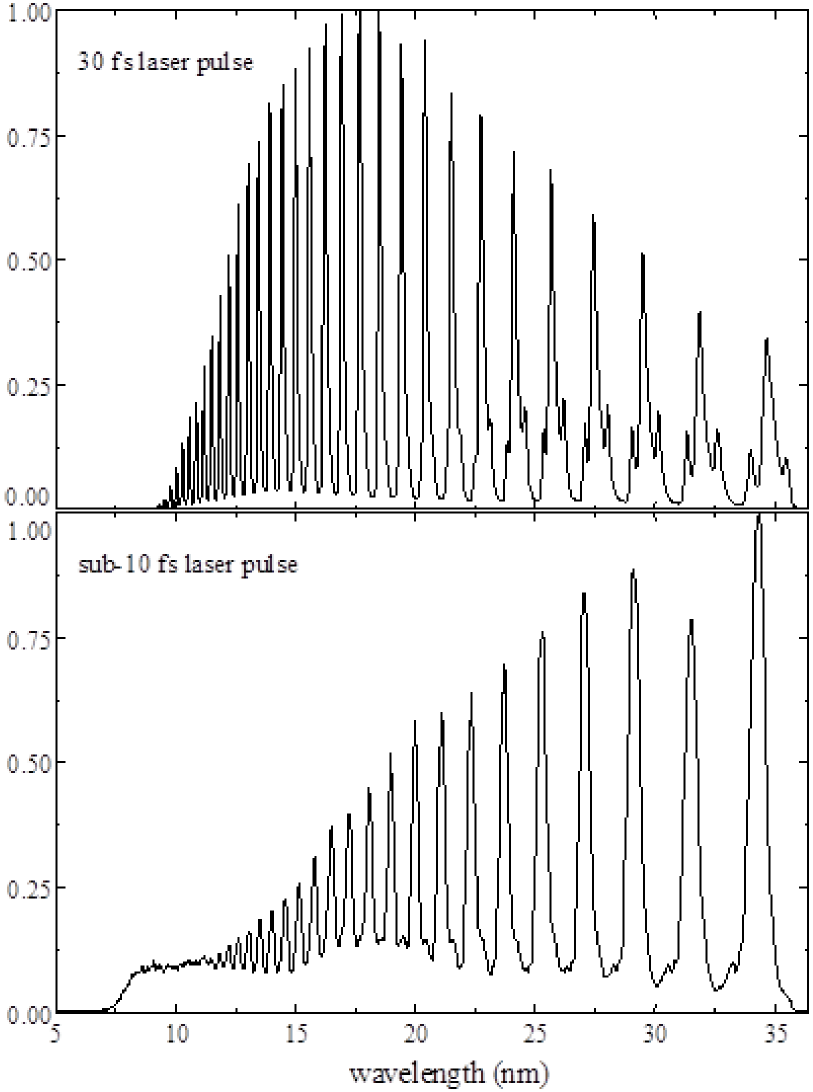

HH spectra in Helium, 300 μJ laser pulse
Hitachi grating, 1200 gr/mm
MCP detector, 40 mm size

Stigmatic configurations at grazing incidence

Two configurations:

- toroidal gratings
- additional mirror for spatial focusing

Option 1: toroidal grating monochromators (TGM), often used for synchrotron beamlines.

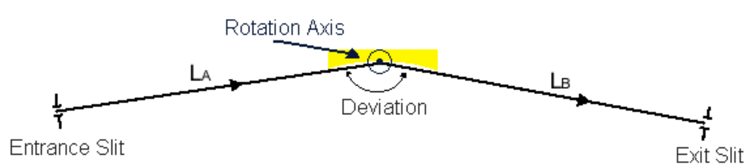

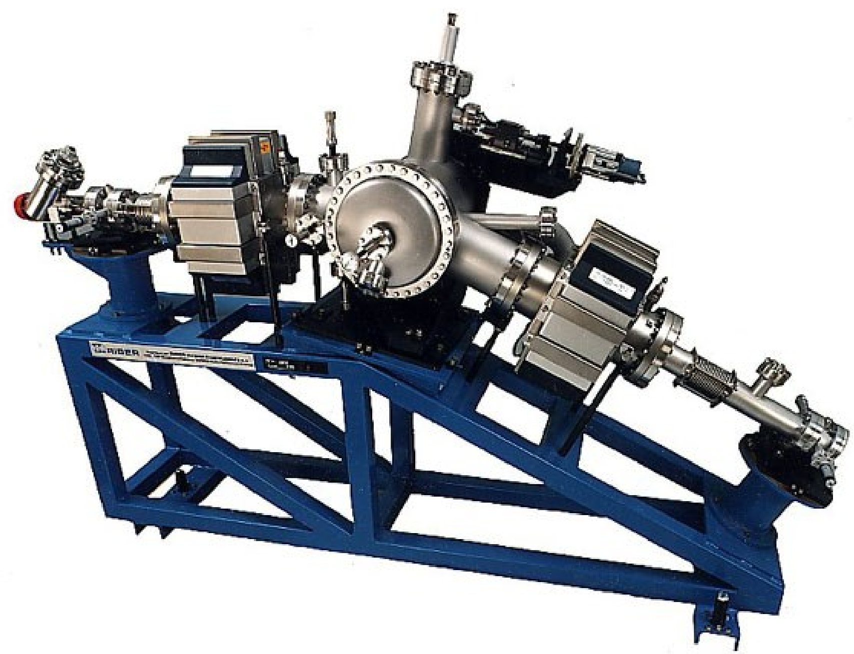

Stigmatic configurations with external toroidal mirror (1)

An external mirror provides the tangential focusing on the entrance plane of the grating and the sagittal focusing on the detector plane.

The configuration gives a ***single stigmatic point for the Rowland configuration***, since the output arm varies rapidly.

The configuration is ***stigmatic on a broad spectral interval with VLS gratings***, since the output arm is constant with the wavelength.

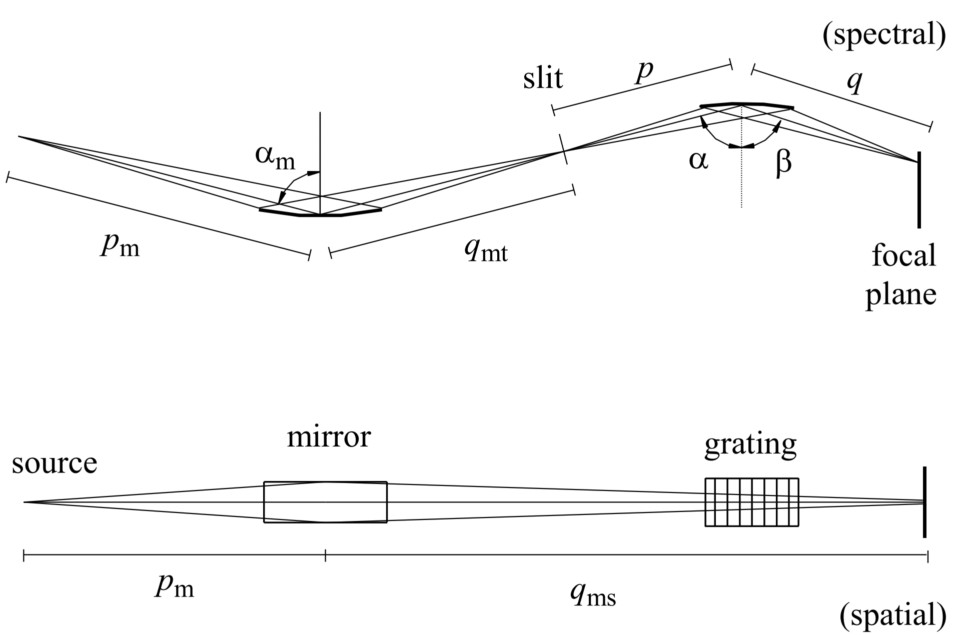

Toroidal mirror and VLS spherical grating

Poletto et al, Rev. Sci. Inst. 72, 2868 (2001)

Example: configuration to measure HH spectrum and divergence

⌘ Toroidal mirror and VLS grating

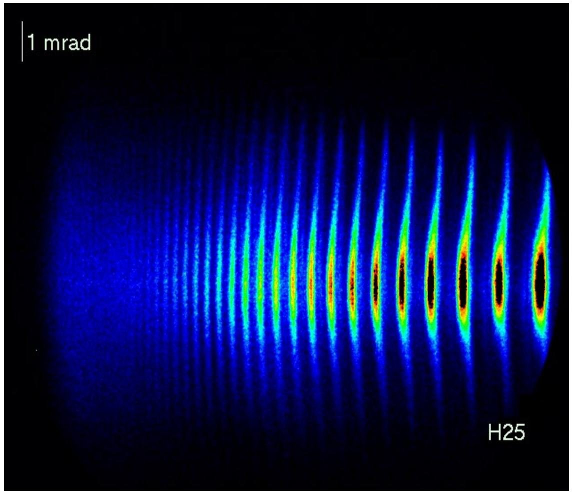

Spectrum in He
10 fs pulses
0.3 mJ/pulse

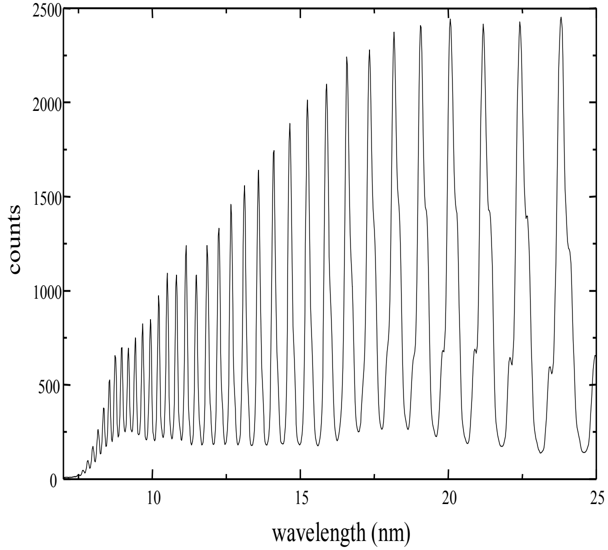

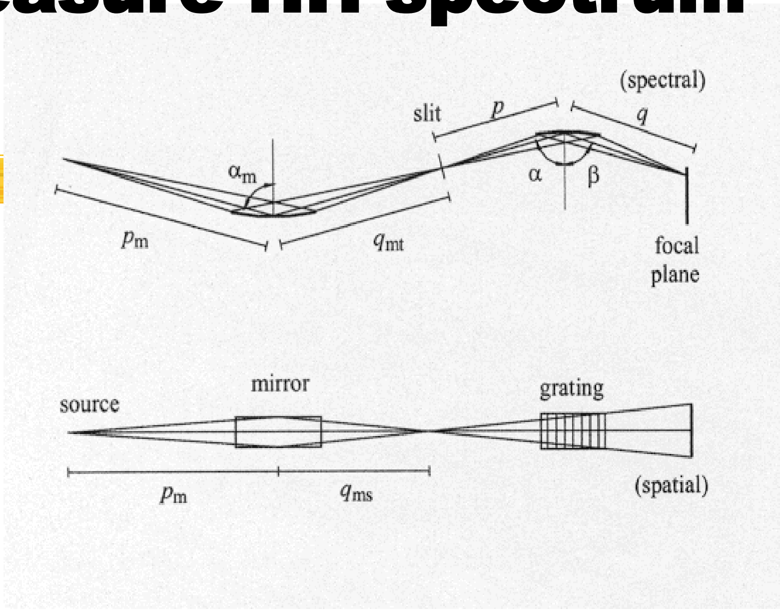

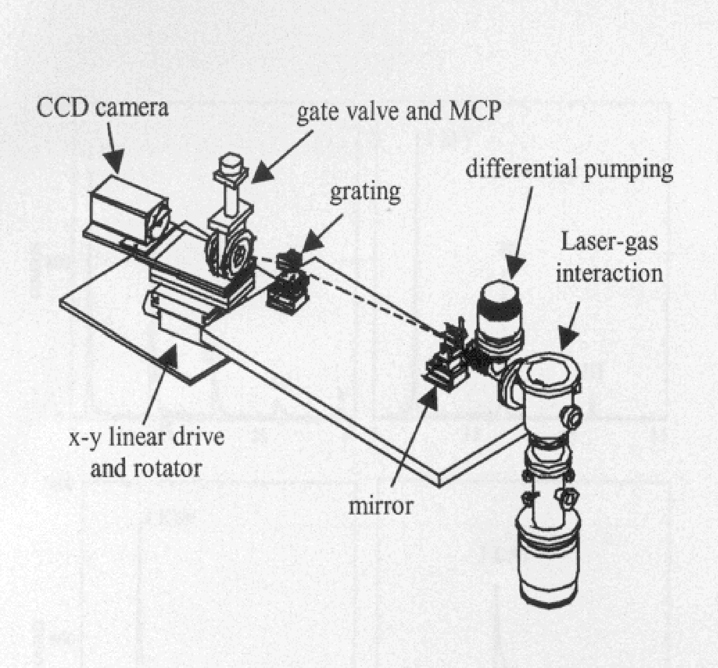

Grating monochromators for ultrafast pulses

Spectral selection of ultrafast pulses

Let us consider the problem of the monochromatization of ultrafast tunable XUV pulses, such as FEL pulses (e.g. suppression of the background or selection of the FEL harmonics)

$\Rightarrow$ XUV TUNABLE MONOCHROMATOR

THE MONOCHROMATOR HAS TO PRESERVE THE TEMPORAL DURATION OF THE XUV PULSE AS SHORT AS THE GENERATION PROCESS

If the wavelength selection is operated by a diffraction grating, a pulse-front tilt has to be accepted at the output.

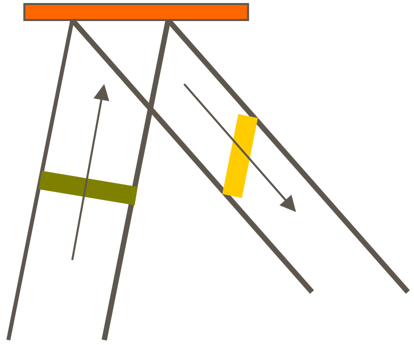

Es: 5-mm FWHM beam, λ=30 nm (41 eV), 300 gr/mm grating, normal incidence

$\Rightarrow$ 1500 illuminated grooves

$\Rightarrow$ path-difference ΔOP_{FWHM} = 45 μm, Δt_{FWHM} = 150 fs

Limit of the grating monochromator

For a given resolution $\lambda/\Delta\lambda$, the minimum number of illuminated grooves (first diffracted order) is $N = \lambda/\Delta\lambda$ (Rayleigh criterion).

This gives a broadening on the focus that is ≈equal to the Fourier limit.

$$\Delta\tau_{FWHM} = \frac{\lambda^2}{\Delta\lambda_{FWHM}} 1.7 \cdot 10^{-3}$$

If the number of grooves that are illuminated is the minimum for a given resolution, the broadening given by a diffraction grating is comparable to the Fourier limit.

OPERATION AT GRAZING INCIDENCE

When working with gratings at grazing incidence, the illuminated area is long and the number of illuminated grooves is normally far superior to the Rayleigh limit.

The problem of time preservation has to be analyzed !

Design of single-grating monochromators

Aim of the design is to keep the number of illuminated grooves as close as possible to the resolution $\lambda/\Delta\lambda$

- The classical diffraction geometry can be used to make the spectral selection with a single grating
- The temporal broadening in the XUV is in the range 100-200 fs FWHM
- The efficiency is limited by the quality of the grating surface ($\approx$10%)

L. Poletto and F. Frassetto, Appl. Opt. **49**, 5465 (2010)

The off-plane mount

OFF-PLANE MOUNT $\Rightarrow$ the incident and diffracted wave vectors are almost parallel to the grooves

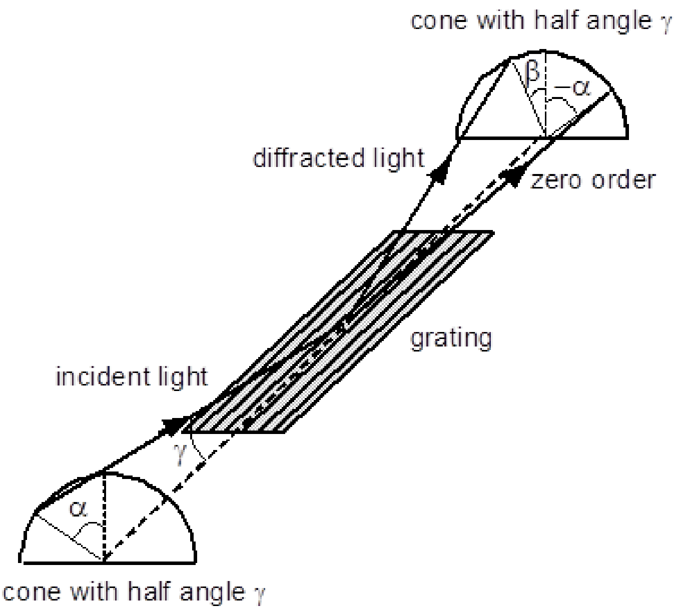

W. Cash, Appl. Opt. **21** 710 (1982)

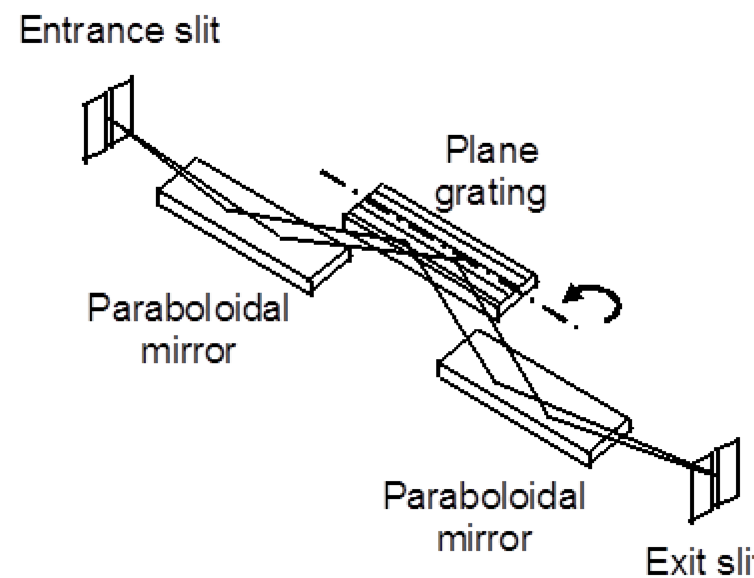

W. Werner and H. Visser, Appl. Opt. **20**, 487 (1981)

Efficiency of gratings for XUV monochromators

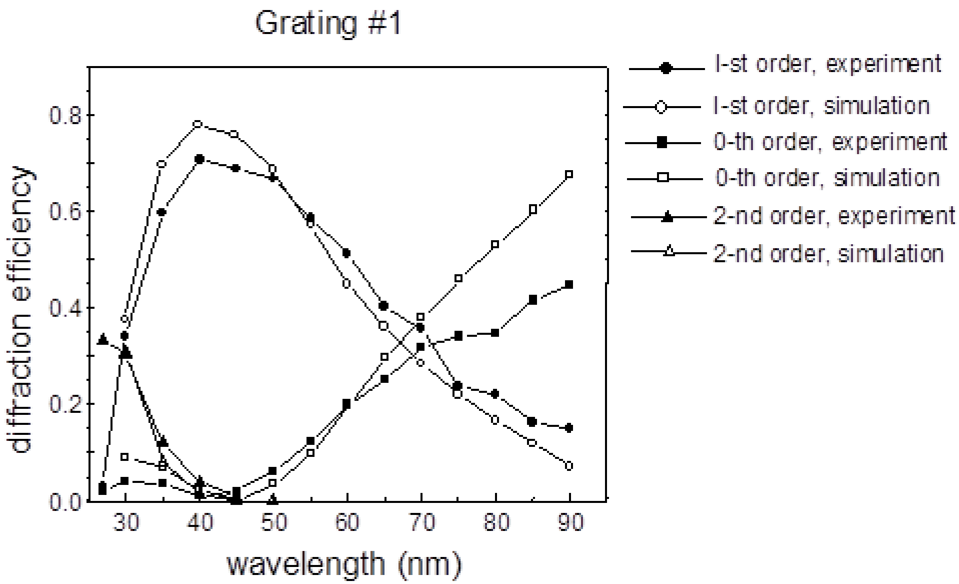

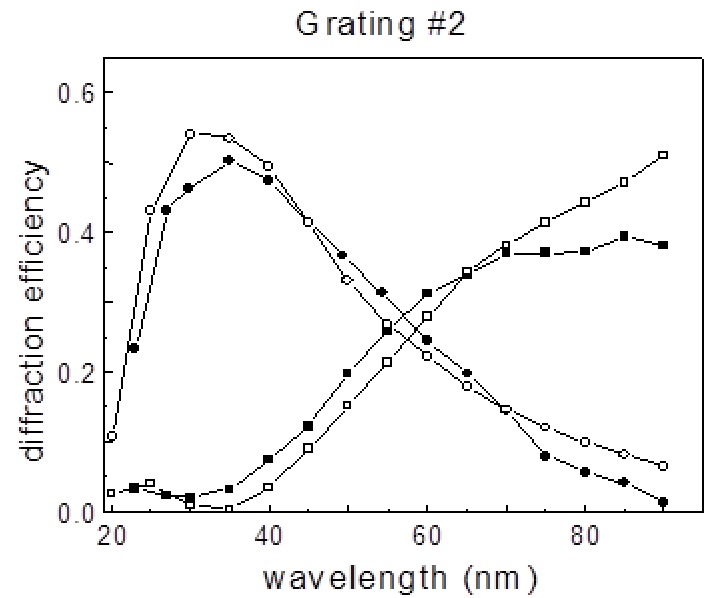

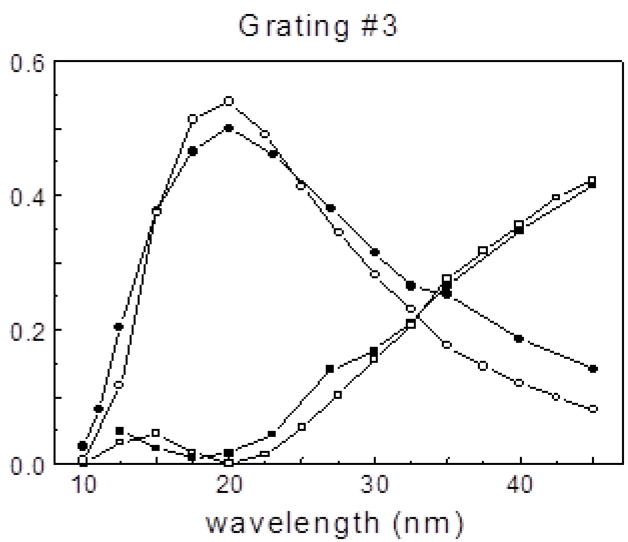

Grating	*gr/mm*	*altitude angle*	*blaze wavelength*
1	400	3°	44 nm
2	400	5.6°	38 nm
3	600	3°	21 nm

VERY HIGH EFFICIENCY !

M. Pascolini et al, Appl. Opt. **45,** 3253 (2006)

Classical design vs off-plane (single-grating mount)

Wavelength 30 nm

Beam size 1 mm half-width

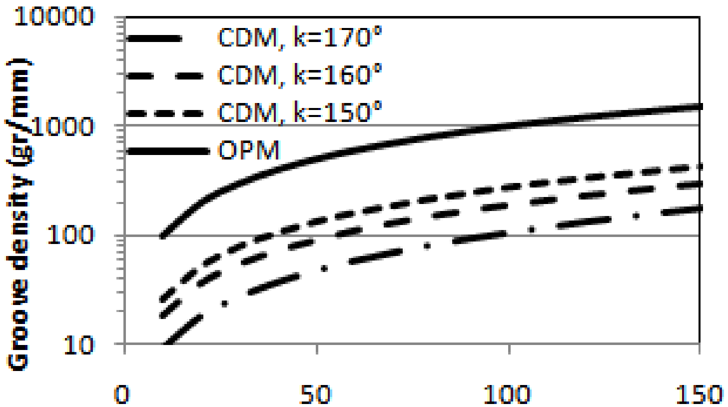

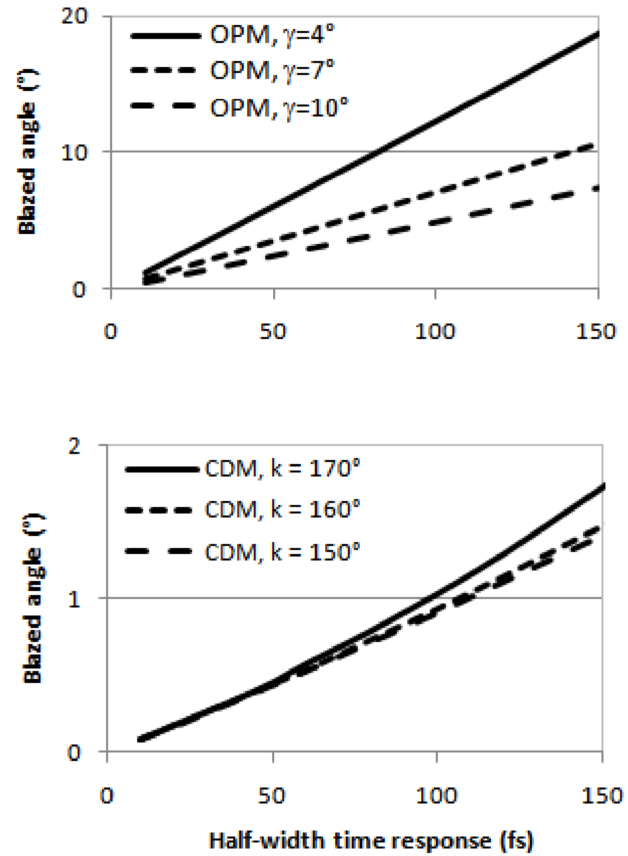

The classical mount is suitable for time response in the 100-200 fs range.

The off-plane mount should be used for time response in the 10-100 fs range.

L. Poletto et al, J. Sel. Top. Quant. Electron. **18**, 467 (2012)

Temporal characterization

The temporal characterization is achieved by cross-correlation measurement of the XUV pulses with a synchronized 800-nm pulse. The harmonic pulse ionizes a gas in the presence of the IR field. When the two pulses overlap in time and space on a gas jet, sidebands appear in the photoelectron spectrum. The sideband amplitude as a function of the delay between the XUV and IR pulses provides the cross-correlation signal.

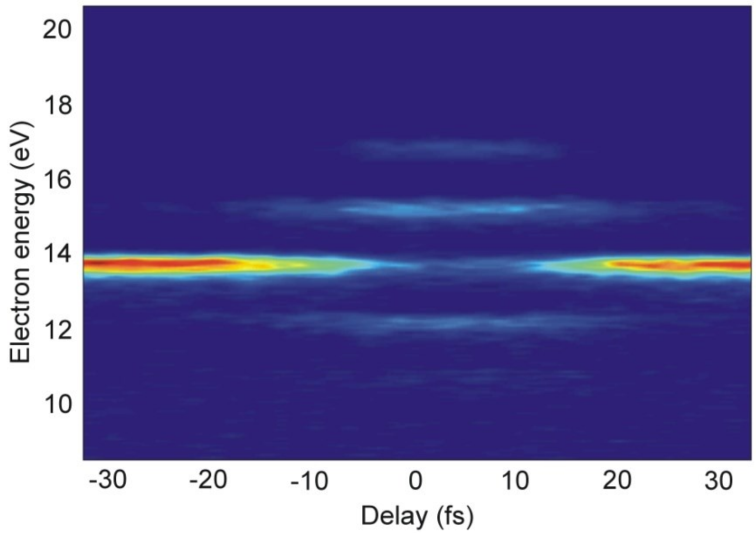

Example: monochromatic beamline at EPFL (1)

Harmonium beamline at EPFL, Lausanne

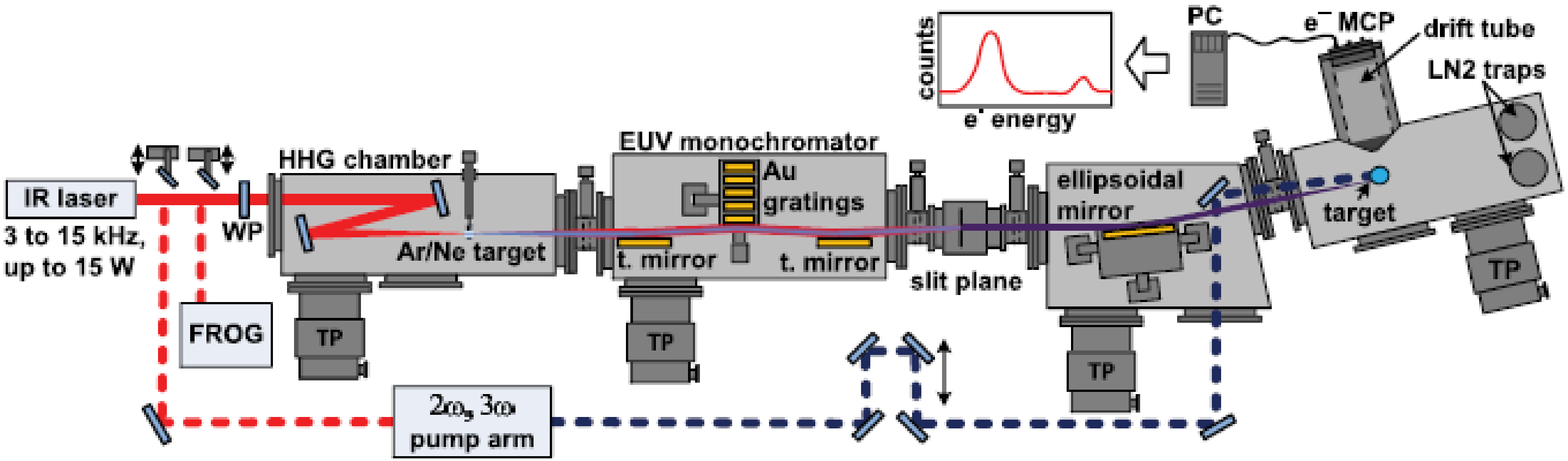

Spectral region	Resolution	Time response
30-40 eV	0.7 eV	20 fs
30-40 eV	0.2 eV	100 fs
80-100 eV	0.7 eV	100 fs
80-100 eV	0.2 eV	100 fs

J. Ojeda et al, Structural Dynamics **3**, 023602 (2016)

Example: monochromatic beamline at EPFL (2)

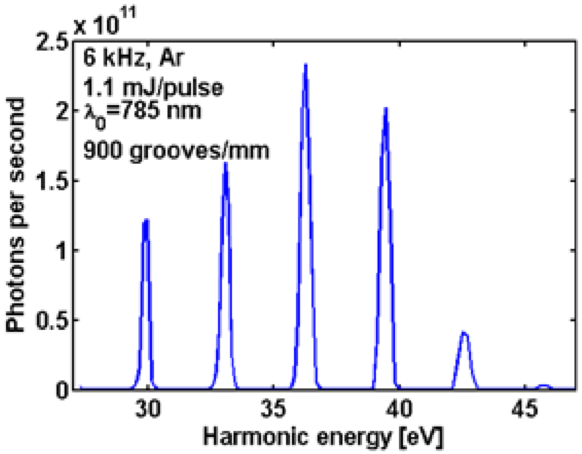

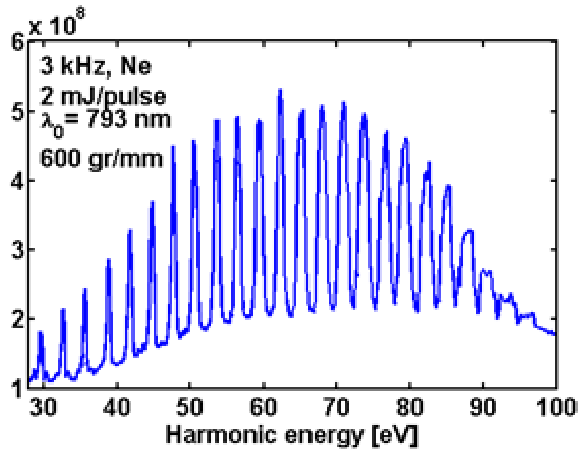

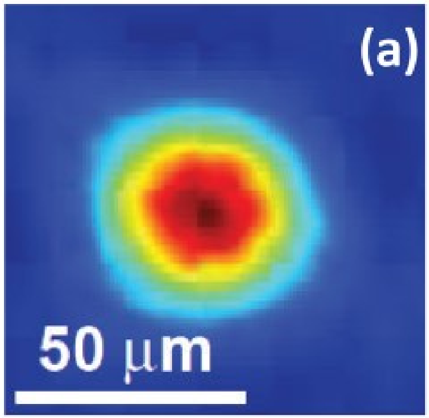

Spot size, 22 um FWHM

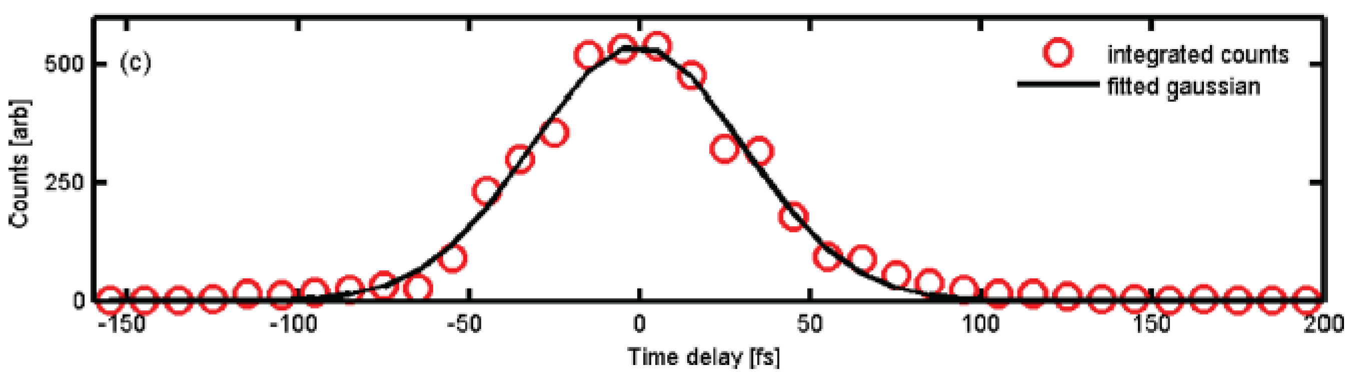

Temporal response

200 gr/mm grating, ≈70 fs FWHM @36 eV

Double-grating design

Scheme for path length equalization: the mechanism which originates the path difference, hence the pulse-front tilt, must be canceled.

- equalization of path length for different rays at the same wavelength
- combination of two diffractive elements in negative dispersion
- correction of the optical aberrations

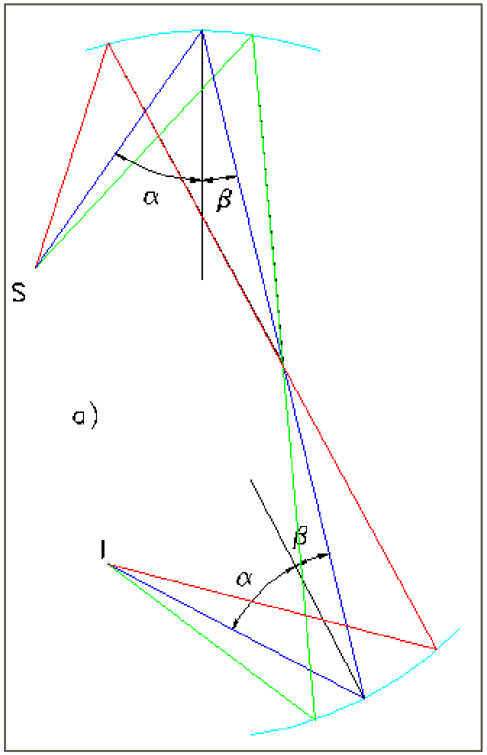

Double-grating monochromators have already been realized for high-order laser harmonics, showing instrumental response of ≈10 fs in the XUV (30-40 eV range)

P. Villoresi, Appl. Opt. **38,** 6040 (1999)

L Poletto, Appl. Phys. B **78**, 1009 (2004)

L Poletto and P. Villoresi, Appl. Opt. **45**, 8577 (2006)

Double-grating design with toroidal gratings

The double-grating design has been realized in a moderate grazing-incidence set-up (142° deviation angle)

Compensation of the pulse-front tilt to 11 fs at 32.6 eV (38 nm, H21) has been demonstrated

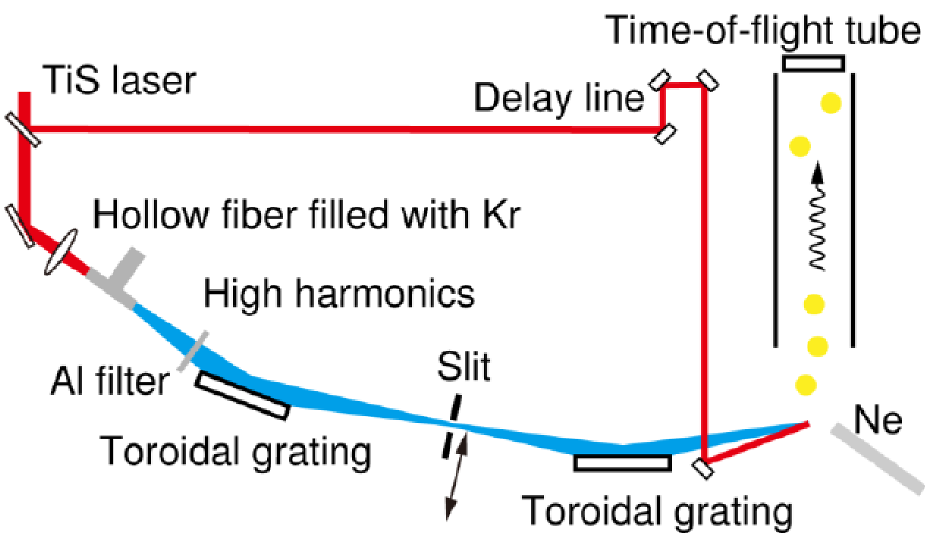

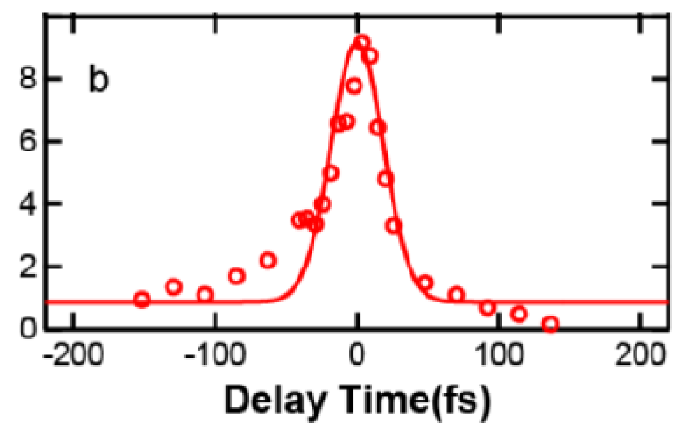

M. Ito et al, Opt. Express 18, 6071 (2010)
H. Igarashi et al, Opt. Express 20, 3725 (2012)

Double-grating design in the off-plane mount

DOUBLE-GRATING CONFIGURATION
The two gratings are mounted in COMPENSATED CONFIGURATION and SUBTRACTIVE DISPERSION.

Time compensation
1) the differences in the path lengths of rays with the same wavelength that are caused by the first grating are compensated by the second grating
2) rays with different wavelengths within the spectrum of the pulse to be selected are focused on the same point

Focusing
The focusing is provided by the toroidal surfaces

Spectral selection
A slit placed on the intermediate focus carries out the spectral selection of the HHs

Wavelength scanning
The wavelength scanning is performed by rotating the gratings around an axis tangent to the surface and parallel to the grooves

Double-grating design in the off-plane mount

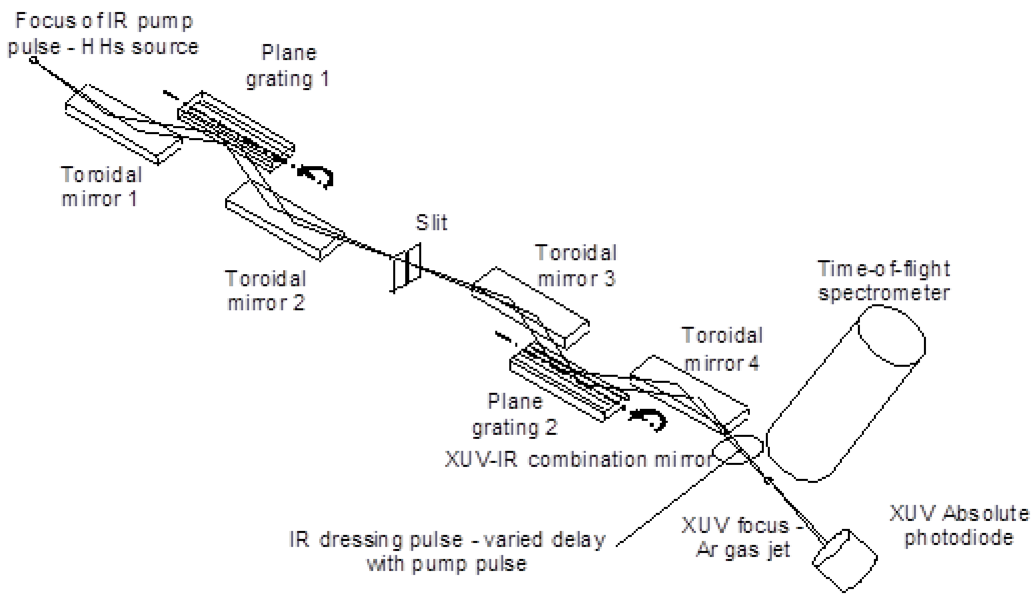

The double-grating design has been realized in the off-plane mounting.

Compensation of the pulse-front tilt down to 8 fs at H23 has been measured

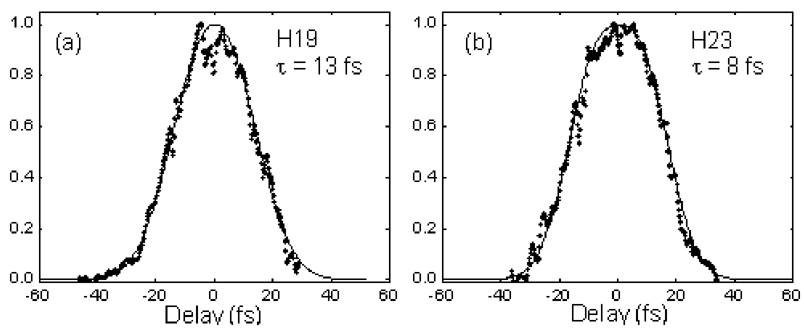

L. Poletto, Appl. Phys. B **78,** 1013 (2004)
L. Poletto and P. Villoresi, Appl. Opt. **45,** 8577 (2006)
L. Poletto, Appl. Opt. **48,** 4526 (2009)

Effect of the monochromator on ultrafast pulses

The temporal response of the monochromator is evaluated considering two effects on the ultrafast pulse given by the time-delay-compensating configuration

1. Compensation of the pulse-front tilt, i.e., ***all the rays emitted by the source in different directions at the same wavelength have to travel the same optical path***. Ideally the compensation is perfect for a double-grating configuration, although aberrations may give a residual distortion of the pulse-front.

2. Group delay introduced by the two gratings, i.e., ***different wavelengths within the bandwidth transmitted by the slit travel different paths***, similarly to grating pulse shapers for the visible range. Within the output bandwidth, the optical path decreases linearly with the wavelength and this forces the group delay dispersion to be almost constant and positive.

L. Poletto and F. Frassetto, Applied Sciences **2018**, 8, 1-9 (2018)

Gratings for pulse compression

Chirped-pulse amplification for FELs

Solid-state laser: frequency chirping is employed to stretch a short pulse before amplification. This mitigates the problem of phase distortion in the amplification medium. After pulse amplification, the chirp is compensated in order to recover short pulses and high power.

CPA in seeded FEL's: the seed pulse is stretched in time before interacting with the electron beam. This allows to induce bunching on a larger number of electrons, and to linearly increase the output energy of the generated pulse. The chirp carried by the phase of the seed pulse is transmitted to the phase of the FEL pulse. Compensating the chirp of the FEL pulse allows to recover a **short pulse** and a **high peak power**.

Grating compressor

The first grating disperses the beam, therefore different wavelengths travel in different directions and with different optical paths, but also introduces a pulse-front tilt because of diffraction. The second grating compensates for the spectral dispersion, therefore all the wavelengths at the output have the same direction than the input, and for the pulse-front tilt. Two additional plane mirrors are required to translate the output beam as the input.

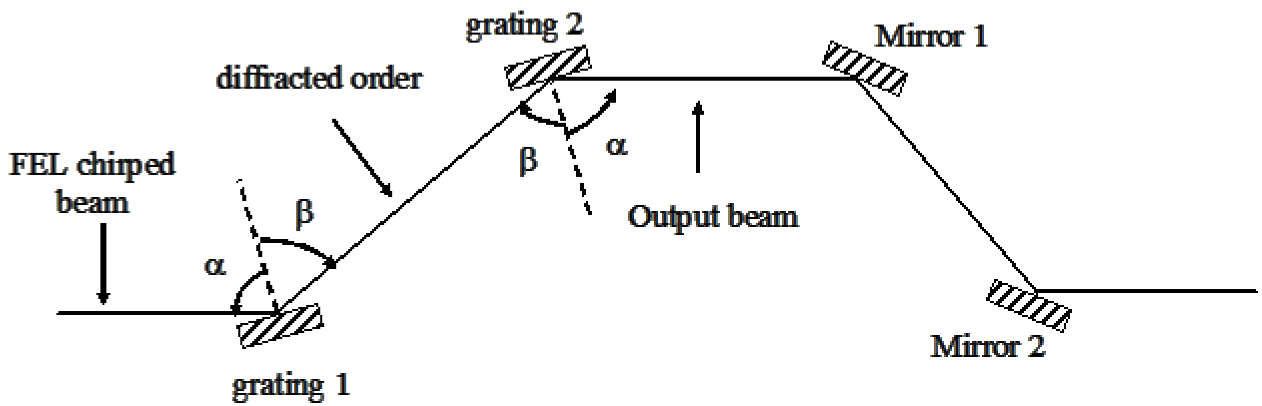

$$OP(\lambda) = q\lambda_c \left(\frac{\sigma}{\cos \beta_c} \right)^2 \Delta\lambda$$

Optical path varies with the wavelength ⇒ negative dispersion

F. Frassetto and L. Poletto, Appl. Opt. **54**, 7985 (2015)

The experiment at FERMI (1)

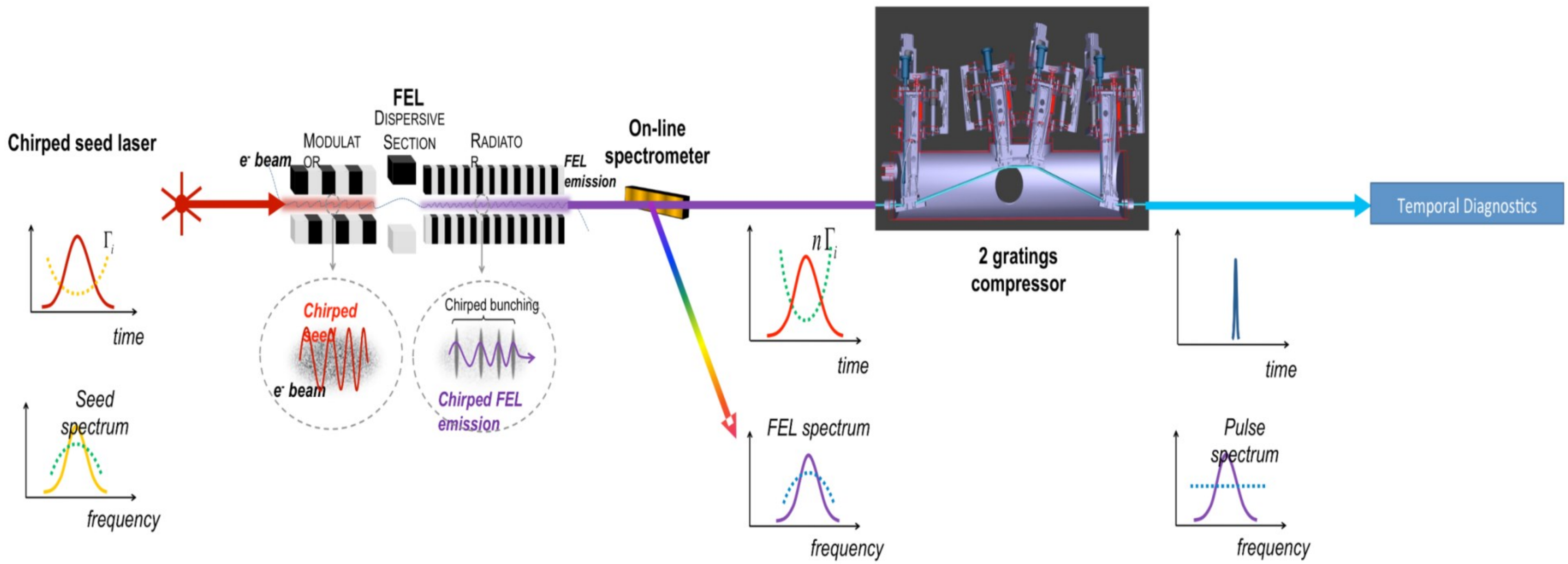

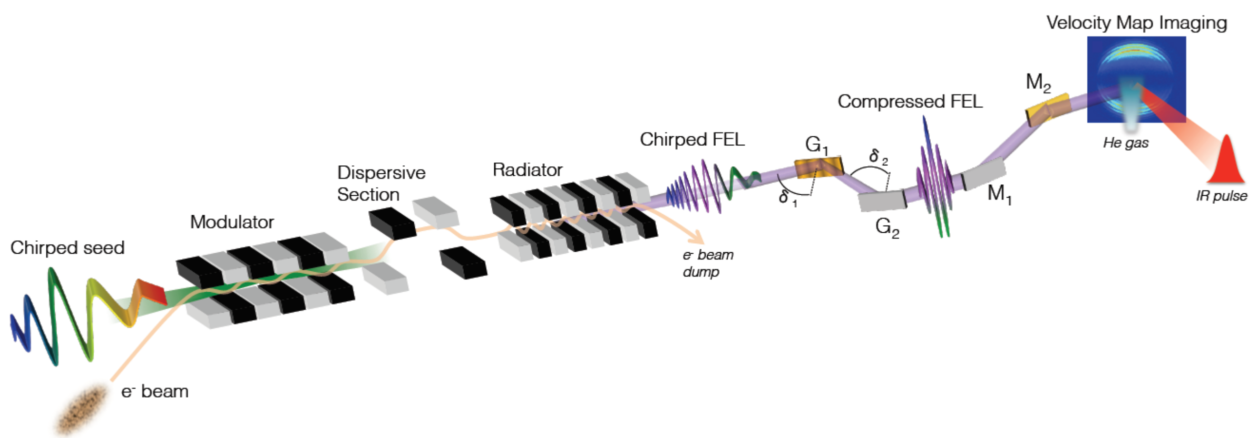

FEL tuned at 37.3 nm

FEL pulse duration measured through IR-XUV cross-correlation

Seeding laser duration: 170 fs (no chirp)

Standard FEL pulse measured to be 91 fs

The experiment at FERMI (2)

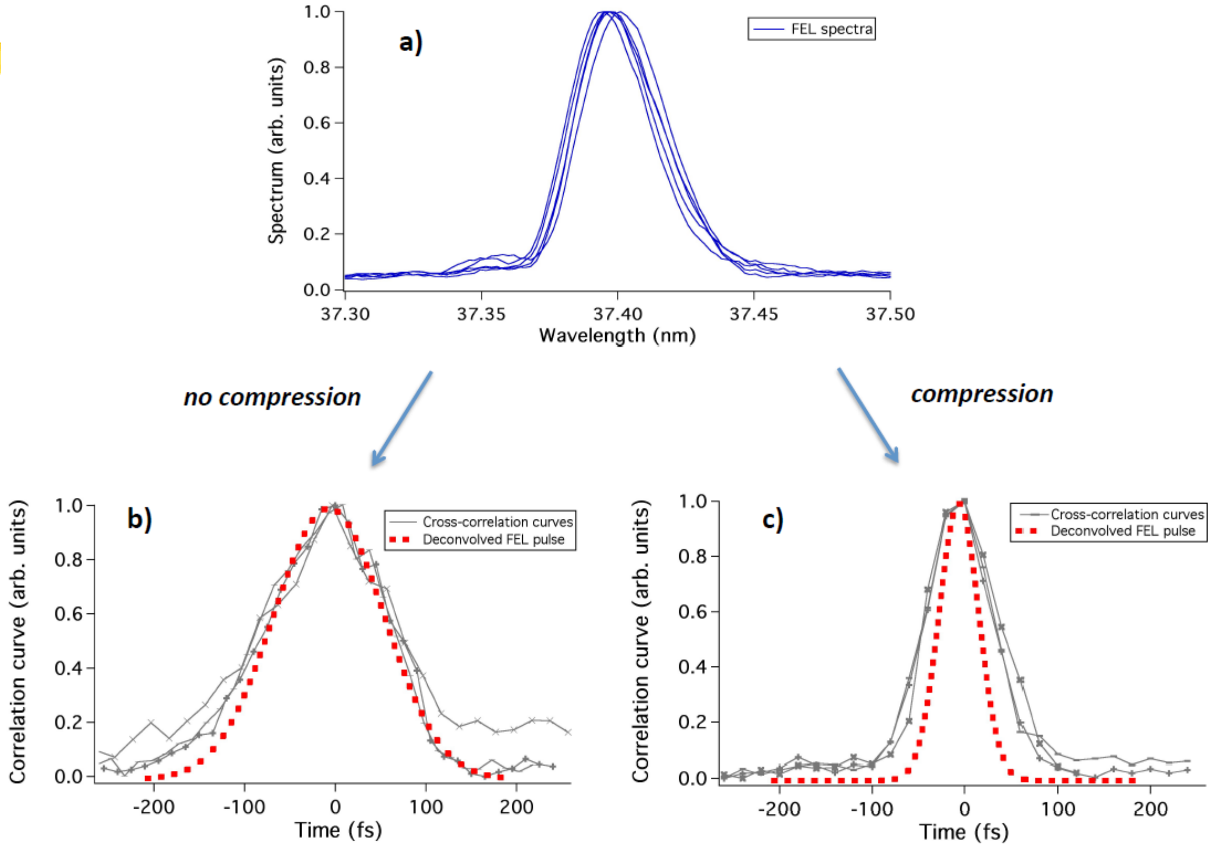

Seeding laser duration with chirp: 290 fs

FEL duration before compression: 143 fs

FEL duration after compression: 50 fs (40 fs Fourier limit)

D. Gauthier et al, Nat. Comm. **7**, 13688 (2016)

Multilayer mirrors

Operation at normal incidence

Operation at normal incidence is preferred for optical systems:

- Low aberrations
- Large collecting angle
- Small optics

Unfortunately, XUV reflectivity of a single layer at normal incidence is very low.

50 nm wavelength	
Platinum	0.18
Silicon	0.006

20 nm wavelength	
Platinum	0.01
Silicon	0.0001

What can be done to operate at normal incidence with high efficiency ?

What is a multilayer?

- Multilayer is a nanostructured stack based on two or more materials
- The layer thickness is regulated in such a way that all the reflected component at each interface add in phase
- A capping layer (i.e. structure on top of it) can be deposited to improve performances or for protection

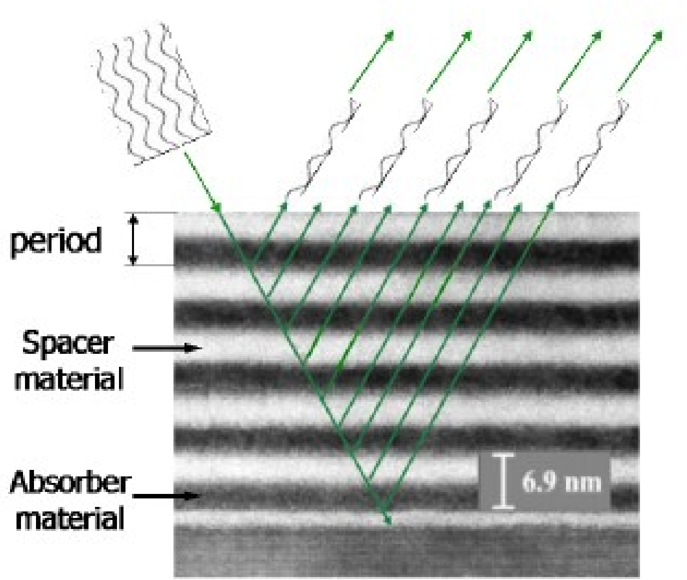

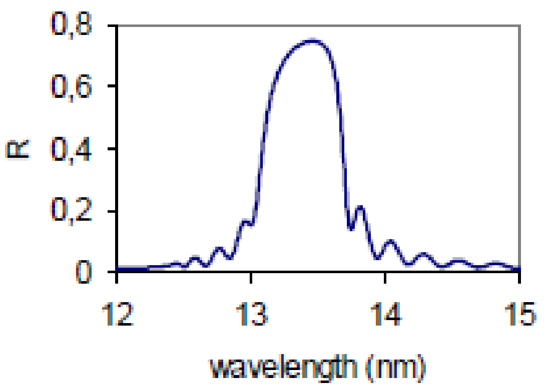

Applications

Lithography

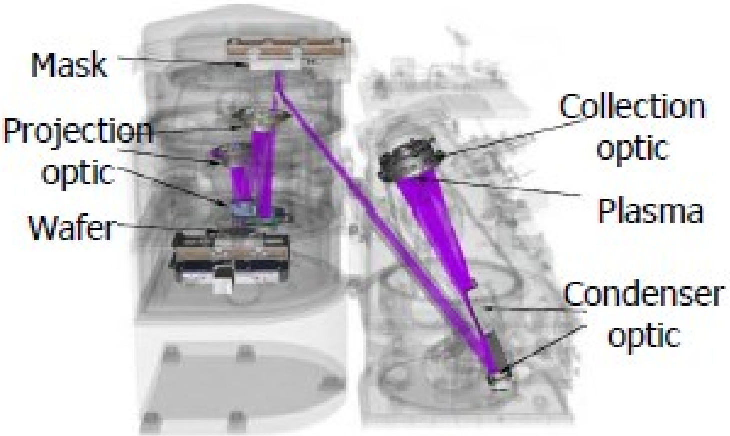

Atto-physics

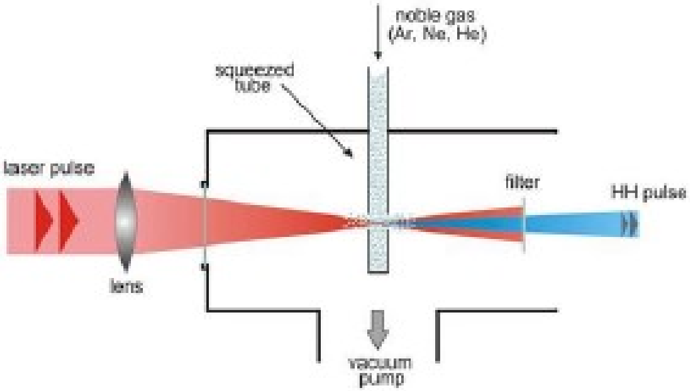

Solar observations from space

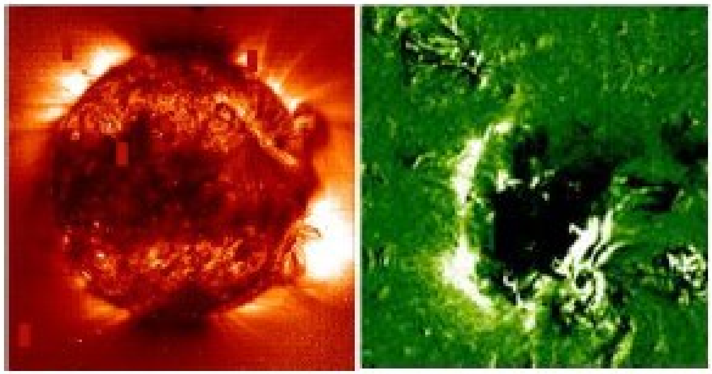

EUV Large scale facilities

Definitions

- **Periodic ML:** structure based on the repetition of a couple of materials deposited using the same layer structure
- **A-periodic ML:** the materials are deposited alernatively, but with different layers
- **Spacer**: material with low absorption
- **Absorber:** material with high absorption
- **Γ** (gamma): ratio between spacer layer and ML period d
- **Capping-layer**: external layers of the structure
- **Barrier layer**: thin layers deposited between the spacer and the absorber to decrease roughness and interdiffusion

Definitions

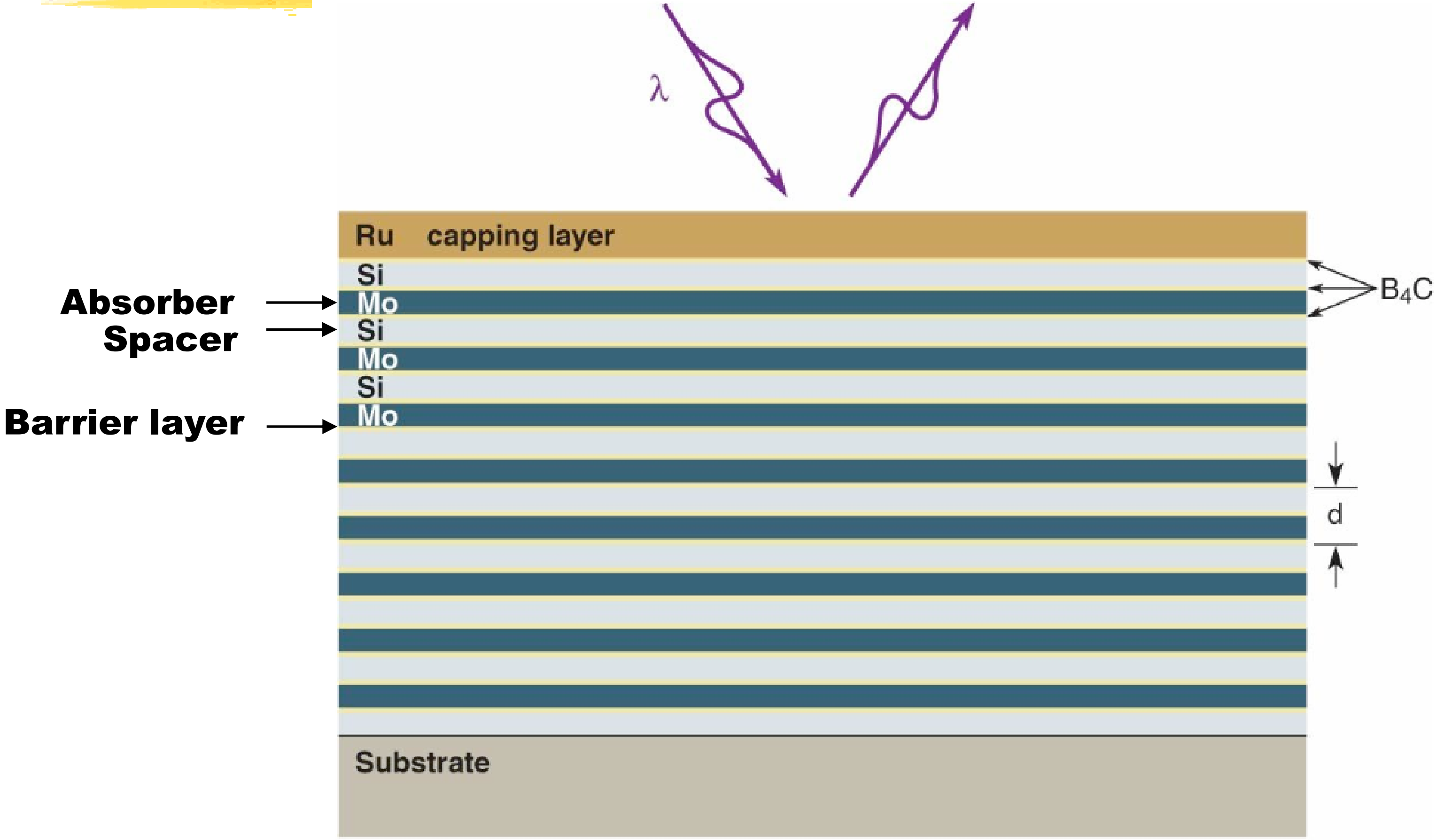

λ = 13.4 nm

Ru (1.70 nm)
Si (4.14 nm)
B_4C (0.25 nm)
Mo (2.09 nm)
B_4C (0.40 nm)

d = 6.88 nm
Γ = 0.34

Multilayer mirrors satisfy the Bragg condition

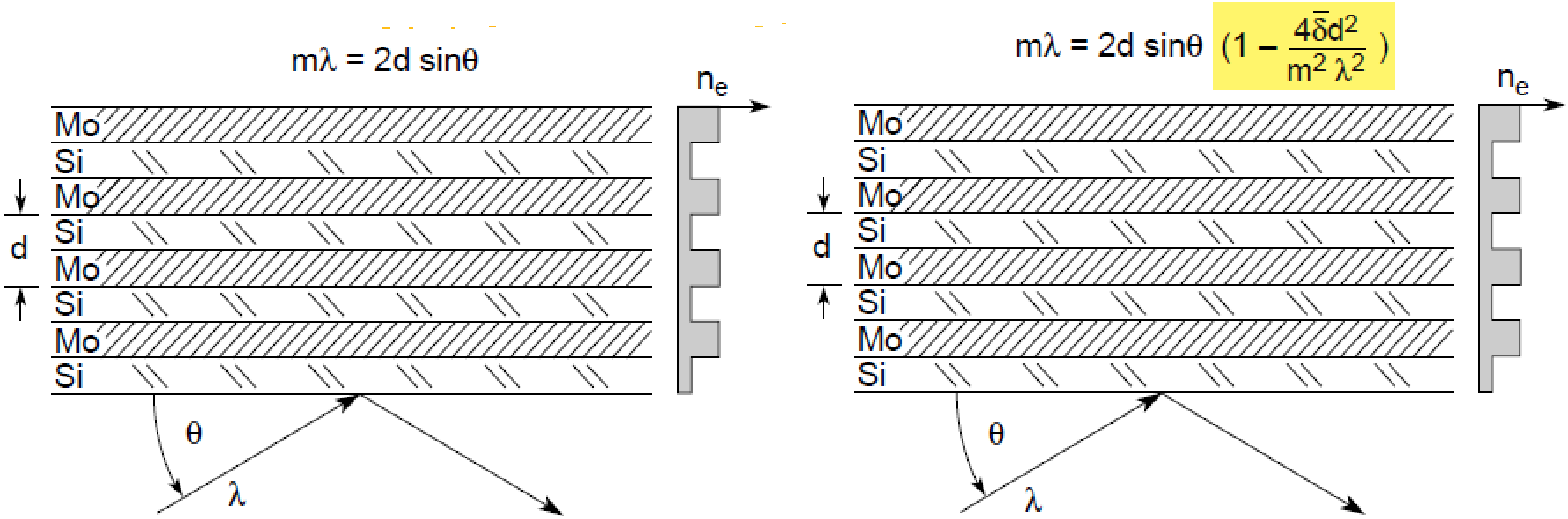

For normal incidence, $\theta = \pi/2$, first order ($m = 1$) reflection

$\lambda = 2d$

$d = \lambda/2$

Just as Bragg's law describes the condition for constructive interference of X-rays in a crystal, the same law describes the condition for constructive interference in a multilayer film (operating in first order): $\lambda=2d\sin\theta$.

Near normal incidence (θ~90°) Bragg's law tells us that the multilayer period d is approximately equal to half the photon wavelength.

Materials and Fresnel diagram

Materials used for ML should satisfy the following criteria:

- Lowest absorption of spacer
- Highest optical contrast between absorber and spacer
- Low chemical reactivity and reactivity with oxygen
- Deposition in smooth layers (amorphous phase)
- No toxic elements

Typical materials

2-4 nm	13 nm	19 nm	30.4 nm
Sc	a-Si	Al	Si
W	Ru	a-Si	a-C
Cr	Mo	Se	B_4C
B_4C	Rh	Ac	Si
	Nb	Mo	Al
		Nb	Mo
		a-C	

Fresnel diagram

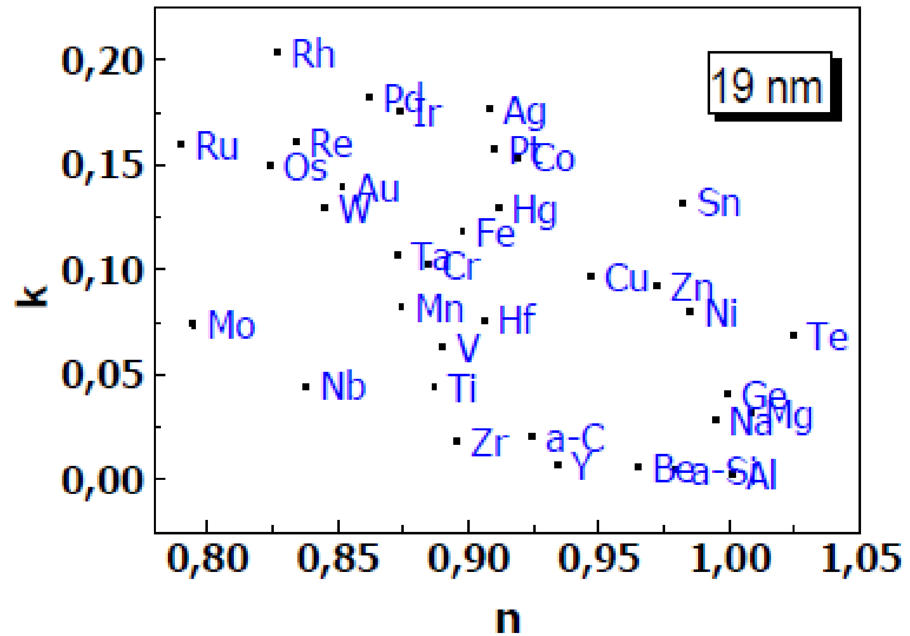

Roughness and interdiffusion

Table 1. Mo/Si and Ir/Si Multilayer Design Parameters

Materials	Multilayer	Capping Layer
Si/Mo	$d = 16.40\,\mathrm{nm}\Gamma = 0.82\ N = 30$	Si (1 nm)
Ir/Si	$d = 16.84\,\mathrm{nm}\Gamma = 0.28\ N = 30$	Ir (2.2 nm) Si (13.5 nm)

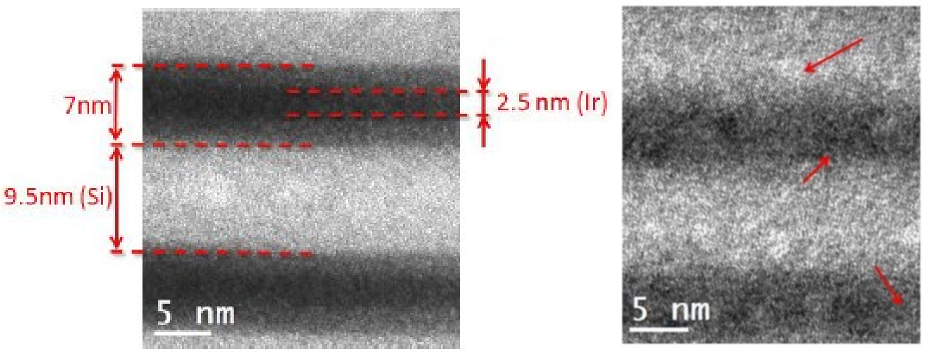

P. Zuppella et al, Optics Letters 36, 1203 (2011)

- Interdiffusion and substrate roughness during the deposition give a rough interface between layers
- Reflectivity is decreasing

Mo-Si ML (simulation)
d=6.9 nm
Γ=0.4
Normal incidence

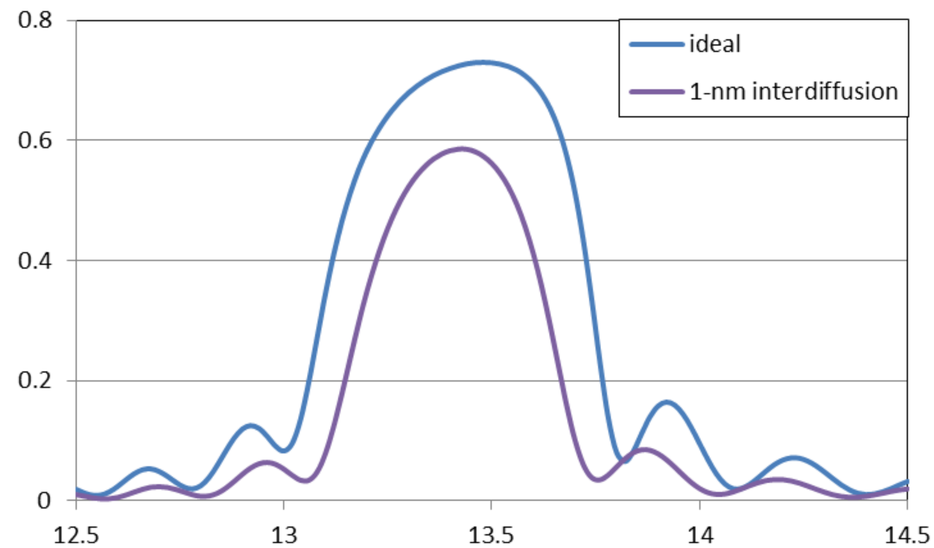

State of art

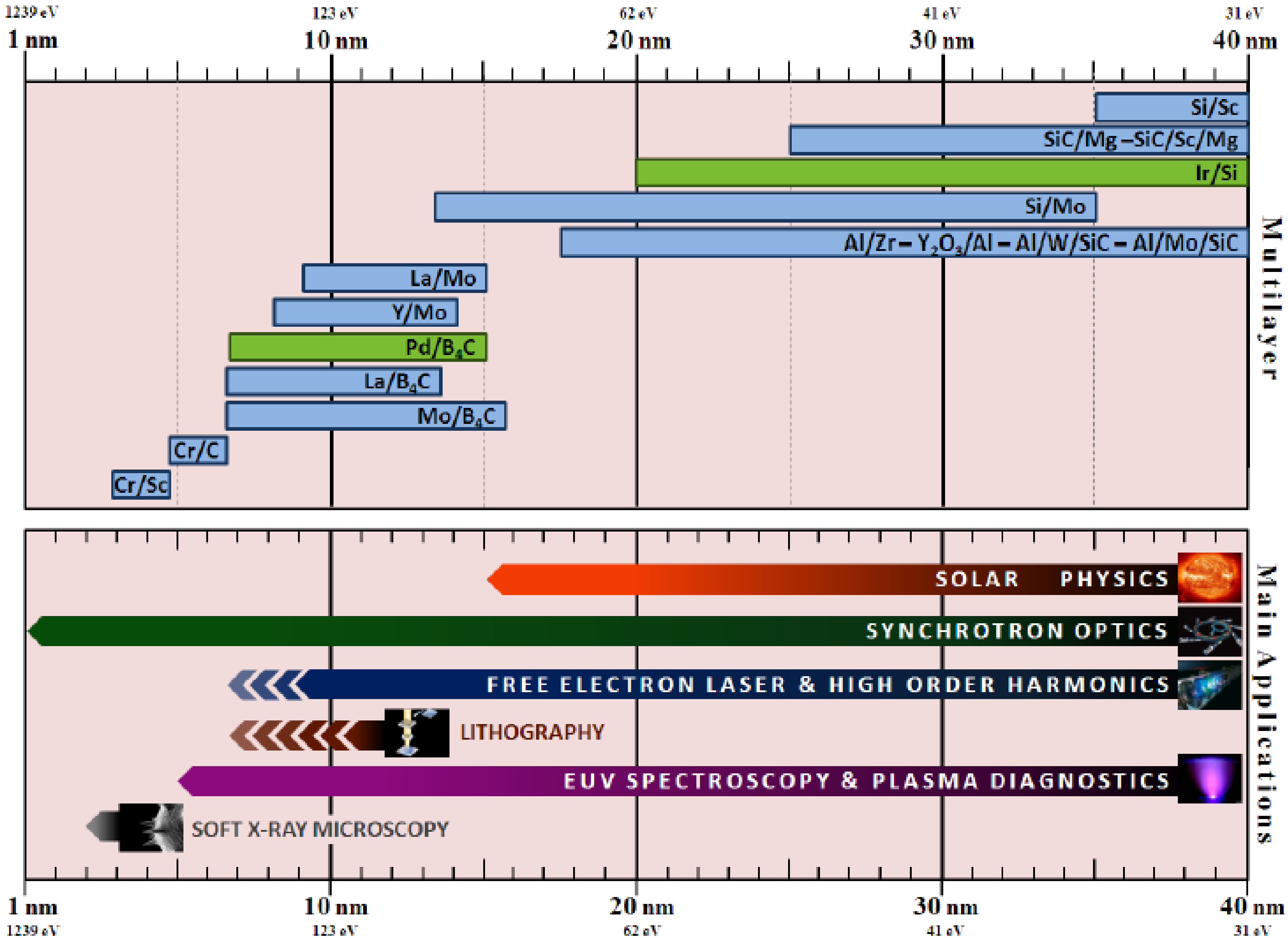
1239 eV
123 eV
62 eV
41 eV
31 eV
1 nm
10 nm
20 nm
30 nm
40 nm
Si/Sc
SiC/Mg –SiC/Sc/Mg
Ir/Si
Si/Mo
Al/Zr – Y_2O_3/Al – Al/W/SiC – Al/Mo/SiC
La/Mo
Y/Mo
Pd/B_4C
La/B_4C
Mo/B_4C
Cr/C
Cr/Sc
Multilayer
SOLAR PHYSICS
SYNCHROTRON OPTICS
FREE ELECTRON LASER & HIGH ORDER HARMONICS
LITHOGRAPHY
EUV SPECTROSCOPY & PLASMA DIAGNOSTICS
SOFT X-RAY MICROSCOPY
Main Applications

Example: XUV lithography

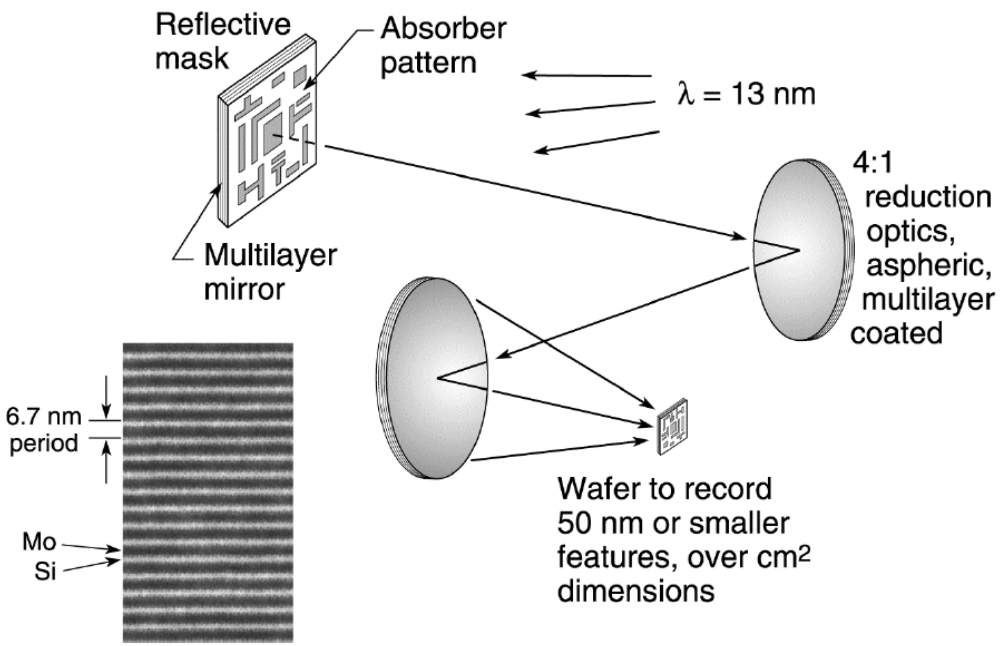

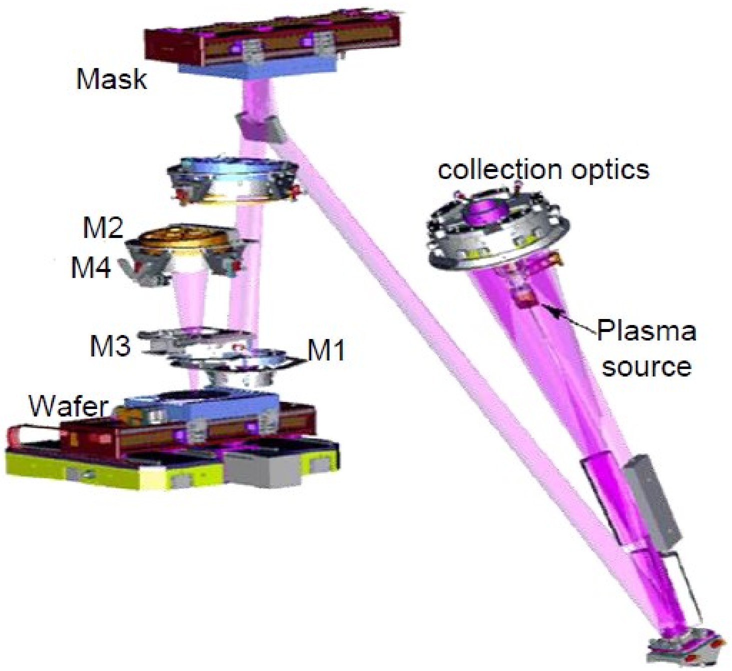

Engineering Test Stand from Extreme Ultraviolet Limited Liability Company (USA)

Example: XUV lithography

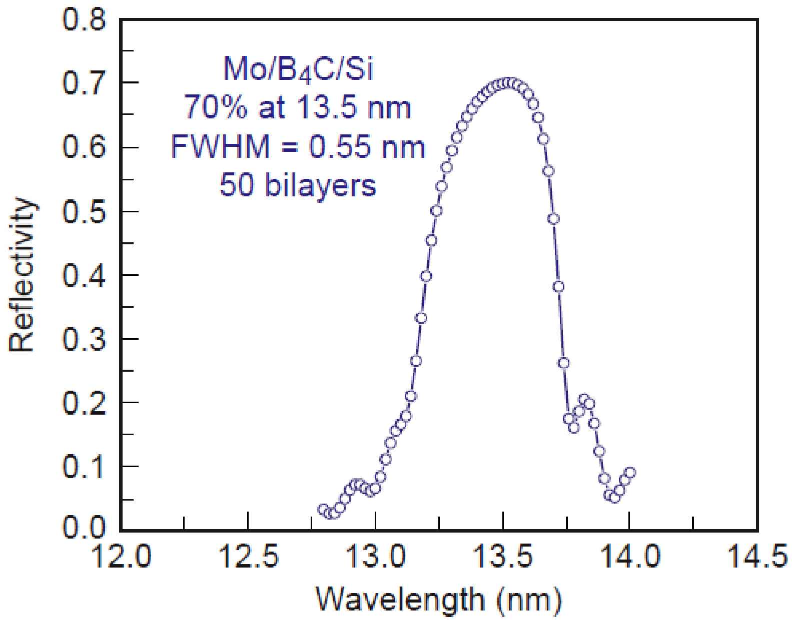

The XUV lithography is realized at **13.5 nm** because of high reflectivity of available ML mirrors

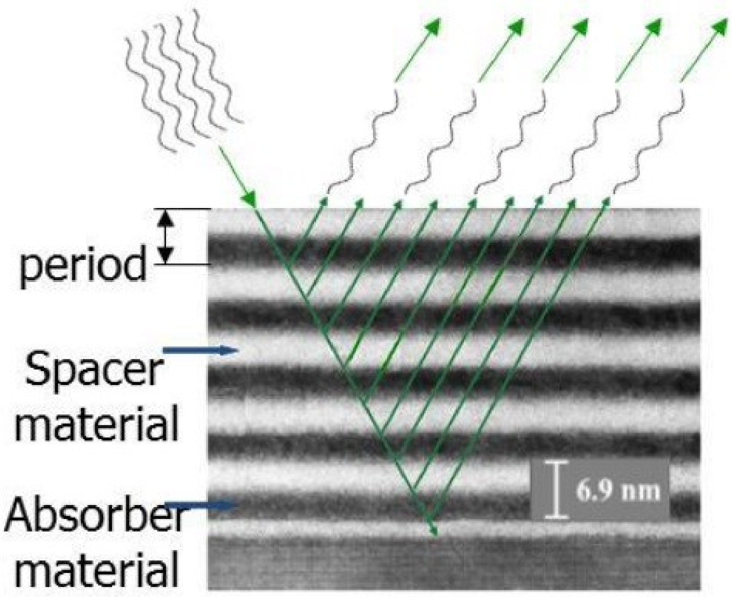

Example: space applications in the XUV

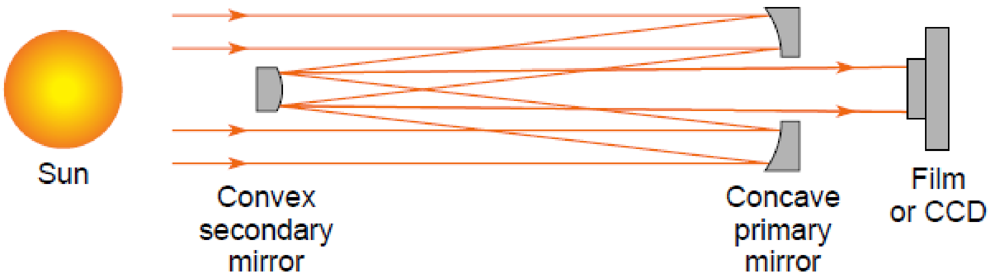

Cassegrain telescope

The solar disk at 28.4 nm, SOHO-EIT (Fe XV)

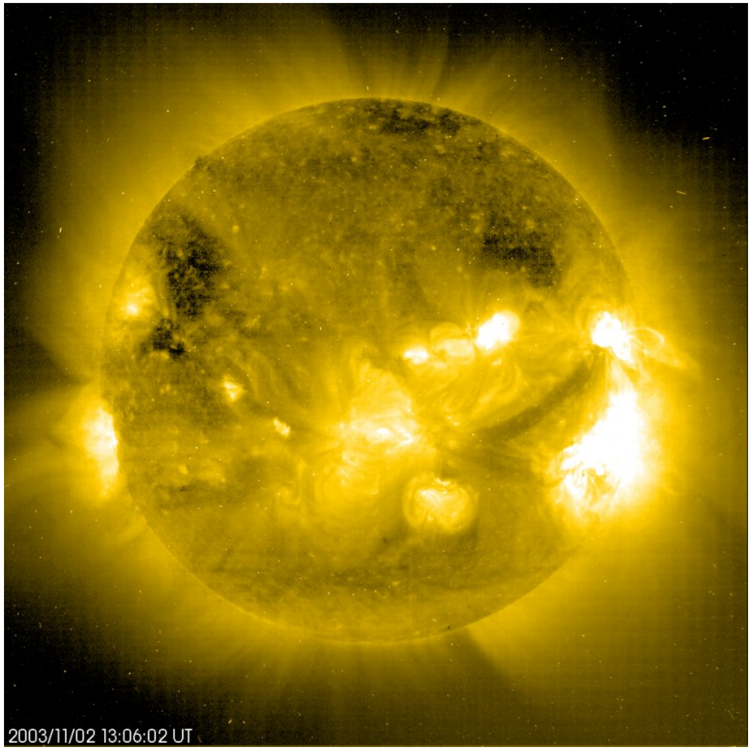

Coronal loop at 17.1 nm, TRACE (Fe IX)

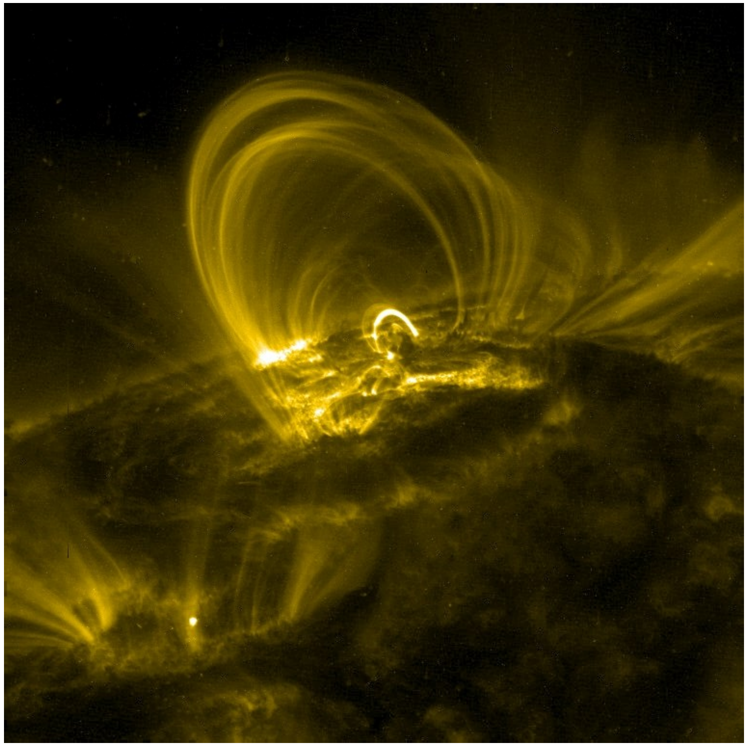

Example: space application in the X-rays

NUSTAR NASA mission

X-ray Wolter-type telescope

133 shells

3-79 keV photons

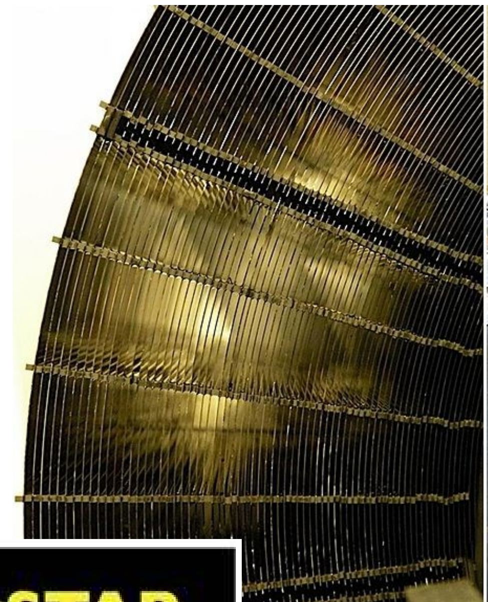

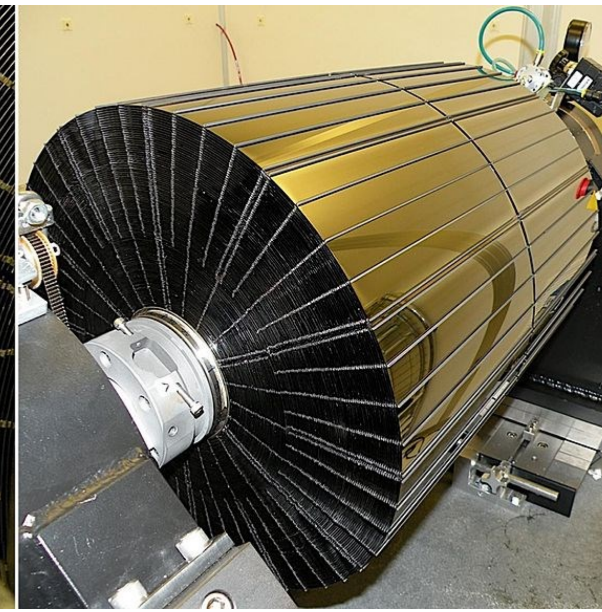

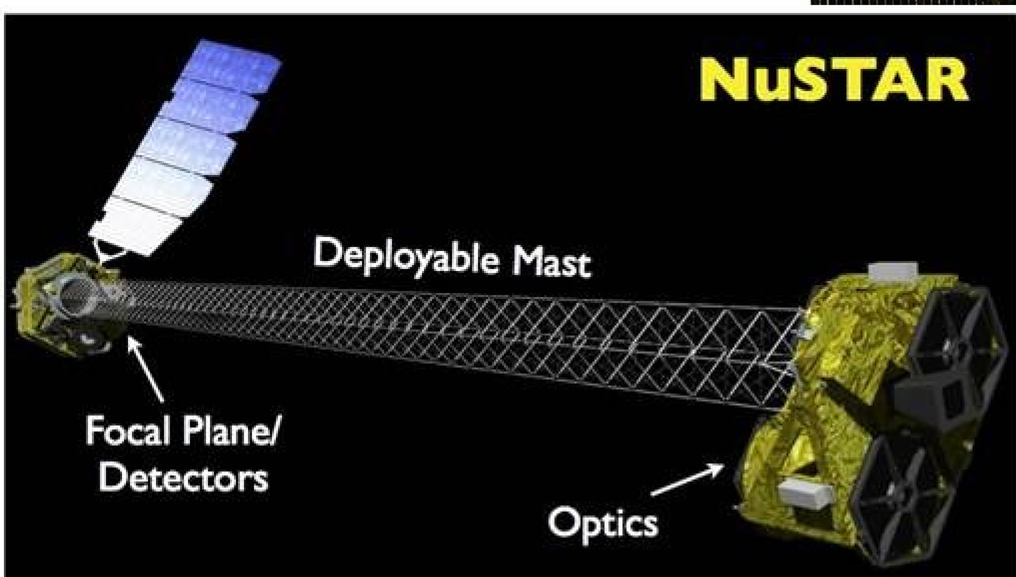

Tight focusing of HHs with ML-coated optics

Multilayer-coated optics at normal incidence have been used to focus HHs to 1-um spot size

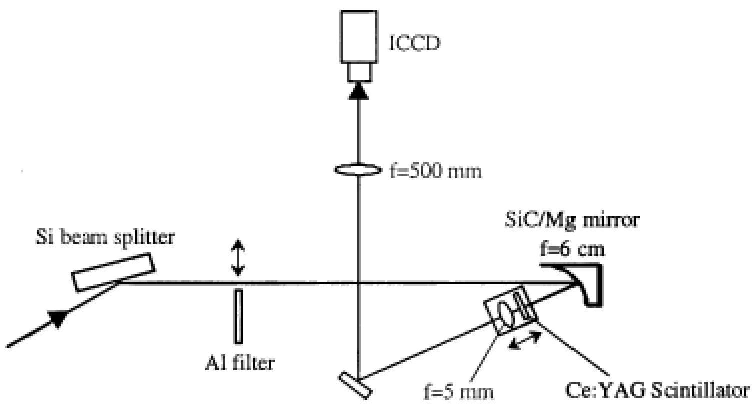

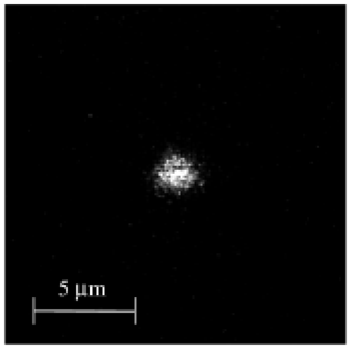

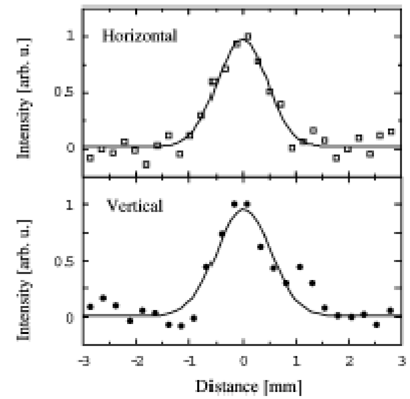

ML coated off-axis parabola, 6-cm focal length

Mashiko et al, Opt. Lett. 29, 1927 2004

Narrow-band ML for the isolation of a single harmonics

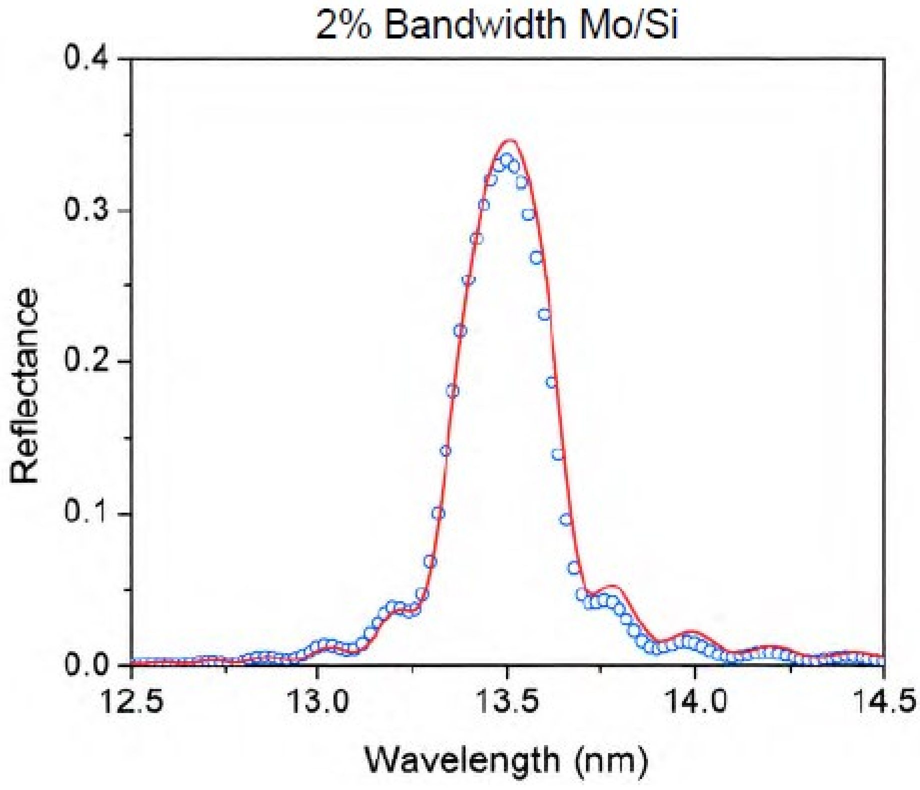

ML to generate attosecond pulses

XUV excitation pulses generated from neon atoms ionized by an 5-fs linearly polarized laser pulse.

Proper adjustment of the laser peak intensity yielded highest-energy (cutoff) XUV emission in the high-reflectivity band of a Mo/Si multilayer mirror, which is used to spectrally confine and focus the XUV pulses. The cutoff emission is confined to the vicinity of zero transition(s) of the laser electric field after the most intense half-cycle(s) in a few-cycle driver.

250-as single pulses have been generated.

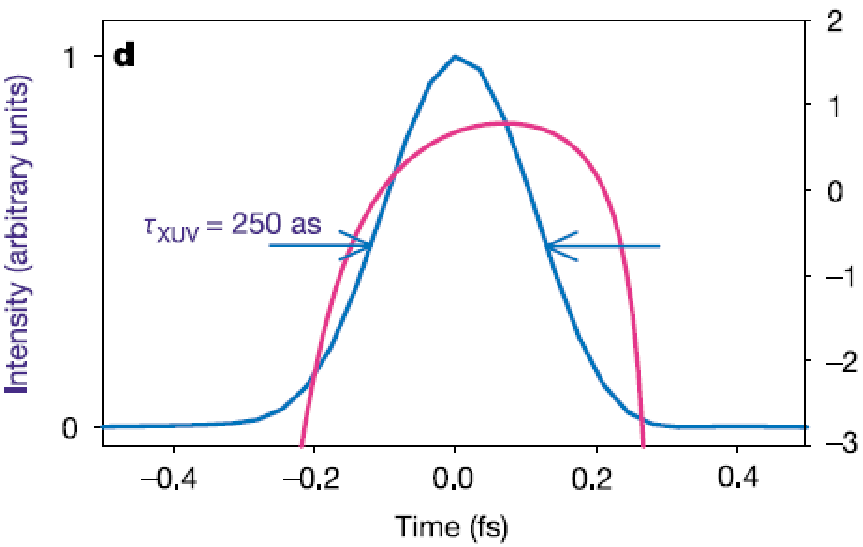

R. Kienberger et al, Nature 427, 817, 2004

Aperiodic ML

Aperiodic multilayers are typically used to achieve broad spectral response at a fixed incidence angle. The individual layer thicknesses are specified numerically.

Performance of an aperiodic Al/Zr multilayer designed for high reflectance at normal incidence from 171 Å to 211 Å, to be compared with the reflectivity curves for the periodic Si/Mo multilayers used for the Hinode/EIS instrument on SOLAR-B and the TXI sounding rocket instrument.

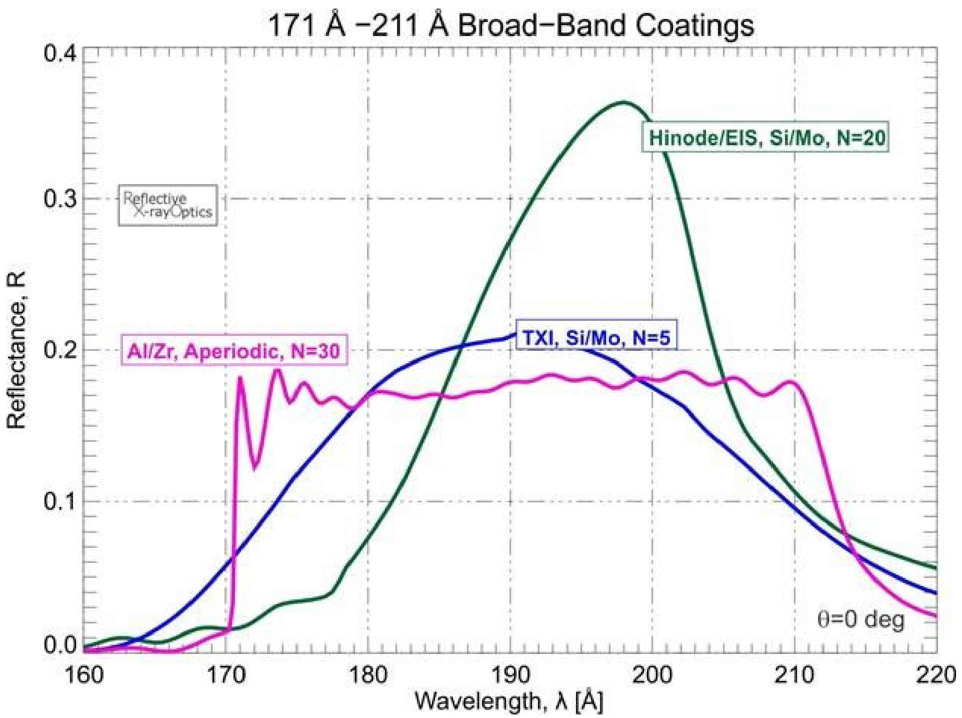

Aperiodic ML to compensate the attochirp

Controlled isolation of a single energetic harmonic pulse requires control of the amplitude of spectral components of the emitted XUV radiation over a broad spectral range. Furthermore, transform-limited XUV pulse production calls for precise control of the phase over the spectral band.

Such a phase control has been demonstrated by utilizing the dispersion of materials near electronic resonances (R. Lopez-Martens et al, Phys. Rev. Lett. 94, 033001, 2005; Sansone et al, Science 314, 443, 2006).

By analogy with broadband dispersion control of optical pulses with chirped multilayer dielectric mirrors, chirped ML mirrors have been proposed and developed for the same purpose in the XUV (A.-S. Morlens et al, Opt. Lett. 30, 1554, 2005; A. Wonisch et al, Appl. Opt. 45, 4147, 2006; M. Schultze et al, New J. Phys. 9, 243, 2007).

Simulations

The electric field of the incident pulse E(t) is Fourier transformed to obtain the spectral composition $E(\omega)$ of the pulse.

Each Fourier component is multiplied by the complex amplitude reflectivity $r(\omega)$ of the ML. To obtain the field of the reflected pulse, an inverse Fourier transform is performed on $E'(\omega)= E(\omega)\, r(\omega)$.

The complex-amplitude reflectivity $r(\omega)=|r(\omega)|\exp[-i\varphi(\omega)]$ with $\varphi(\omega)$ as the phase shift $\varphi(\omega)$ is calculated by a recursive Fresnel equation code by using the atomic scattering factors for the layer materials.

The pulse duration of the reflected pulse can be determined by calculating the FWHM of the pulse intensity envelope $I(t)=E(t)^2$

The two main parameters for designing a chirped mirror that can compress HH pulses are a large bandwidth and a negative GDD.

Results (1)

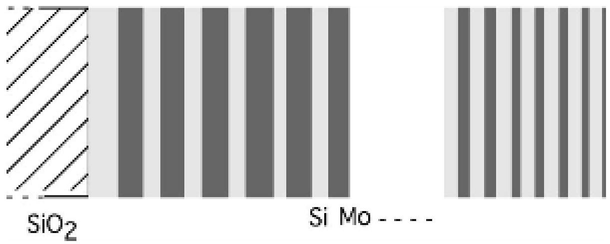

Fig. 2. Designed chirped mirror consisting of alternating Si (light gray) and Mo (dark gray) deposited on a SiO_2 substrate.

A.S. Marlens et al, Opt. Lett. 30, 1554, 2005

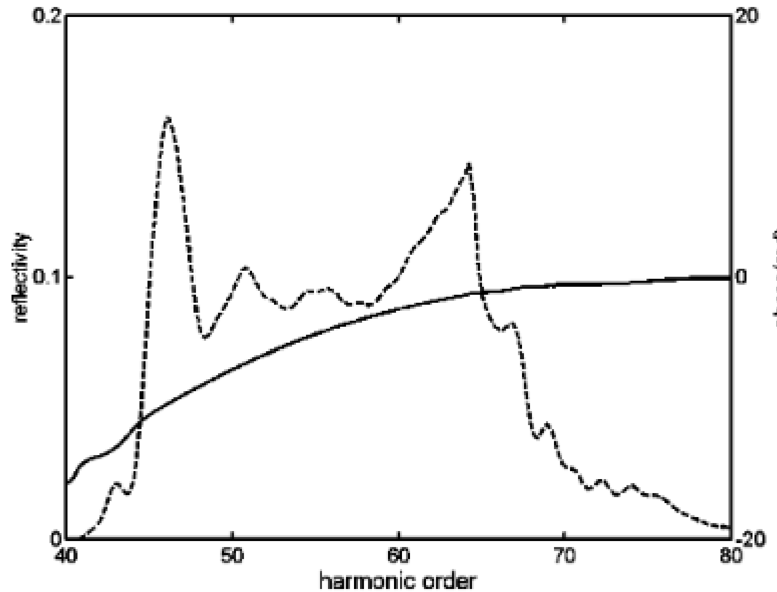

Fig. 3. Reflectivity (dashed curve) and phase (solid curve) at normal incidence for the chirped mirror represented in Fig. 2.

H25-H61, GDD = 10,000 as^2 at 5 10^{14} W cm^{-2}

H25-H101, GDD = 6,500 as^2 at 7.5 10^{14} W cm^{-2}

Results (2)

ML coating for reflection of attosecond pulses:

● Large bandwidth: for a Gaussian-shaped 100 as pulse a bandwidth of approximately 26 eV is required.

● Linear phase shift: When a nonchirped incident pulse is reflected from a multilayer coating, its duration and shape are conserved only if the multilayer has a linear phase shift

● High reflectivity

● Gaussian or rectangular reflectivity profile:

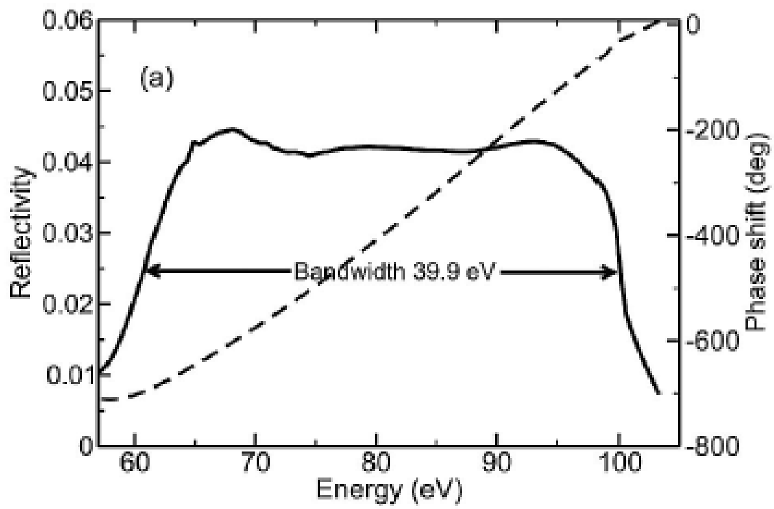

A. Wonisch et al, Appl. Opt. 45, 4147, 2006

Diffractive optics

Zone plate

A **zone plate** is a device used to focus light using diffraction.

A zone plate consists of a set of radially symmetric rings (Fresnel zones), which alternate between opaque and transparent. Light hitting the zone plate will diffract around the opaque zones. The zones can be spaced so that the diffracted light constructively interferes at the desired focus, creating an image.

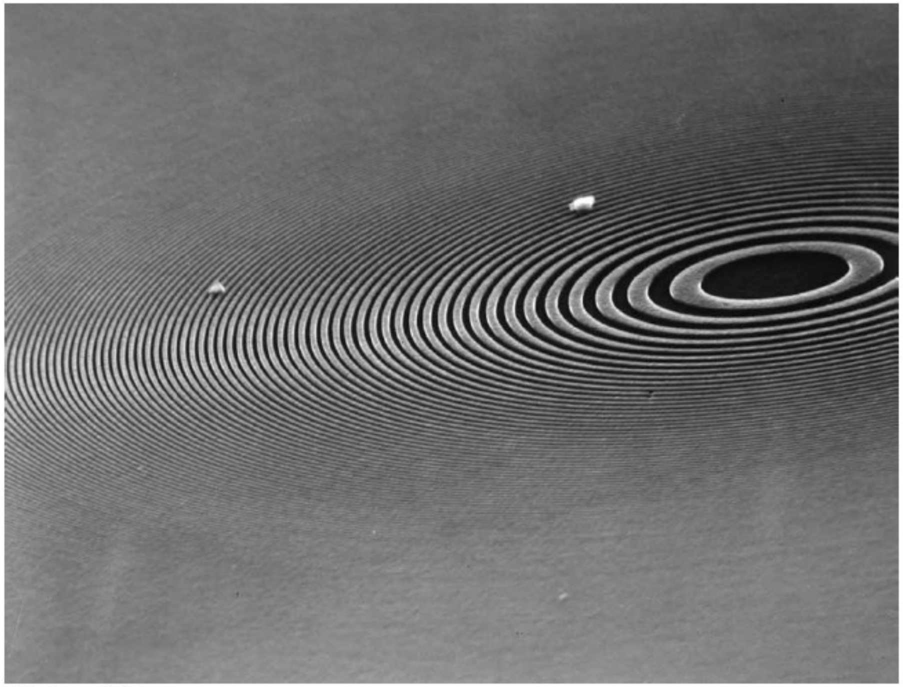

E. Anderson, LBNL

Diffractive focusing

- Selection of the paths that are added in phase with the central path
- Image formation from the contributions having path multiple of the wavelength
- Chromatic effect (strongly dependent on the wavelength)

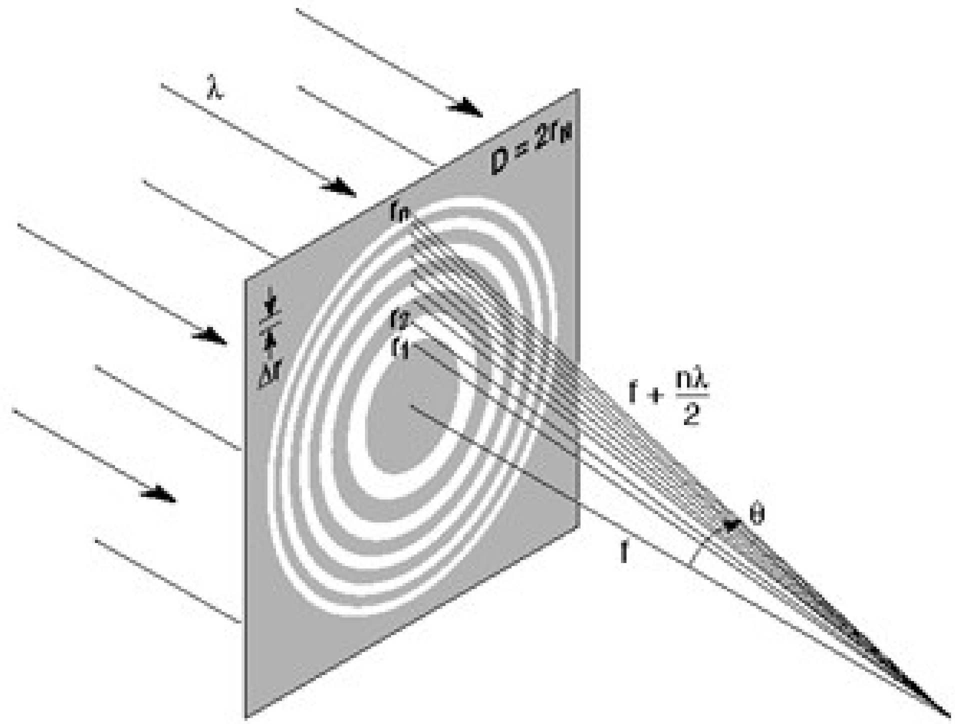

Zone plate: radius of single zones

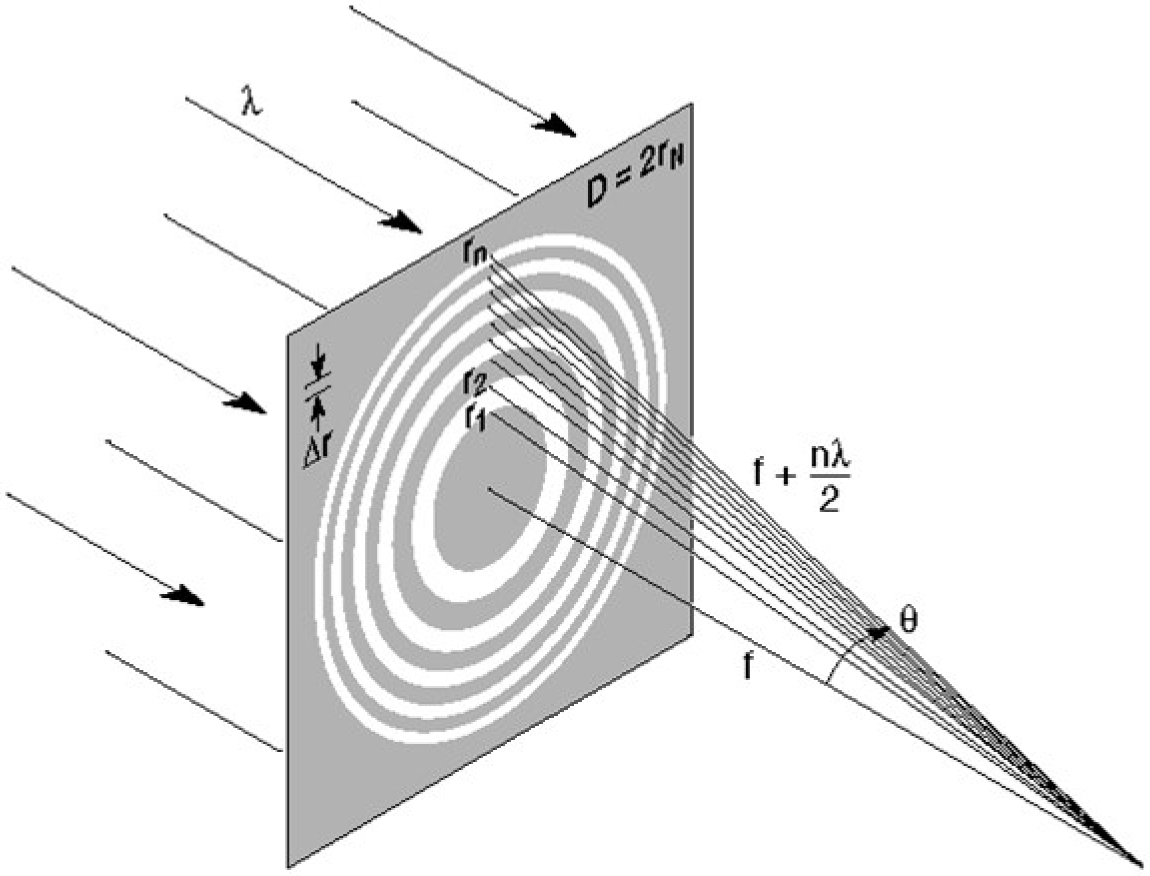

$$f^2 + r_n^2 = \left(f + \frac{n\lambda}{2} \right)^2$$

$$r_n^2 = n\lambda f + \frac{n^2\lambda^2}{4}$$

$$r_n \cong \sqrt{n\lambda f}$$

Zone plate: focal length and numerical aperture

N = number of zones

D = zone plate diameter

NA = numerical aperture

$$\Delta r \equiv r_N - r_{N-1}$$

$$2r_N \Delta r = D\Delta r \cong \lambda f \cong \frac{r_N^2}{N} = \frac{D^2}{4N}$$

$$D \cong 4N\Delta r$$

$$f \cong \frac{D\Delta r}{\lambda} = \frac{4N(\Delta r)^2}{\lambda}$$

$$NA = \frac{r_N}{f} \cong \frac{\lambda}{2\Delta r}$$

Zone plate: point by point imaging

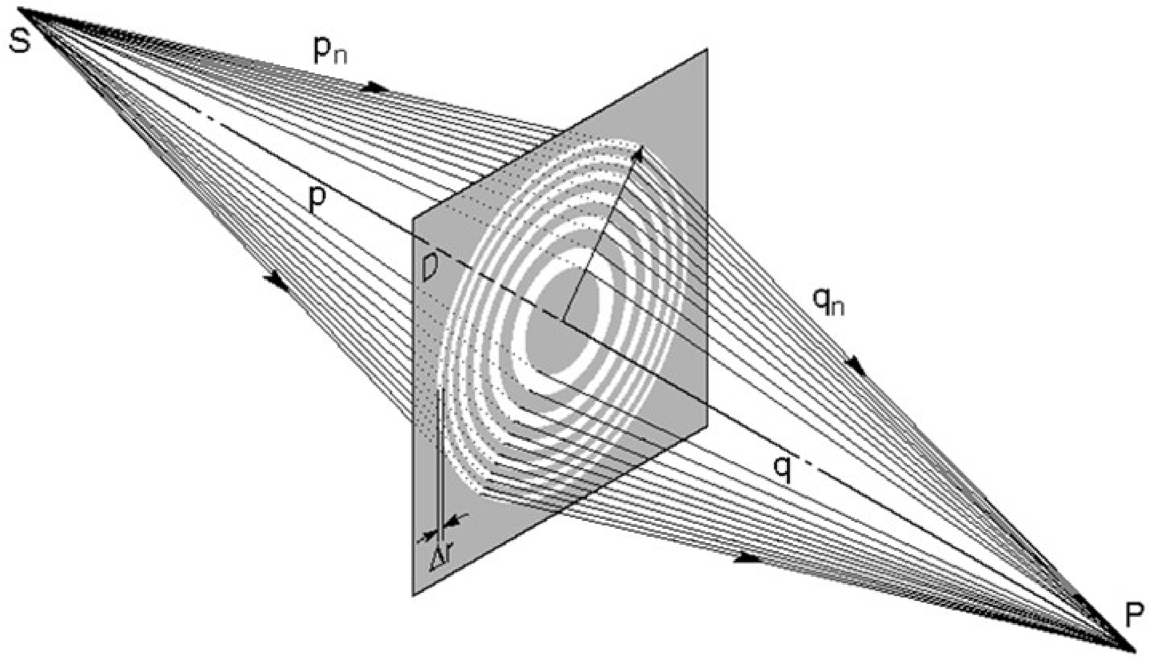

$$q_n + p_n = q + p + \frac{n\lambda}{2}$$

$$q_n = \sqrt{q^2 + r_n^2} \cong q + \frac{r_n^2}{2q}$$

$$p_n = \sqrt{p^2 + r_n^2} \cong p + \frac{r_n^2}{2p}$$

$$\frac{1}{p} + \frac{1}{q} \cong \frac{n\lambda}{r_n^2} = \frac{1}{f}$$ focusing equation

$$M = \frac{p}{q}$$ magnification

Zone plate: diffraction limit

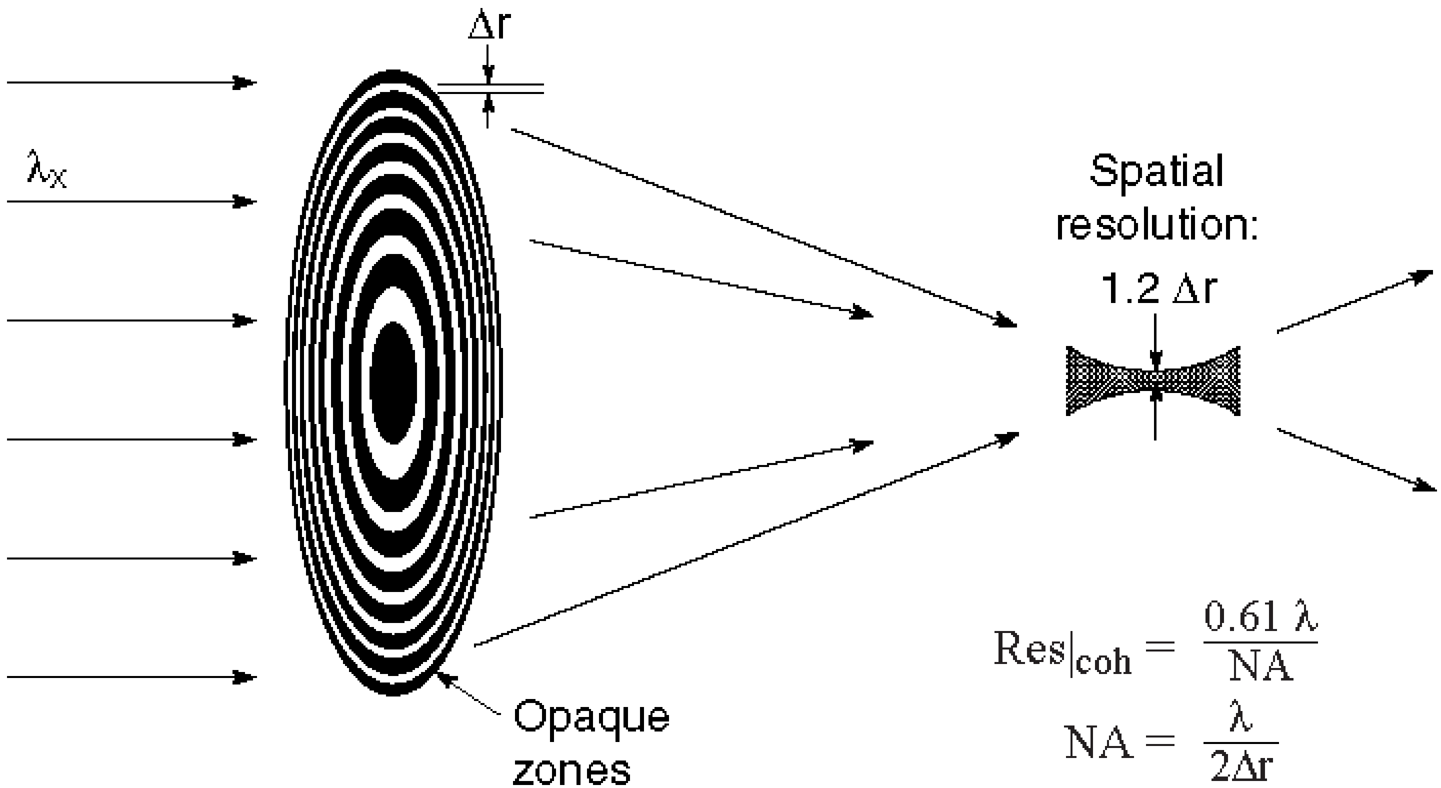

$$\mathrm{Res}|_{coh} = \frac{0.61\,\lambda}{NA}$$

$$NA = \frac{\lambda}{2\Delta r}$$

$$\therefore\ \mathrm{Res}|_{coh} = 1.22\,\Delta r$$

Some numbers

Zone Plate Formulae

$r_n^2 = n\lambda f + \dfrac{n^2\lambda^2}{4}$		$\lambda = 2.5$ nm, $\Delta r = 25$ nm $N = 618$
$D = 4N\Delta r$		63 μm
$f = \dfrac{4N(\Delta r)^2}{\lambda}$		0.63 mm
$NA = \dfrac{\lambda}{2\Delta r}$		0.05
$\text{Res.} = k_1 \dfrac{\lambda}{\text{NA}} = 2k_1\Delta r$	$k_1 = 0.61$ $(\sigma = 0)$	$1.22\Delta r = 30$ nm
$\text{DOF} = \pm \dfrac{1}{2}\dfrac{\lambda}{(\text{NA})^2}$		1 μm
$\dfrac{\Delta\lambda}{\lambda} \leq \dfrac{1}{N}$		1/700

Example: XM-1 beamline at ALS

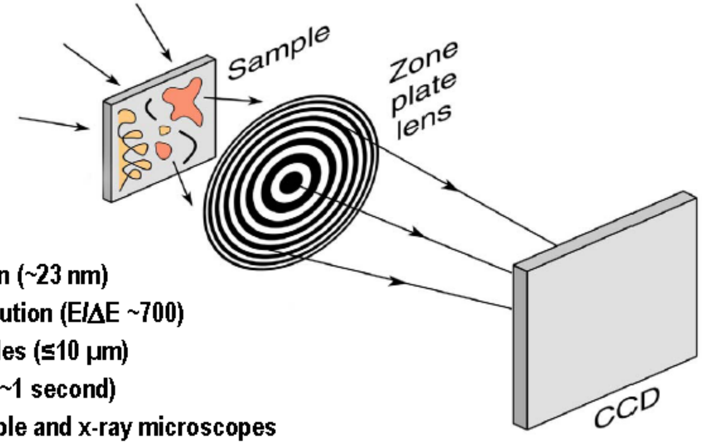

- High spatial resolution (~23 nm)
- Modest spectral resolution ($E/\Delta E$ ~700)
- Hydrated, thick samples (≤10 μm)
- Short exposure time (~1 second)
- Mutually indexed visible and x-ray microscopes
- High throughput (up to a thousand images per day)
- Large image fields by montage assembly
- Easy access, user friendly

E = 250 eV - 900 eV
λ = 1.4 nm - 5.1 nm

Courtesy of W. Meyer-Ilse and G. Denbeaux, CXRO/LBNL

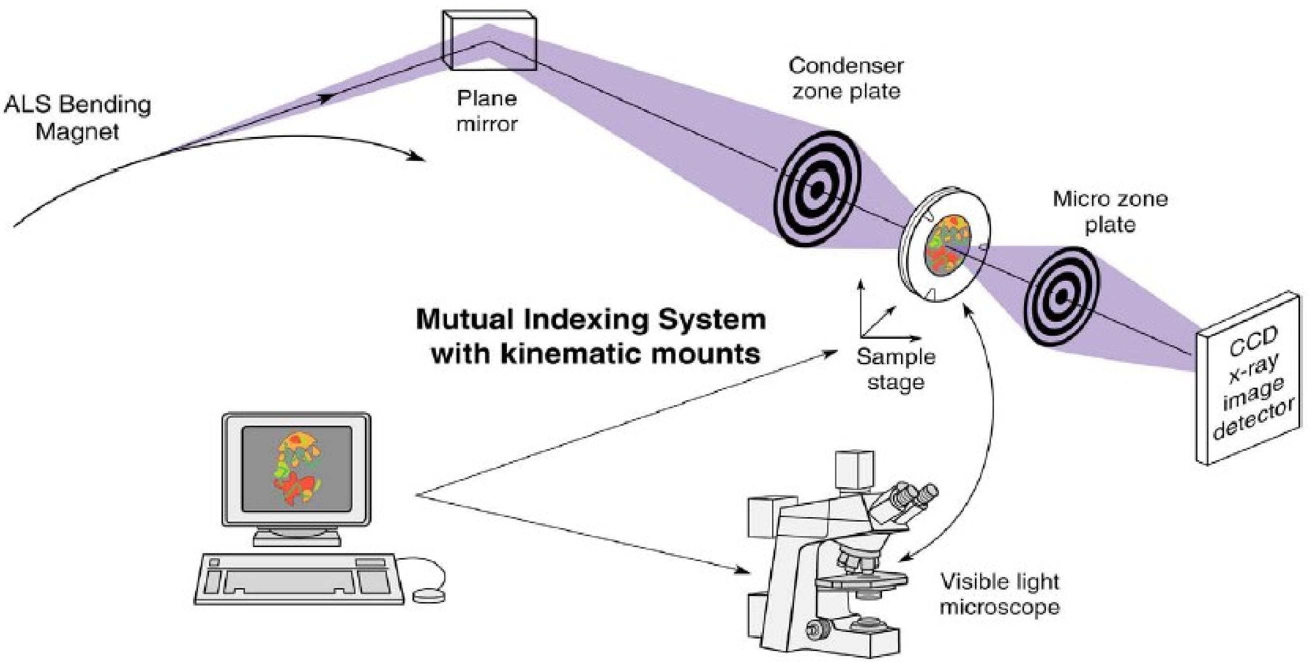

Courtesy of W. Meyer-Ilse, CXRO/LBNL

Nanometer focusing

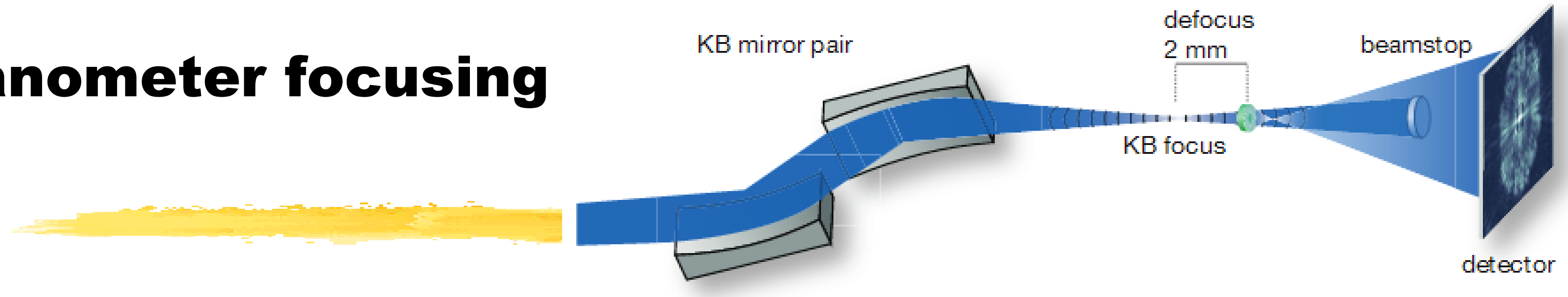

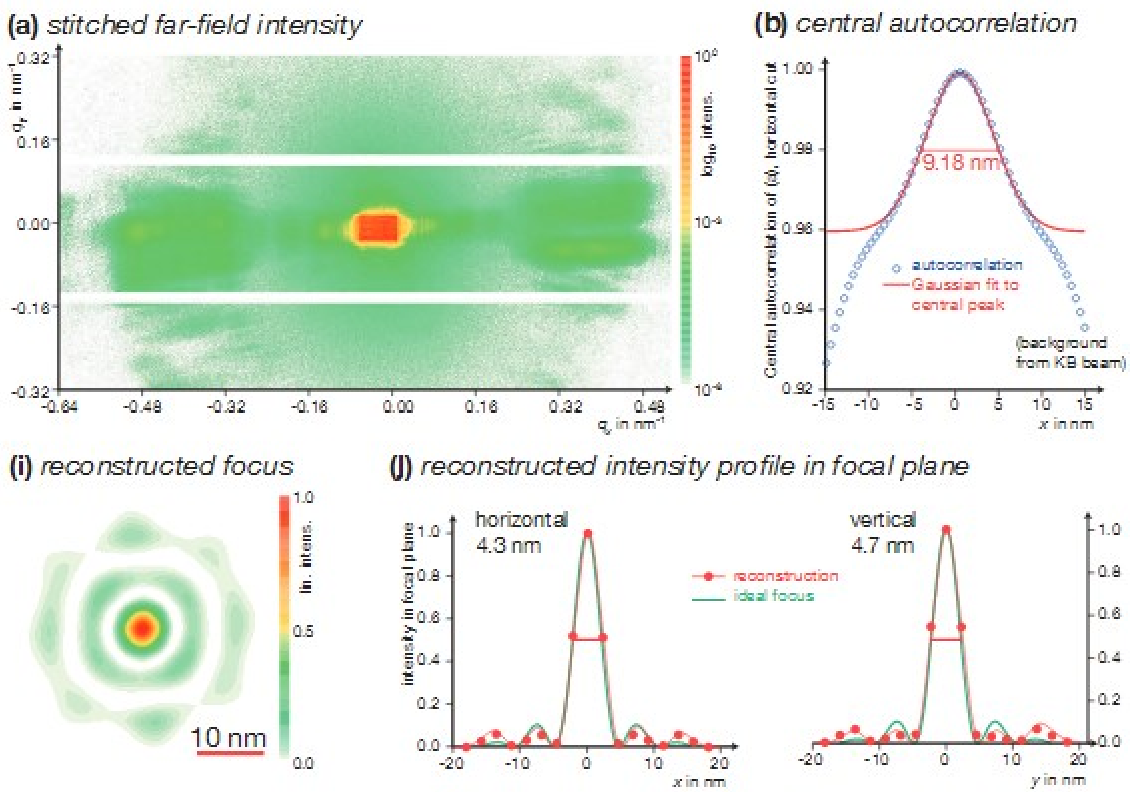

150 nm focus at 8 keV (0.16 nm)
Yun et al, Rev. Sci. Inst. 70, 2238, 1999

Sub-5 nm focusing at 8 keV
Doring et al, Opt. Express 21, 19311, 2013

Zone plates for high-order laser harmonics

The zone plate monochromator

An off-axis reflection zone plate (RZP) is imprinted as a projection of a conventional transmission zone plate on a totally reflecting mirror surface. The structure, being a laminar grating of variable line spacing in two dimensions, is capable of imaging the source by diffraction onto a certain distance along the optical axis, acting as both a dispersive and focusing optical element. However, owing to the high chromaticity of a zone plate, i.e. the dependence of the focal length on wavelength, different energies are focused on different positions along the optical axis.

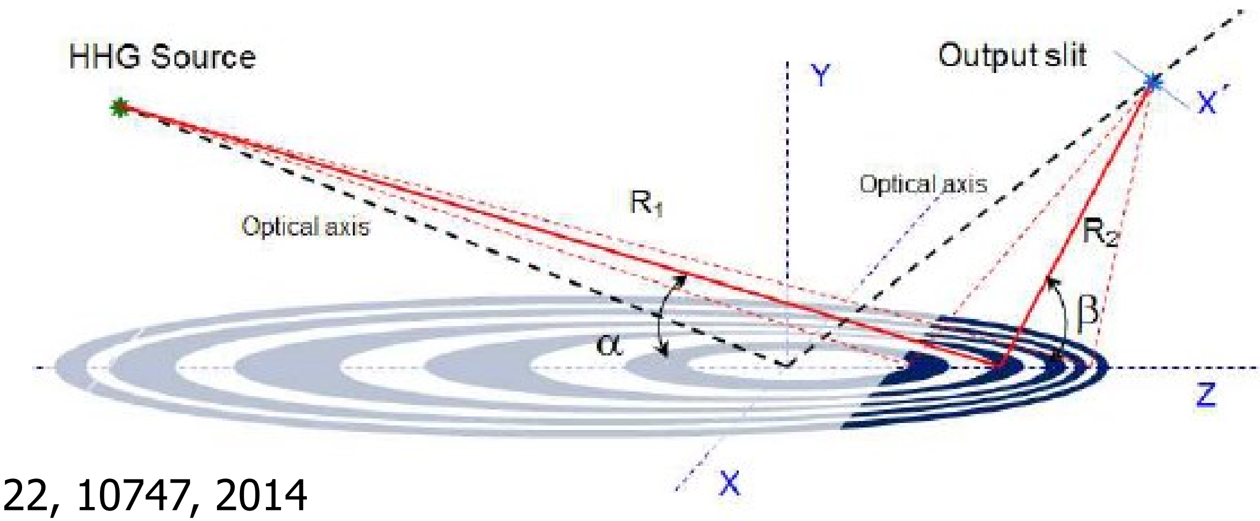

J. Metje al, Opt. Express 22, 10747, 2014

Zone plates for high-order laser harmonics

Energy dispersion $$\frac{\Delta E}{\Delta x'} = \frac{E^2 d \sin\beta}{hcR_2}$$

Optimal structure period *d* $$d = \frac{\lambda}{\sin\alpha}\left[\left(1+\cot^2\alpha+\left(\frac{R_2}{\Delta x'}\frac{\Delta E}{E}\right)^2\right)^{\frac{1}{2}}-\cot\alpha\right]$$

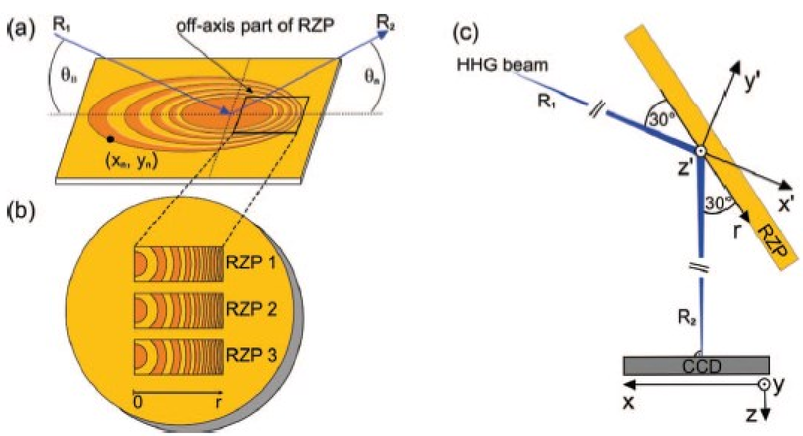

M. Brzhezinskaya et al, J. Synch. Rad. 20, 522, 2013

Beamline for HHs

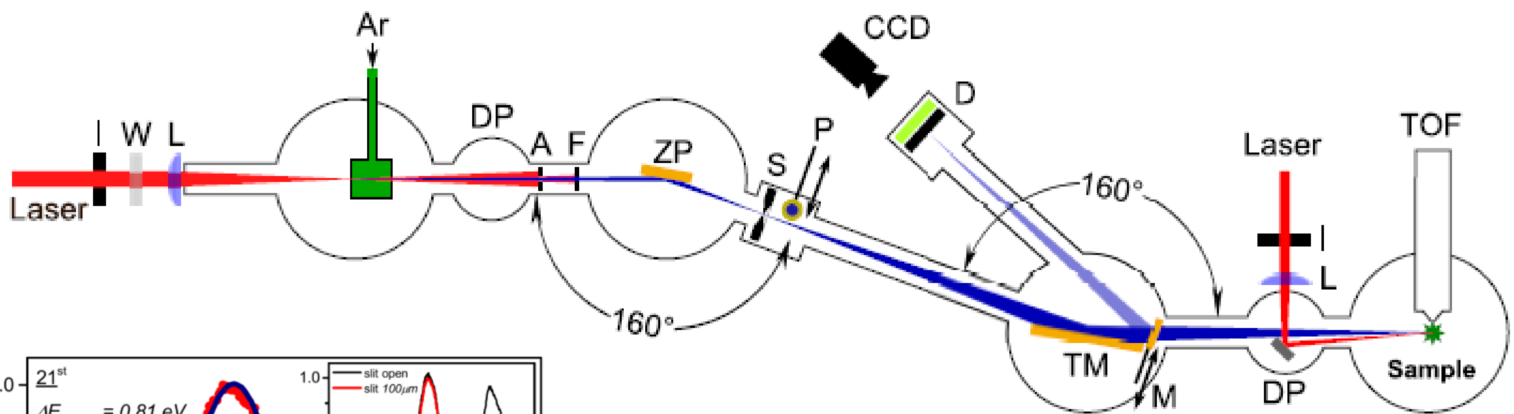

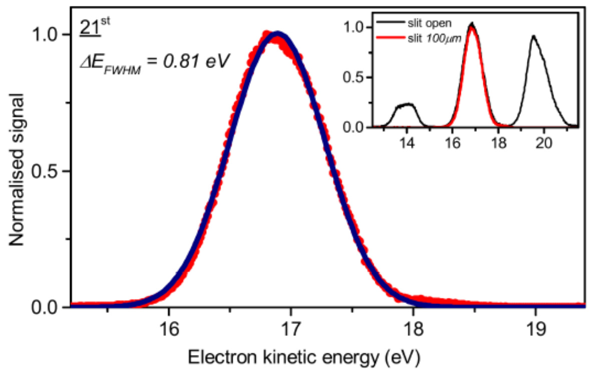

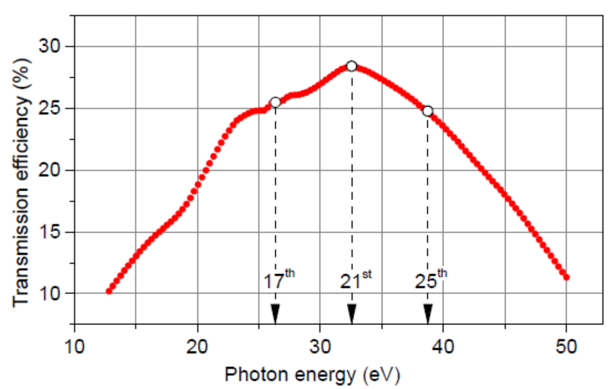

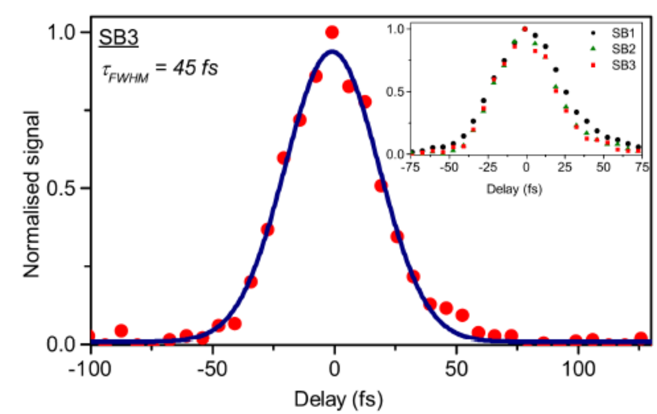

Conclusions

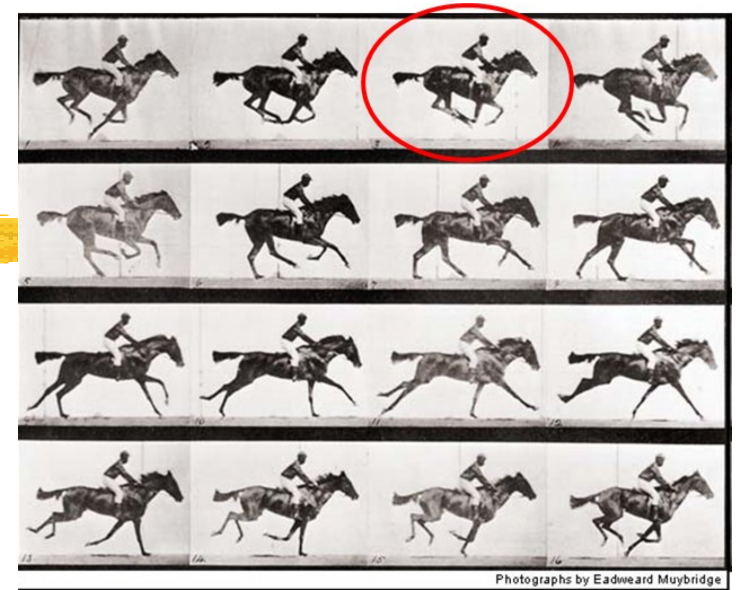

After ≈50 years from the use of dye lasers (ps time scale), ultrafast optics broke the femtosecond barrier and reached the attosecond time scale to watch at electron motion in real time.

XUV optics play an important role in handling and conditioning the XUV photon beam toward the sample